THESIS ON MECHANICAL ENGINEERING E97

Titanium Carbide Cermet as Ballistic Protection Material

MAREK JÕELEHT

TUT PRESS

TALLINN UNIVERSITY OF TECHNOLOGY
Faculty of Mechanical Engineering
Department of Materials Engineering

This dissertation was accepted for the defence of the degree of Doctor of Philosophy in Engineering on March 21st, 2016.

Supervisor: D Eng Jüri Pirso, Department of Materials Engineering, Tallinn University of Technology

Kristjan Juhani PhD, Department of Materials Engineering, Tallinn University of Technology

Opponents: Richard T. Fingers PhD, Acting Deputy Director, Aerospace Systems Directorate, Air Force Research Laboratory, United States of America

Renee Joost PhD, Program Director, Skeleton Technologies OÜ, Estonia

Defence of the thesis: April 26, 2016 at 14.00, Tallinn University of Technology, Ehitajate tee 5, 19086 Tallinn, Estonia, room NRG-621.

Declaration:

Hereby I declare that this doctoral thesis, my original investigation and achievement, submitted for the doctoral degree at Tallinn University of Technology, has not been submitted for any academic degree.

ISSN 1406-4758
ISBN 978-9949-23-917-7 (publication)
ISBN 978-9949-23-918-4 (PDF)

MEHHANOTEHNIKA E97

Titaankarbiidkermis ballistilise kaitse materjalina

MAREK JÕELEHT

TTÜ
KIRJASTUS

CONTENTS

ABBREVIATIONS

List of abbreviations and symbols used in the dissertation

AD – Areal mass density [kg/m^2]

AEP – Allied Engineering Publication

AFV – Armoured Fighting Vehicle

Al_2O_3 – Aluminium oxide

AP – Armour piercing

a.u. – Arbitrary Unit for better visual comparison or estimation

DoP – Depth of Penetration [mm]

EDF – Estonian Defence Forces

KE – Kinetic energy [J]

HBS – Brinell hardness with steel indenter

HIP – Hot Isostatic Pressing

HV10 – Vicker's hardness

MBT – Main Battle Tank

MoD – Ministry of Defence

NATO – North Atlantic Treaty Organisation

RD – Relative density [%]

SEM – Scanning Electron Microscope

SiC – Silicon carbide

STANAG – Standardization Agreement in NATO

TGA – Thermogravimetric analysis

TiC – Titanium carbide

TRS – Transverse Rupture Strength [MPa]

TUT – Tallinn University of Technology

WC – Tungsten carbide

XRD – X-ray diffraction

wt% – Weight percent [%]

1 INTRODUCTION

1.1 Motivation

Motivation for the current dissertation comes from a research project focused on the development of light weight vehicle armour. Conducted from 2008 to 2010, the project ended successfully and in 2012, a follow-on project was started. The idea and the request were proposed by the Estonian Defence Forces (EDF) but the funding and contract were made by the Ministry of Defence of Estonia. As the only technical university, Tallinn University of Technology (TUT) was chosen to conduct research and development of these projects.

In the first project, the purpose was to design and optimise an armour system for transport vehicles rather than for fighting platforms such as main battle tanks (MBT) or armoured fighting vehicles (AFV). The vehicles in question that the armour system to be implemented on were MAN 4520 trucks manufactured by MAN SE in Germany and Pasi XA-180EST made in Finland [1]. The threat level defined for the armour system was set to NATO STANAG 4569 level III. Level III indicates 7.62 mm calibre rounds with armour piercing (AP) capability fired from assault or sniper rifles. The resulting armour panel weight was 61.3 kg/m^2. The term STANAG stands for the Standardization Agreement often used both between the NATO nations and with nations that wish to offer their products to NATO member countries.

The second project is aimed at the further development of the armour panel to reduce the weight and the cost. Additionally, the goals are to test and develop the panel to withstand any operational conditions including the weather (temperature fluctuations, moisture, UV radiation etc.) and mechanical conditions (vibration and torsion on the vehicle). Since there are various types of threats, the EDF also wanted to obtain different solutions to NATO STANAG 4569 threat levels II–IV. The project's contract includes an agreement to develop additional solutions for level II and IV, which compared to level III are expected to be lighter and heavier, respectively.

Throughout this dissertation the focus remains on NATO STANAG 4569 level III with 7.62x51 AP (WC core) rounds as the used material selection is expected to remain the same for other threat levels with extrapolated thicknesses.

1.2 Armour panel concept

1.2.1 Threat level

In today's world, specialisation is of strong connotation. This applies also in the case of ballistic threat and protection. The range of potential threats is wide, starting from hand guns, medium calibre anti-armour sniper rifles to high calibre anti-tank rounds with various penetration mechanisms. Therefore, first, it is important to understand so-called "enemy" that the research project has to work

against. The threat level under consideration is NATO STANAG 4569 level III with key characteristics illustrated in Table 1.1.

Table 1.1. NATO STANAG 4569 level III kinetic threat (Edition 2, 18 December 2012 Annex A)

Threat level	Weapons	Calibre	Core	Distance	Angle
3	Machine gun, sniper rifle	7.62 mm	WC core Steel core	30 m	Azimuth 360°

The rounds with tungsten carbide (WC) core are heavier and the material properties of WC hardmetals are superior compared to hard steel core. Even though the standards usually refer to the core as being tungsten carbide, the actual material is a cermet, i.e. cemented carbide where the hard WC grains are in a binder metal matrix such as Co. Several companies produce such ammunition and at the beginning of the project, the Estonian Defence Forces used ammunition from Lapua, Ruag and Nammo.

The design and properties of ammunition from different manufacturers vary slightly. The design of each bullet and corresponding core are shown in Figure 1.1. The weight of the bullet and the respective cores as well as the velocities of the fired shots were measured by the EDF using Kurzzeit BMC 19. The values are presented in Figure 1.1 and Table 1.2.

a) b) c)

Figure 1.1. Bullet and core design of AP ammunition used by the EDF: a) Lapua 7.62x51 AP492; b) Ruag 7.62x51 AP; c) Nammo 7.62x51 AP8

Table 1.2. Parameters of ammunition used by the EDF

Manufacturer	Ammunition type and model	Bullet weight [g]	Core weight [g]	Bullet velocity [m/s]
Lapua	7.62x51 AP492	10.7	6.3	871±8
Ruag	7.62x51 AP	12.7	5.6	792±7
Nammo	7.62x51 AP8	8.4	6.0	955±7

Using Eq. (1.1), the kinetic energy (KE) in J of each bullet but also their corresponding cores were calculated to compare the ballistic threats:

$$KE = \frac{m \cdot v^2}{2}, \tag{1.1}$$

where m is the weight of the bullet or core in kg and v is the velocity of the bullet after firing in m/s. The kinetic energy values are shown in Figure 1.2.

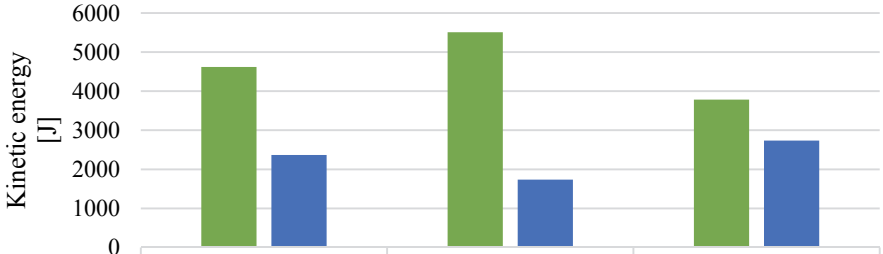

	Lapua	Ruag	Nammo
Bullet KE	4619	5509	3785
Core KE	2369	1735	2736

Figure 1.2. Kinetic energy of ammunition used by the EDF

The kinetic energy values indicate that the Nammo bullet has the smallest weight and overall energy; on the other hand, the core has the highest kinetic energy because of the increased velocity. According to NATO STANAG 4569 [2] and AEP-55, level III threat level WC core ammunition velocity is set to 930±20 m/s and Nammo AP8 is mentioned as a suitable ammunition for testing purposes.

The material used in the Nammo 7.62x51 AP8 uses tungsten carbide hardmetal with nickel as the binder metal – WC-Ni. The analysis suggests that the composition of the bullet core is a relatively common WC-10Ni, i.e. the ratio between tungsten carbide and nickel is 90:10 by weight, respectively. Mechanical properties of such material are influenced by the starting powder (particle size, purity etc.), green body preparation (mixing, pressing etc.) and by sintering (regime, furnace etc.). Nammo 7.62x51 AP8 bullet core properties are outlined in Table 1.3.

Table 1.3. Nammo 7.62x51 AP8 bullet core mechanical properties [3, 4]

Material	**Density [g/cm^3]**	**TRS [MPa]**	**HV10**	**Toughness [MPa·m$^{1/2}$]**
WC-10Ni	14.4–14.5	2100–2500	1280–1360	15.6–16.4

The values were compiled by comparing different sources with some of the properties that could be measured. The microstructure image of the bullet core material is illustrated in Figure 1.3.

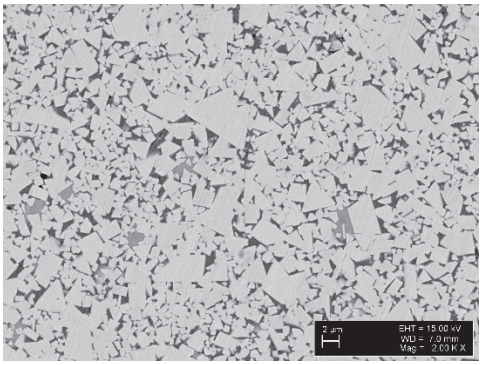

Figure 1.3. SEM microstructure of Nammo 7.62x51 AP8 bullet core

1.2.2 Armour panel configuration

Vehicle armour for lower level threats usually implements armour steel with 6 – 8 mm in thickness against handguns and rifle ammunition without any armour piercing cores. Steel has several characteristics that make it a good armour solution since it is simple to integrate sheet metal onto the vehicle and it has better multi hit capability than ceramic tiles that are destroyed during the impact. The main downfall of armour steel solutions is the weight of the added material. For level III, it is also possible to use only armour steel plates but the areal mass density (AD) is around 190 kg/m^2 (see Table 1.4.), i.e. for a MAN 4520 truck cabin with an area of 10 m^2, the added weight would be 1900 kg. Such added weight will greatly impair the mobility of the vehicle and may require additional improvements to the drive system and suspension.

Table 1.4. Steel armour properties and weight [5, 6]

Material	Yield strength [MPa]	Tensile strength [MPa]	Elongation [%]	HV10	Thickness [mm]	AD [kg/m^2]
Ramor 500	1450	1700	7	580	25.1	196
Miilux 500	1250	1600	8	580	24.0	187

Alternatively, instead of only armour steel plates, composite materials are implemented to provide protection against STANAG 4569 level III. A composite armour panel consists of two main layers working during a ballistic impact. The principal schematic of a typical armour panel configuration is illustrated in Figure 1.4.

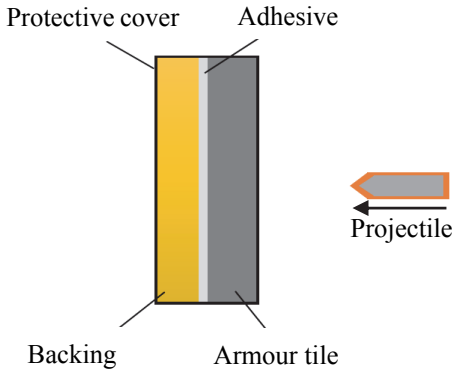

Figure 1.4. Schematic of armour panel construction

The purpose of the first layer, armour plate (dark-grey), is to reduce the kinetic energy of the core of the bullet by shattering the core into smaller fragments and disrupting their linear translational vectors. This means that the penetration potential of each fragment is significantly reduced compared to the initial bullet core as a whole. In addition to the fragmentation of the projectile, the armour tile is also shattered into a debris of fragments. The armour tile debris then acts as an abrasive media against the bullet fragments and it is estimated that around 40% of the kinetic energy of the projectile is absorbed by erosion [7]. The second important layer is the backing indicated in yellow. Backing can offer structural integrity if the armour plate consists of individual tiles, i.e. creating a mosaic but the main function of this layer is to stop the fragments. Additional layers include an adhesive (light-grey) to fix the armour plates to the backing and finally cover material (black) that protects the inner layers from environmental influence such as moisture, UV radiation etc.

1.2.3 Armour tile material

The material of armour tile has to satisfy mainly two criteria – areal mass density and ballistic performance. Density is mostly driven by the application whereas vehicles on land for transport or close combat as well as airborne platforms engaged on low altitude combat areas, such as helicopters, need the lightest possible armour solutions for mobility. Usually, the area that needs protection is around the cabin where the driver or pilot is located but may also be needed for sections of the vehicle/platform where other passengers are situated. This means that the total area for armouring is several square meters. In metallurgy, light metals are considered elements that have lower density values compared to iron with a density of 7.87 g/cm^3. Such metals can be, for example, aluminium (Al) and titanium (Ti) with densities at 2.70 g/cm^3 and 4.51 g/cm^3, respectively. Both of these materials are used for armouring solutions in the form

of alloys or intermetallic compounds but not against STANAG 4569 level III solely on their own.

Determining the ballistic performance of a material requires either actual test-firing experiments or computational methods that have been verified together with experimental equivalents [8]. There is still open discussion on the correlation of more commonly tested mechanical properties of the material and the resulting ballistic behaviour. It has been concluded that the hardness of the armour plate material has to be higher than the projectile's material but further increase of hardness does not improve the ballistic performance of the armour material alone [9]. This can also be seen in [10] where the ballistic performance of a material is evaluated by the required impact velocity for the projectile to cause interface defeat, i.e. cause penetration. In this study, TiB_2, SiC, B_4C and Syndie (synthetic diamond with Co catalyst) were used with increasing hardness values but the corresponding interface defeat velocities placed the boron carbide last with the lowest required impact velocity (Figure 1.5).

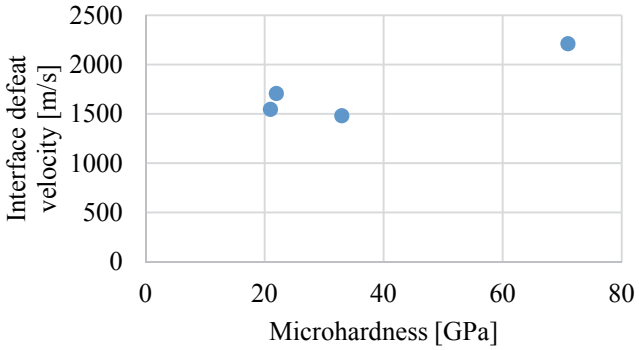

Figure 1.5. Influence of material hardness on interface defeat velocity [10]

The most common light weight material used against armour piercing rounds with hard cores is aluminium oxide (Al_2O_3). It has sufficient hardness against both hard steel core and hardmetal core with hardness of HV10 1500–1900 and low density of 3.8–3.9 g/cm^3 [8]. As aluminium oxide is widely used also against 7.62x51 AP (WC core), which is the main focus of this research, it was suggested that titanium carbide based cermets being developed in TUT could have the potential as an alternative armour material. Capabilities are available in Estonia to manufacture it locally.

1.3 Objective of the dissertation

The objectives of this research are to develop reactive sintered titanium carbide (TiC) based cermets to increase the mechanical properties of these cermets and to evaluate the feasibility of implementing TiC based cermets as armour tile material against 7.62x51 armour piercing rounds with hardmetal core. Main hypotheses stated are as follows:

Hypothesis I. *Reactive sintering technology enables preparation of TiC based cermets with similar or superior mechanical properties compared to conventional powder metallurgy route.*

Hypothesis II. *TiC based cermets are suitable as armour material against 7.62x51 armour piercing rounds to destroy the bullet's hardmetal core.*

Hypothesis III. *TiC based cermets have competitive mass efficiency as armour material compared to commonly used Al_2O_3 and SiC.*

The objectives of this dissertation are based on the research project LKM12179 and contract no. 447/1211 between Tallinn University of Technology and the Ministry of Defence of Estonia.

1.4 Outline of the dissertation

The dissertation is divided into two main sections. The first part focuses on the development and characterisation of reactive sintered TiC based cermets. Materials research studies microstructure formation, composition, powder preparation and sintering regimes. This is the main area of research with published results. In section two, ballistic capability of titanium carbide cermet is evaluated and compared against a certified Al_2O_3 ceramic solution from the market and SiC ceramic also considered as a light weight armour material in the research project. During ballistic testing, both small scale testing of individual armour tiles and full armour panel configurations are evaluated. Conclusions are followed by suggestions for future research.

2 MATERIAL DEVELOPMENT

2.1 Titanium carbide ceramics and cermets

Titanium is the lightest element in group IV of the transition metals and is very reactive compared to many other transition metals. Titanium is able to form several compounds with non-metals such as monocarbides (TiC) and mononitrates (TiN), but also carbonitrides (TiC_xN_{1-x}). Then, the ratio of metal to non-metal atoms is 1:1 but in reality, the materials provided as powder have some deficiencies of non-metal atoms and may also have "free" (unbounded) material in the case of carbon. The carbon deficit can vary between $TiC_{0.97}$ to $TiC_{0.56}$ [11]. Corresponding mechanical properties of TiC with different C content are shown in Table 2.1.

Table 2.1. Properties of TiCx depending on C content [12]

TiC_x	x=0.97	x=0.87	x=0.78	x=0.68	x=0.58
HV10	3370	2800	2300	-	-
Microhardness [GPa]	28	23	21	15.5	12
Young's modulus [GPa]	494	492	446	406	385
Shear modulus [GPa]	196	195.5	180	161	152
TRS [MPa]	570	550	360	270	250

Titanium carbonitride is also referred to as TiC/TiN or Ti_2CN to emphasise the ideal ratio of 1:1 between Ti atoms and non-metal atoms (C and N). The ratio between carbon and nitrogen can be varied but industrial powders usually come in two grades at 50/50 or 70/30, respectively or other, also referred to as $TiC_{0.5}N_{0.5}$ and $TiC_{0.7}N_{0.3}$. Additionally, titanium may form oxides and borides in which case the ratio between the metal and non-metal/metalloid is 1:2, respectively. As TiC and TiN are both face-centred cubic crystal structures, TiO_2 has body-centred tetragonal and TiB_2 hexagonal crystal structures. The resulting mechanical properties of these ceramics are represented in Table 2.2.

Table 2.2. Properties of titanium ceramics [13–20]

Ceramic	Crystal structure	Density [g/cm^3]	Micro-hardness [GPa]	Young's Modulus [GPa]	Toughness [MPa·m$^{1/2}$]
TiC	Face-centred cubic	4.93	28–32	497	-
TiN	Face-centred cubic	5.22	20–24	250	5.5
TiO_2	body-centred tetragonal	4.23	9–10	230	3.2
TiB_2	hexagonal	4.52	26–30	543	6.2

Considering the mechanical properties, the best option for ceramic armour would be TiB_2 since it has the lowest density at sufficient hardness and higher fracture toughness than other ceramic armour plate materials such as Al_2O_3, SiC and B_4C. Several studies about implementing TiB_2 as an armour plate material in the scientific community [10, 20-23], military research [24] have been reported and offered by industry as an alternative material for armour solutions [25-27]. Other titanium ceramics have not been found to be used as armour plates so far. In the case of titanium dioxide, the hardness of the ceramic does not meet the required value of the level III 7.62x51 Nammo tungsten hardmetal core of HV10 1320. Titanium carbide and nitride have inferior mechanical properties and higher densities, which make them less attractive for armour solutions as pure ceramics.

Instead of pure ceramic armour plate, this research focuses on ceramic-metallic composite materials, i.e. cermets. Common cermets usually employ two phases in their microstructure – high hardness ceramic grains and ductile metallic matrix, also referred to as binder [8, 28]. This combination of two very different phases results in a material with promising ballistic capability. As the armour tile is subjected to a projectile, the fragmented armour tile begins to expand in volume in all directions including radial directions, which loads the neighbouring tiles. Due to low fracture toughness of pure ceramic tiles, the adjacent armour tiles can be easily damaged. The existence of metal matrix surrounding the ceramic grains means that crack propagation is less severe. The ductile metal increases the fracture toughness and strength of most common titanium based cermets around 2–4 times compared to armour ceramics (Table 3.1).

During armour panel development in the current project a significant decrease in damaged armour tiles per hit was found when ceramic SiC tiles were compared to those of cermet TiC-NiMo. Similar conclusions were made in [29] where Al_2O_3 ceramic tiles were compared against TiC cermets with different amounts of binder in the cermet. With increased toughness and strength, the size of the fragments was larger and retained still some ballistic protection capability.

In 2014, small scale armour panels were tested where the construction of the panel was kept the same but only the armour tiles were varied. Two panels for each armour tile material were made. In both cases, armour plate thicknesses of 10 mm, 8 mm and 6 mm tiles were used. The backing material was kept the same, composed of 20 layers of S2-fiberglass with epoxy resin and additionally two layers for packing. After firing experiments, the panels were disassembled to investigate the damage caused to the armour tiles. A comparison between the TiC-NiMo cermet and SiC ceramic tiles is shown in Figure 2.1.

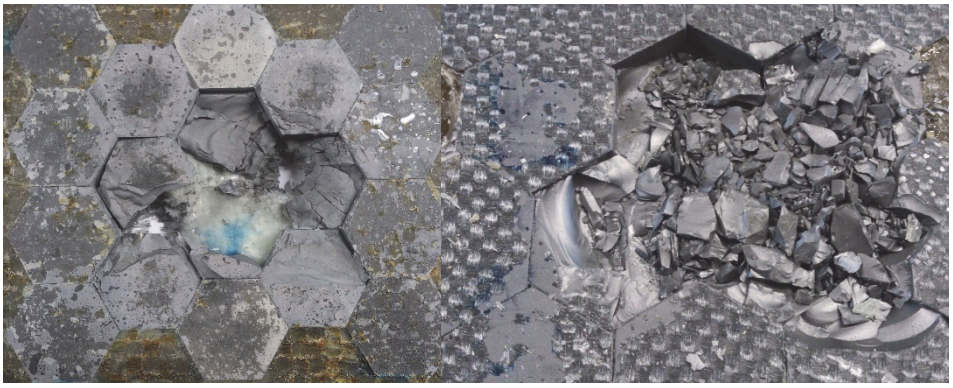

a) b)

Figure 2.1. Comparison of damaged armour plates after impact: a) panel with TiC-NiMo tiles after two shots; b) panel with SiC tiles after one shot

It can be clearly seen that the number of adjacent tiles that are damaged during the impact is higher for the SiC ceramic armour plates. These results were consistent throughout the firing experiments, as indicated on the graph (Figure 2.2). As an average, 2.25 tiles were damaged per shot for the TiC-NiMo cermet and 5.67 for SiC ceramic armour plates. This is a serious advantage for cermet armour plates when considering multi hit capability and the firing arrangement described in AEP-55. This difference is believed to be caused by the reflection of a compressive wave front caused by the initial tensile wave from the impact. With low tensile strength compared to metals and cermets, the ceramic materials are likely to fracture due to any reflected tensile wave [8]. The created wave front in the tile with impact is then carried to adjacent tiles where also the wave front is dissipated amongst further tiles but still a reflection occurs, which can be sufficient to initialise cracks in the first adjacent tile.

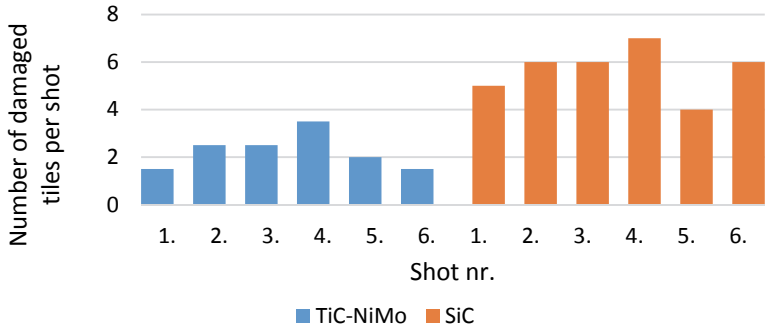

Figure 2.2. Comparison of damaged tiles per shot

The main drawback of implementing cermet materials for armour solutions is the higher density of the material compared to commonly used ceramic tiles. In order to counter this issue, it is hypostasised that the thickness of the cermet tile can be reduced to achieve ballistic protection at similar areal mass density.

2.1.1 Properties of titanium carbide cermets

Titanium carbide based cermets were introduced in 1929–1931 to find an alternative to the success of WC-Co hardmetals [3, 30]. However, they did not find a wide use until the 1960s because of their higher brittleness and difficulty to braze [3, 20]. A variety of alloying elements and binder metals have been tested for TiC based cermets and so far the optimum mixture of components has been TiC, Ni and Mo. In this case, nickel serves the purpose of creating a metal matrix binding the TiC grains. Molybdenum is an alloying element to aid the connection between TiC grains and Ni phase since the wetting angle of liquid Ni is 30˚ [31]. Molybdenum substitutes some of the titanium atoms in TiC, forming an outer ring of Ti(Mo)C on the carbide grains (Figure 2.3).

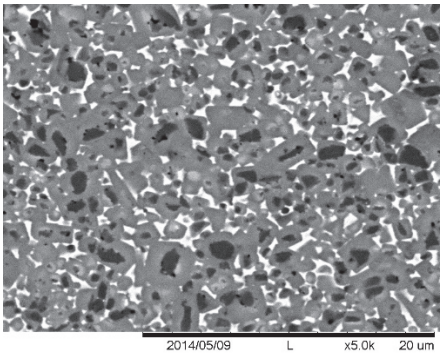

Figure 2.3. Core-rim structure of TiC-NiMo cermet

The dual-carbide phase has a wetting angle of 0˚ with nickel [32]. Molybdenum can decrease the wetting angle of TiC also with aluminium as

matrix material in [33]. Another option is to use cobalt as the binding metal but it is not used in the industry because of its higher price and sintering temperatures without advantages over nickel in terms of mechanical properties [34]. Iron based binders investigated for TiC based cermets have shown comparable mechanical properties to Ni-Mo binders [35-40]. So far, the use of iron based binder cermets is limited. A more exotic composition investigated are TiC/Al with Mo addition by SHS [33], a mixture of TiC-Al_2O_3-Ni-Co-Mo sintered at high temperatures of 1750 ˚C was produced for cutting hardened steels in [41] and TiC with iron aluminide intermetallic binder was prepared by liquid state sintering and pressureless melt infiltration of TiC preforms in [42].

In this research, the starting TiC based cermet was taken from the previous project as a reference material. The selection of the exact composition of the cermet is based on three key aspects:

- sufficient hardness > HV10 1400;
- maximum toughness > K_{Ic} [MPa·$m^{1/2}$];
- minimal density < ρ [g/cm^3].

An overview of typical TiC-NiMo properties depending on the composition of the cermet is presented in Table 2.3.

Table 2.3. Mechanical properties of TiC-NiMo cermets with common composition [43]

TiC [wt%]	Ni [wt%]	Mo [wt%]	HV10	TRS [MPa]	Density [g/cm^3]	Toughness [MPa·$m^{1/2}$]
80	10	10	1650	730	5.54	11.3
	13	7	1510	990	5.50	11.8
	16	4	1400	1010	5.47	11.9
70	15	15	1590	1090	5.68	10.4
	20	10	1420	1180	5.77	15.5
	24	6	1300	1210	5.74	17.3

As fracture toughness is in strong correlation with strength, i.e. higher strength values also indicate higher fracture toughness, the reference material selected for this research project was 80TiC-20NiMo(2:1).

2.2 Manufacturing of titanium carbide based cermets

There are several technological routes for manufacturing cermet materials. The most common industrial method consists mainly of ball milling followed by liquid state sintering. Alternatively, in literature, numerous articles have used the spark plasma sintering (SPS) method [44, 45], self-propagating high-temperature synthesis (SHS) [36, 39, 46, 47], and the pulse current sintering (PCS) process [48]. The main drawback of these technologies arises from scaling up the manufacturing of cermet products, as the financial costs could not compete with conventional manufacturing.

In essence, powder metallurgy (PM) comprises four steps: mixing/milling of powders, powder preparation, pressing of "green bodies", and sintering [4, 49]. Usually, the starting powders for cermet and hardmetal mixtures employ ceramic powders of the main hard phase (TiC, WC, Cr_3C_2 etc.), binder metal powders (Ni, Co etc.) and alloying element powders if needed (Mo, VC etc.). These powders with required ratios are mixed using ball mills, followed by drying and granulating. When the powder mixture is ready, the "green bodies" of the product are pressed to about 50–60 % theoretical density and finally sintered. Sintering can be done in two steps, using different furnaces – a pre-sintering furnace is used to remove any pressing aid substances such as paraffin wax and the second furnace to fully densify the parts. These steps can be combined into one sintering cycle, which will decrease cycle duration (Figure 2.4) but requires a high temperature furnace able to withstand pressing aid removal.

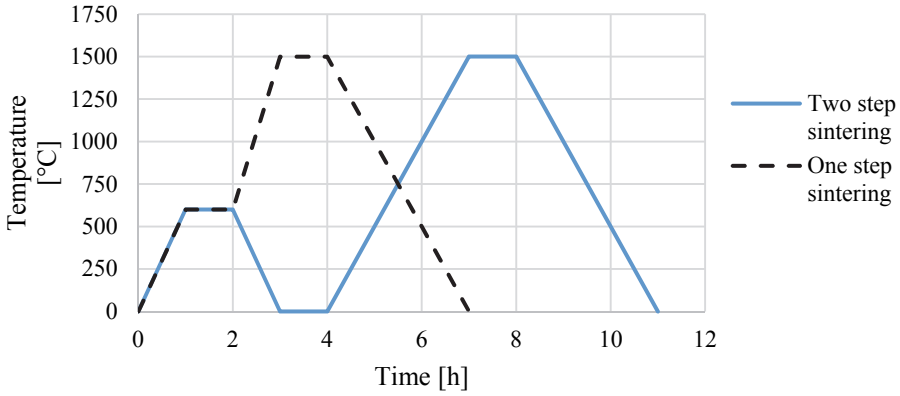

Figure 2.4. Sintering cycle durations with one and two step sintering regimes

In case pre-sintering is performed separately, sufficient temperature and time is needed for the powder particles to undergo initial fusion. This enables manipulation of the pre-sintered parts without destroying them. Pre-sintering has two advantages as the parts are strong enough to be additionally machined (milled, drilled etc.) and the vapour of pressing additives is removed before sintering in a high-temperature furnace. Pre-sintering temperature is around 600–700 °C and duration depends on the volume of the parts. Final sintering uses temperatures where the binder metal has entered liquid state. The melting temperature of most common binder metals is – cobalt 1495 °C, nickel 1455 °C, iron 1538 °C. During sintering of cermet parts, the melting temperatures of the binder metals are lower compared to pure metals. Still, the final sintering temperature can be between 1350–1500 °C, depending on the materials used, the ratio between the ceramic and binder phase and the engineered microstructure of the cermet. Higher final temperatures result in less viscous binder, which helps to prevent porosity and to form more homogeneous microstructure using shorter

sintering cycles but additionally facilitates grain growth. An example of different final sintering temperatures and resulting microstructures is illustrated in Figure 2.5.

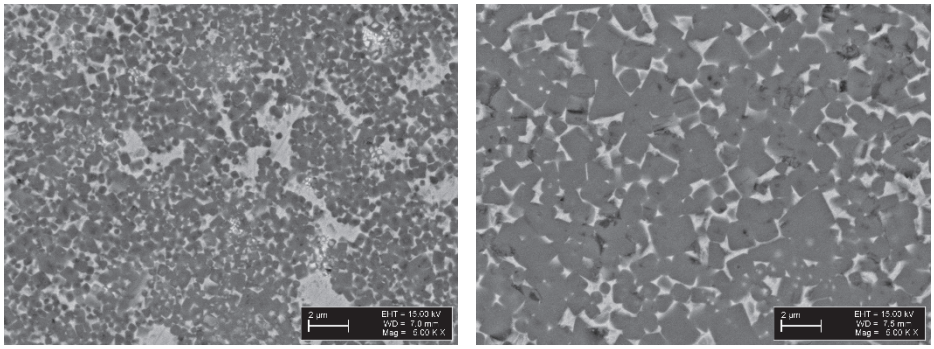

a) b)

Figure 2.5. Microstructures of reactive sintered Ti(Mo)C-Ni cermets at different temperatures: a) at 1330 °C; b) at 1500 °C

It is clearly visible that the lower sintering temperature of 1330 °C has resulted in finer carbide grains (~0.5 µm) compared to grains at 1500 °C with ~1.5 µm in diameter. Also, the lower sintering temperature microstructure is less homogeneous with areas of binder "lakes".

2.2.1 Reactive sintering technology

In principle, reactive sintering follows the main four steps as normal powder metallurgy. The main difference is in the starting powders used to mix the required cermet mixture. When conventional PM uses ceramic powder (TiC, TiCN etc.) for the hard phase of the cermet, then in reactive sintering, the base elements of the ceramic are used instead of TiC powder, replacing it with Ti and C (carbon black) powders. This, in turn, means that the formation of ceramic compounds (in this case TiC) occurs *in situ* during the final sintering of the part. Traditionally, titanium carbide is produced separately in high-temperature kilns by using one of these chemical reaction options Eqs. (2.1) and (2.2):

$$Ti + C \rightarrow TiC \tag{2.1}$$

$$TiO_2 + 2C \rightarrow TiC + CO_2 \tag{2.2}$$

In both cases, the temperature in the kiln is around 2000 °C for titanium carbide to synthesise. This process also requires long sintering durations and has therefore high energy consumption. In literature, alternative routes are suggested for procuring TiC. Low cost starting materials of TiO_2 and carbon black were mechanically activated and sintered between 1250–1500 ˚C in [50]. In [51, 52], polymeric precursors (furfuryl alcohol – FuOH) are prepared by titanium alkoxides (titanium butoxide – $Ti(O\text{-}n\cdot Bu)_3$) and organic compounds at

temperatures of 1100–1300 °C. Another alternative is gas phase reduction of $TiCl_4$ using hydrocarbons as presented in [53]. Additionally, autoclaving titania (TiO_2) with magnesium and magnesium carbonite has been reported to synthesise TiC in [54]. Long milling for 40 hours has produced TiC from titanium and carbon powders in [55]. Using high-energy planetary mill TiC has been produced by mechanical alloying combining titanium powder with different carbon sources – activated carbon, carbon fibres and carbon nanotubes [56].

In reactive sintering, the lower temperature for titanium carbide synthesis is a result of two factors. Firstly, with the presence of other elements in the powder mixture (binder metal) it is believed that nickel in the case of reactive sintered Ti(Mo)C-Ni cermets acts as a catalyst for the reaction of Ti and C to form TiC. Secondly, during milling, the powders are also mechanically activated, reducing the amount of required energy later in the furnace by heating. With sufficient kinetic energy of the milling balls, TiC can already form during the milling process at near room temperature. This phenomenon has been called by various terms: mechanical alloying, reactive milling, mechanical activation for TiC and other carbides, e.g. SiC, Co_6W_6C [57–61]. The synthesis of carbides occurs before the binder enters the liquid phase and it may be required to have an additional dwell steps at carbide formation temperatures with larger mass parts.

The possibility of manufacturing reactive sintered cermet samples has been shown for different cermet compositions. In 2000, Choi used elemental Ti, C and Ni powders to fabricate ultrafine TiC-Ni cermet powder using a spex-milling technique with a particle size of 0.2–1.5 μm after sintering [62]. He concluded that compared to the commercial cermet powder with grains of 3–5 μm, the mechanical alloying process results in a more effective formation of the final microstructure of the cermet. In 2006, Pirso et al. used reactive sintering to produce Cr_3C_2-Ni cermets with increased mechanical properties compared to conventional route [63]. In 2008, the same group published results of reactive sintered WC-Co hardmetals [64].

In 2006, Kabayashi and Ozaki used mechanical alloying and pulse current sintering to produce TiC-20Ni cermets from Ti, C and Ni as starting powders. In 2014, Hosokawa et al. used a two-stage milling process to produce powder mixtures for $(Ti_{0.8}Mo_{0.2})$C-Ni cermets that were then sintered for 1 h under vacuum [65]. In this process, the initial mixture contained only carbide elements (Ti, Mo and C) that were milled for 250 h. After initial milling, Ni powder was added and additional milling was done for 72 h. Green bodies were sintered at different temperatures depending on the binder content at 1400–1450 ˚C.

An illustrative schematic of conventional powder metallurgy and reactive sintering technologies is presented in Figure 2.6.

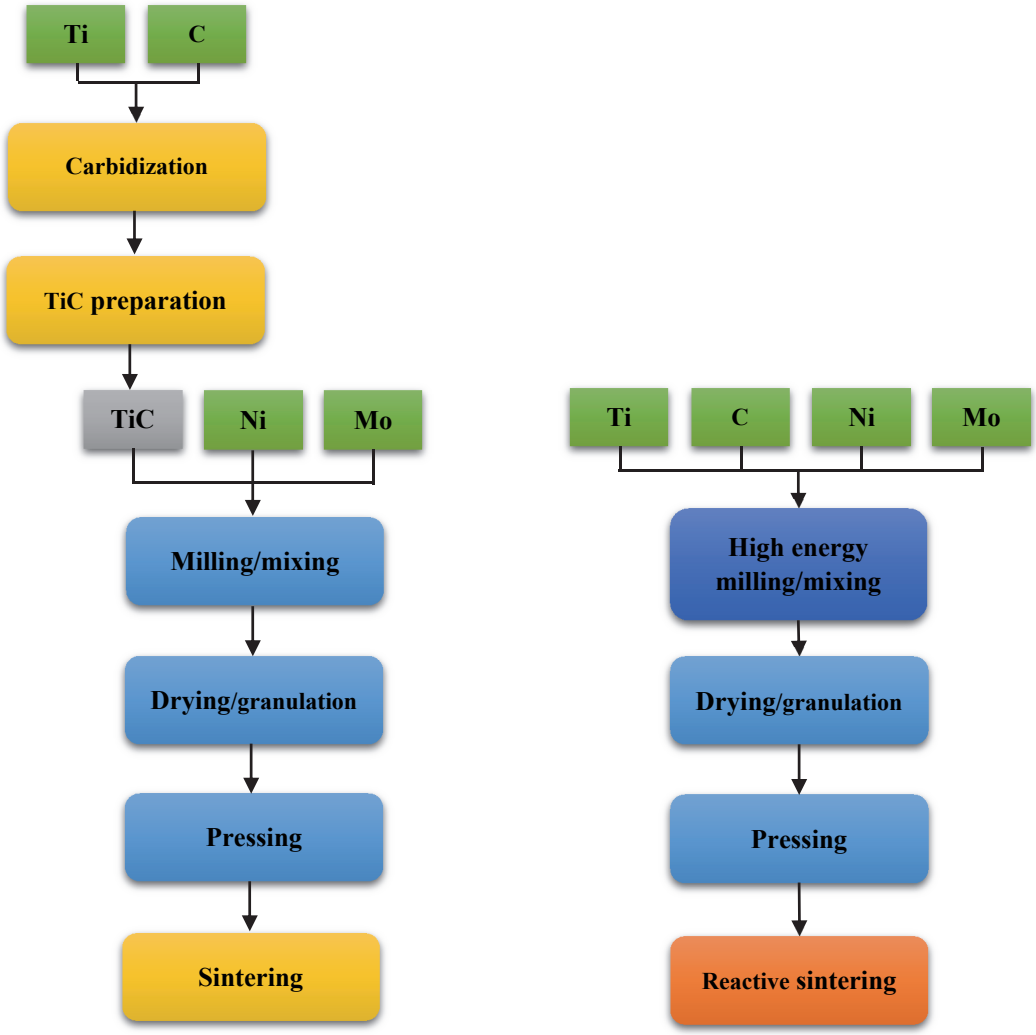

Figure 2.6. Process schematic of: a) conventional powder metallurgy; b) reactive sintering

The main differences between conventional and reactive sintering are the starting powders used, milling energy and sintering regime. The reduced cost of reactive sintering comes from excluding the high temperature TiC powder synthesis and preparation. Milling of the final mixture and final sintering need to be adjusted for reactive sintering but in general the same or similar equipment can be utilised without any major investments.

2.3 Development of reactive sintered titanium carbide based cermets

2.3.1 Formation of reactive sintered Ti(Mo)C-Ni cermet

Final microstructure and mechanical properties of a cermet material are influenced by several aspects. Most importantly, these are the composition of the mixture and the sintering regime. In the early stage of this research, a base mixture was chosen based on the experience and knowledge acquired in the pre-project and research stage. The mixture was sintered in steps to understand the processes and reactions occurring during sintering of the material and the final samples were first sintered as the reference material.

In order to achieve the required mechanical properties, the reactive sintered cermet was chosen to have 75 wt% of titanium carbide elements and 25 wt% of binder and alloying elements. A very strong factor on the resulting microstructure is carbon content. According to the titanium-carbon phase diagram, the homogeneity range of TiC is relatively large from 15–20 wt% of carbon [66]. The ideal ratio of 1:1 of Ti and C atoms would have 20.03 wt% of carbon and any carbon deficiency reduces the mechanical properties of carbide, as was indicated in Table 2.1. Still, the amount of carbon was reduced to compensate the inhomogeneous mixing of the cermet powder mixture, which would result in free carbon in the final material. As free carbon possesses no noteworthy mechanical properties, the carbon agglomerates are equal to pores in the material. Molybdenum in the case of titanium carbide based cermets is also involved in the formation of carbides and during reactive sintering, only Ti(Mo)C dual-carbide grains are distinguishable in the final microstructure. As titanium's main carbide form has the ratio of metal to carbon ratio of 1:1 (MC[1]), molybdenum's preferable carbide has a ratio of 2:1 (M_2C). This, in turn, means that molybdenum requires less carbon per atom. The exact chemical composition of the dual-carbide in reactive sintered Ti(Mo)C-Ni cermet is complex and the amount of carbon deficiency in $Ti_xMo_yC_z$ is difficult to determine. The microhardness and other mechanical properties of the dual-carbide depend on both the amount of bonded carbon as well as on the ratio between Ti and Mo. From a financial perspective, it is more cost effective to reduce molybdenum content, as it is considerably more expensive than titanium. As there is no capability to exactly determine the chemical composition of the dual-carbide, the ratio of Ti:Mo:C was calculated theoretically. The amount of carbon was selected to be 17 wt% out of the combined weight of titanium and carbon powders based on the results from [67] and previous experiments before the project and research discussed in this

[1] Describing transition metal carbides, the chemical formula of M_xC_y is often used to describe different carbides where M stands for metal atom.

dissertation. Commercial TiC-NiMo cermets indicate a ratio between Ni and Mo, which is usually 1:1, 2:1 or 4:1, respectively. This indication was also used during this research and a ratio of 2:1 of nickel and molybdenum was used as in the reference material. Essentially, this ratio also determines the amount of binder in the final microstructure since Mo is mostly involved in carbide formation and only nickel enters the liquid phase during sintering.

2.3.1.1 Experimental methods for microstructure formation

Elemental powders of Ti, Mo, Ni and C (carbon black) were used as starting powders. The mixture was milled using a high energy attritor mill for 10 hours. Tungsten carbide hardmetal balls were used with a ball to powder ratio of 10:1, respectively. The attritor container and rotary blades were also made from WC-Co hardmetal, which means that a small amount of contamination with WC and Co was present due to milling. Wet milling agent (heptane with 3 wt% of paraffin wax) was used, which also formed a protective cover on the powder particles, preventing from oxidation after milling and drying. Green bodies were pressed using a uniaxial press with 60 MPa pressure to achieve approximately 55 % density. The composition of the powder mixture is presented in Table 2.4.

Table 2.4. Starting powders of reactive sintered Ti(Mo)C-Ni cermet

	Titanium	**Carbon**	**Nickel**	**Molybdenum**
Composition [wt%]	62.2	12.8	16.7	8.3
Powder size [µm]	20.0	6.5	6.0	2.5
Purity [%]	99.7	99.8	99.8	99.8
Molar quantity [mol]	1.30	1.07	0.28	0.09

In order to estimate temperature ranges where phase changes and synthesis of carbides occur, thermogravimetric analysis (TGA) was conducted using SETARAM Setsys Evolution 1750 with THERMO Scientific Nicolet 380 FTIR emission gases analyser. X-ray diffraction (XRD) samples were sintered with high-temperature furnace R.D. Webb 107 and analysed using Bruker AXS D5005 with CuKa radiation. Microstructure images were made with scanning electron microscope ZEISS EVO MA-15.

2.3.1.2 Microstructure and phase formation of Ti(Mo)C-Ni cermets

Thermogravimetric analysis resembles a sintering furnace where a very small amount of material can be sintered to 1400 °C. This temperature range is sufficient in order to indicate all of the major phase changes occurring in the samples investigated. During the process, argon gas is used as a carrier gas for

gas emission analysis and sintering atmosphere. The first parameter monitored was the change in the sample's mass illustrated in Figure 2.7 including the first derivative of weight loss over time, i.e. speed of mass change.

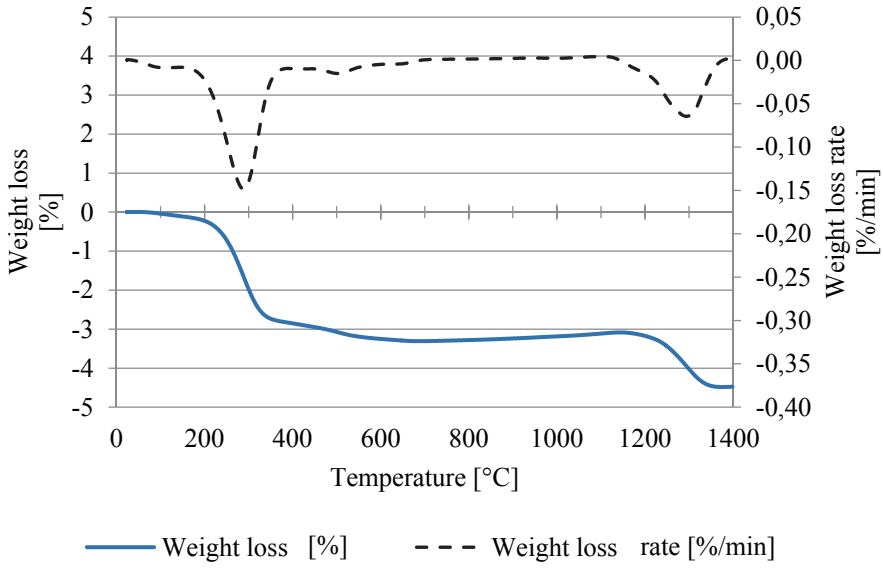

Figure 2.7. Weight loss of reactive sintered Ti(Mo)C-Ni cermet material during thermogravimetric analysis [68]

The analysis indicates two distinctive stages where a total of 4.5 % of sample's mass is removed. The initial mass loss of approximately 3 % occurs before 500 °C and is due to the evaporation of paraffin wax from the powder. The second step from 1200 °C to 1350 °C where 1.5 % of mass was reduced results from the reduction of metal oxide impurities. This is also indicated by a small amount of carbon oxide (CO) and carbon dioxide (CO_2) registered by the gas emission analyser. Some of the oxygen is already introduced into the cermet mixture from elemental powders but even with wet milling, using paraffin wax to prevent additional oxidation oxygen levels can increase since the milling and powder preparation is done under regular atmosphere.

The second parameter monitored during TGA analysis is the change in the heat flow within the sintering chamber. After removing the baseline of the sintering cycle, both exothermic (positive peak) and endothermic phase (negative peak) changes are registered and illustrated in Figure 2.8.

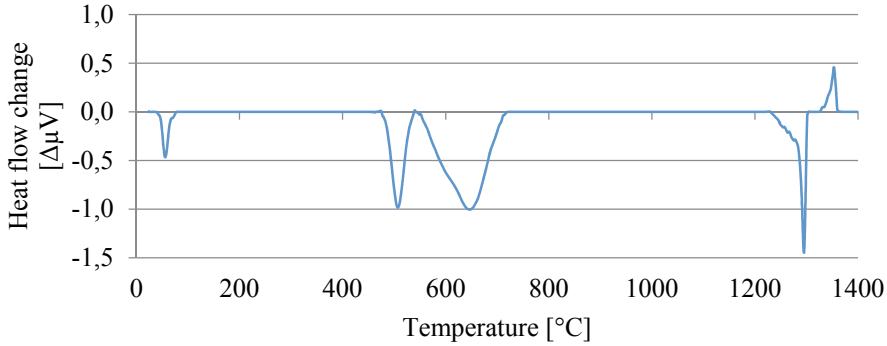

Figure 2.8. Thermal fluctuations during sintering of reactive sintered Ti(Mo)C-Ni cermet [68]

The initial endothermic peak at 56 °C is in the range of the melting point of paraffin wax, which is around 46–68 °C depending on the exact composition. Paraffin consists of hydrocarbons including molecules with twenty to forty carbon atoms and the chemical formula of C_xH_{2x+2}. Following peaks at 507 °C and 647 °C are no longer related to paraffin evaporation since the majority of the mass loss is finished before 400 °C, which corresponds to the boiling temperature of paraffin at 370 °C. Therefore, these temperature ranges are of interest for XRD analysis where reactions between cermet components are expected. Microstructure image of the sample heated to 720 °C (Figure 2.9b) indicates visually no changes that could be compared to the milled powder Figure 2.9a. In the final stages of the sintering cycle, additional two peaks are visible at 1295 °C and 1353 °C. The first of these peaks is an endothermic one and together with the XRD sample sintered at 1200 °C (Figure 2.9c) it is concluded that this peak indicates the melting of nickel metal in the Ti(Mo)C-Ni eutectic. TGA suggests that nickel starts to enter the liquid phase already at 1200 °C. Even after 30 minutes, in the relatively small sample, (10x10x3 mm) binder metal has not fully entered the liquid state. At 1270 °C, the binder metal is fully melted and the sample's microstructure is indicating a two-phase structure of carbide grains and binder matrix (Figure 2.9d). Nickel is still unevenly distributed, as areas between carbide grain agglomerates are not fully infiltrated. The final peak in the thermogravimetric analysis is located at 1353 °C, which was previously attributed to the reduction of metal oxide impurities. As an exothermic reaction, this seems most plausible since no further phase changes seem to be occurring in the samples. The changes in the microstructure are due to carbide grain growth and homogenising (Figure 2.9e, Figure 2.9f).

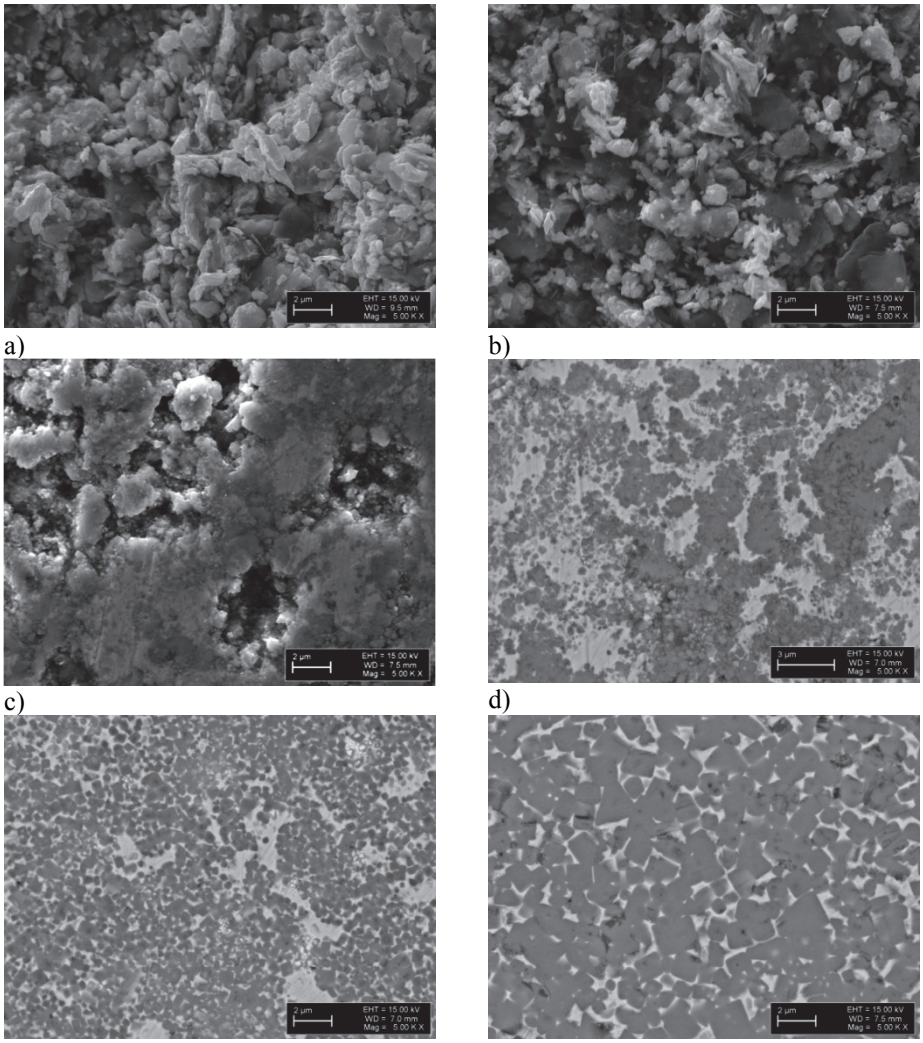

Figure 2.9. Microstructure images of reactive sintered Ti(Mo)C-Ni cermet powder samples sintered at different temperatures for 30 minutes: a) as milled powder; b) 720 ˚C; c) 1200 ˚C; d) 1270 ˚C; e) 1330 ˚C; f) 1500 ˚C [68]

An additional parameter that can be observed from the XRD samples is the dimensional change due to compaction during heating and the resulting phase changes. This compaction, i.e. shrinkage, was measured for samples at different stages of the heating cycle and is illustrated in Figure 2.10.

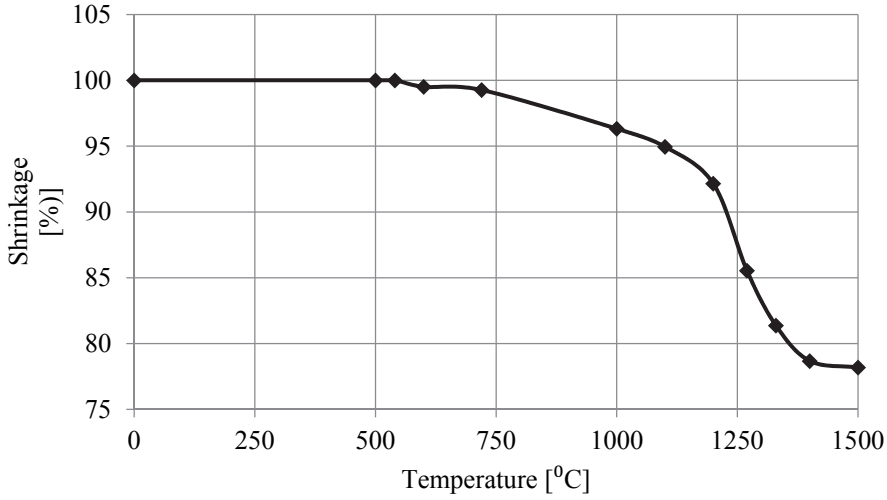

Figure 2.10. Shrinkage of reactive sintered Ti(Mo)C-Ni samples during heating [68]

From the results, it can be seen that no compaction occurs during the melting and evaporation of paraffin wax. In turn, this suggests that no reaction between the elements is present before 500 °C. The total amount of shrinkage is 22 % and most of it (about 15 %) starts intensely at 1200 °C, which corresponds with the thermogravimetric analysis and microstructure images since at that period, nickel starts to melt. With liquid phase sintering, the majority of densification occurs when the binder metal is liquid and the carbide grains are able to orientate and fuse together to form the final microstructure of the cermet. Even in the final structure, 100 °C densification occurs after 1400 °C at much slower rates. It is common knowledge that faster densification occurs at elevated temperatures since the viscosity of the binder metal is lower, helping ceramic compounds relocate quicker. The graph suggests that full density can already be achieved at lower temperatures, e.g. at 1400 °C, but will require longer dwell duration. The initial compaction of 7 % in the temperature range 500 °C to 1200 °C together with the microstructure images suggests that significant phase changes are present in this temperature range. From Figure 2.9c and Figure 2.9d, it was concluded that carbide formation has already occurred, indicating that the synthesis of carbides begins earlier.

A clearer overview of the phase changes and reactions occurring during the sintering cycle is given by the XRD analysis of various samples heated to different temperatures (Figure 2.11). A baseline analysis was conducted in order to establish the locations of the starting powder peaks (Table 2.3, Figure 2.11).

Table 2.3. XRD peak locations of elemental powders before milling in 2θ scale between 25°–65° using CuKa radiation

	Titanium	Carbon	Nickel	Molybdenum
Phase identification angle (°)	35.1 38.4 40.2	26.5	44.7 51.9	40.8 59.0

As the peaks of elemental particles are clearly distinguishable before milling, after high-energy attritor milling, all of the peaks are distorted and wider. This is to be expected as the milling process refines the powders but also creates amorphisation and accumulation of strain energy. The dislocations in the crystal structures, in turn, create disturbances in the reflection of X-ray's angles, resulting in a less intense peaks, widening them. Additionally, as discussed earlier, the synthesis of carbides already occurs during milling, which also explains the shifts in the peak angles at roughly 36° and 42°. Two additional small peaks were introduced after milling that correspond with tungsten carbide reflection angles at 32° and 43°. These peaks are also expected to appear due to contamination and wear of milling balls and an attritor made from WC-Co hardmetal.

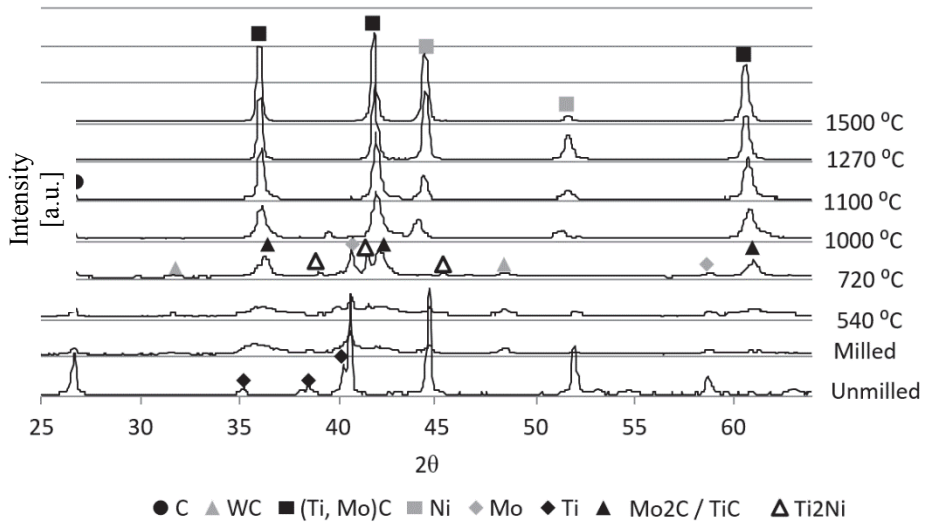

Figure 2.11. XRD patterns of Ti-Mo-C-Ni powder mixtures unmilled, milled and after sintering at different temperatures for 30 minutes [68]

Comparing the XRD peaks of milled powder with the sample heated to 540 °C, no clear phase changes were noticed, which means that the exact cause of the endothermic peak at 507 °C indicated by TGA analysis is still uncertain. On the other hand, the following TGA peak at 647 °C can be explained with the XRD results of the sample sintered at 720 °C. The endothermic peak is wide in the range of roughly 550–720 °C and as a result, several phases and peaks appeared.

First of all, the location of the carbide grains suggests that molybdenum has formed MoC but still molybdenum and carbon peaks are present separately. Titanium on the other hand, has completely disappeared and has formed two phases – titanium carbide and an intermetallic compound with nickel – Ti_2Ni. Pure nickel peaks at 44.7° and 51.9° have disappeared, indicating that all of the nickel metal is in the form of intermetallic Ti_2Ni.

Considering the composition of the starting powders, the theoretical chemical reactions that occurred before 720 °C can be mathematically estimated by Eq. (2.3):

$$1.30Ti + 1.07C + 0.28Ni + 0.09Mo \rightarrow \quad (2.3)$$

$$\rightarrow 0.28Ti_2Ni + 0.09MoC + 0.74TiC + 0.24C$$

As nickel has bonded with titanium atoms, the mixture, in turn, has excess free carbon left in the system. In addition, it must be considered that the samples are still porous with only roughly 75 % density and not all the atoms in the system are able to move freely in the material, which means that ideal reactions are unable to occur using all of the potentially available atoms. With increasing temperature, the intermetallic Ti_2Ni peaks disappeared at 1000 °C. This can be explained considering Ti and Ni phase diagram where at 984 °C the intermetallic compound decomposes [62].

As a result, titanium is able to continue to synthesise carbides with increased TiC peak intensities and also nickel peaks reappeared at 45° and 52°. The carbide peaks are also in the process of shifting and the analysis suggests that from this point onward, the two carbide phases of TiC and MoC are fusing into Ti(Mo)C dual-carbide. There is still some excess carbon in the system even at 1100 °C, most likely due to the absence of the liquid phase, which has finally vanished once the liquid phase of Ni was introduced. At 1270 °C, only two phases remained, as shown on the microstructure images (Figure 2.9 d, e). Assumed synthesis of carbides was following the chemical reactions ideally and not considering any solubility and precipitation, the formula of the dual-carbide would be $(Ti_{0.94}Mo_{0.06})C_{0.77}$. This means that 6 % of the metal atoms in the carbide grains are molybdenum and there is a 23 % carbon deficiency. The ideal hardness of TiC with 6% molybdenum is unknown but it could be estimated from Table 2.1 that the hardness of this dual-carbide with 23% carbon deficiency would be close to HV10 2300. From the project's perspective, this hardness is sufficient against hardmetal projectiles. The macrohardness of the resulting cermet is understandably lower with the inclusion of softer binder phase, as nickel has a hardness of HV10 80, but also defects in the microstructure such as the lower hardness o the composite material and interface strength on grain boundaries.

.

2.3.2 Influence of sintering parameters on Ti(Mo)C-Ni cermet

Sintering regime has an important role in ensuring that the cermet composition reaches its maximum mechanical properties. Sintering parameters that influence the final microstructure and can be fine-tuned are numerous. The parameters under investigation for reactive sintered cermets are the sintering temperatures (T), dwell durations (t) and pressure (p). Based on the microstructure images in Figure 2.9 and the formation of carbides, it was found reasonable to add an additional dwell step for the purposes of investigation. This step would have to ensure that the synthesis of carbides is finished. The carbide synthesis temperature is referred to as T_1 with a dwell duration of t_1 and the final sintering temperature as T_2 with a dwell duration of t_2 (Figure 2.12).

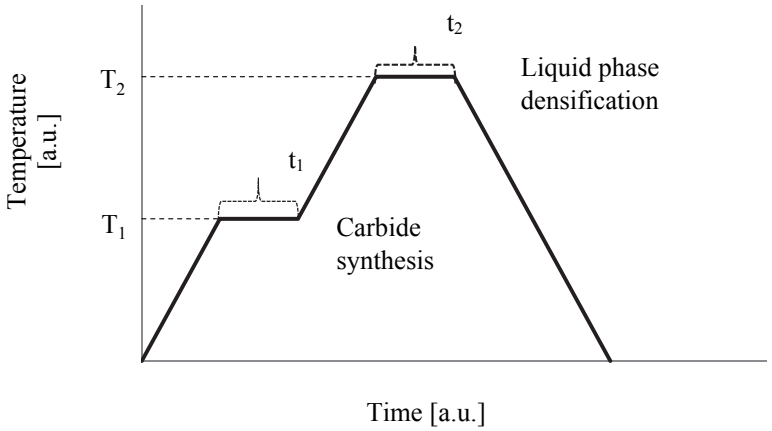

Figure 2.12. Temperature-time graph of reactive sintered cermet

Samples were evaluated by two characteristics. Initial assessment was done by microstructure images using SEM equipment, followed by testing of mechanical properties. Properties considered were hardness (HV10), transverse rupture strength (TRS), fracture toughness (K_{Ic}), and density (ρ).

2.3.2.1 Experimental methods of sintering parameters

Sintering parameters were investigated using the same cermet mixture as described previously in the microstructure formation. Green bodies were also prepared in the same fashion, using uniaxial pressing to achieve 55–60% density. Sintered samples were grinded using a 40 µm grinding wheel for a three-point bending test according to standard EVS-EN ISO 3327:2009. Sample dimensions for three point TRS testing were 5x5x20 mm. Bending tests were conducted using Instron 8516. Samples for microstructure imaging and hardness indentation measurements were polished with 3 µm polishing media. Vicker's hardness

(HV10) was measured using Identec 5030SKV. Fracture toughness indentation marks were using the same Vicker's hardness machine but with 294 N load (HV30) and resulting cracks measured using optical microstructure and software. Fracture toughness was calculated using the median crack system formula Eq. (2.4) [69]:

$$K_{Ic} = 0.0726 \frac{F}{c^{3/2}}, \tag{2.4}$$

where F is the indentation loading force N and c is the average crack length m. Density was measured with the Archimedes method using Mettler-Toledo ME204.

2.3.2.2 Results and analysis of sintering parameters

Dwell duration

The first series of experiments had fixed temperatures of T_1 and T_2 at 1270 °C and 1500 °C, respectively. Dwell durations for the carbide synthesis (t_1) were 0, 10 and 30 minutes while the dwell durations at the liquid phase sintering temperatures (t_2) were 10, 30 and 60 minutes. The resulting hardness and strength values are presented in Figure 2.13 and Figure 2.14.

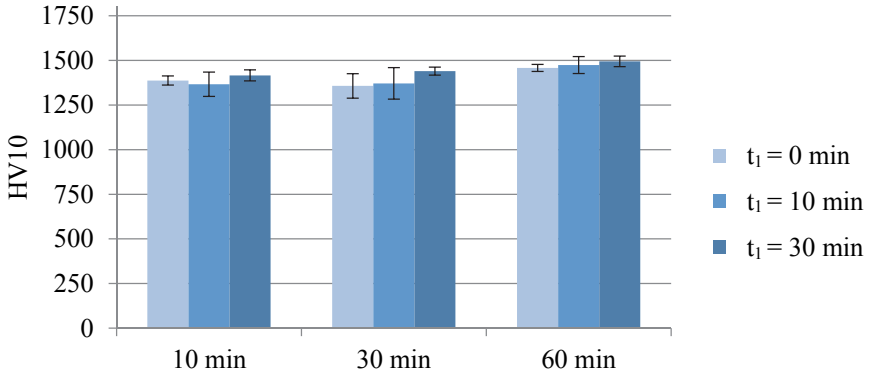

Figure 2.13. Hardness influenced by dwell durations sintered at T_1=1270 °C and T_2=1500 °C [68]

Considering the hardness values and error margins, an increased dwell duration at T_1 temperature shows insignificant difference. Longer dwell duration at the final sintering temperature at 1500 °C seems to increase the hardness values slightly, decreasing the error margins. A final hardness of HV10 1500 was achieved. One of the reasons that may explain the small overall values of hardness results is likely to be the measuring method. As the operator is able to manipulate the exact location of the indentation, it is possible to ignore visual defects on the surface of the sample. In the case of bending tests, the whole sample is under

pressure and the cracks initiating failure can be aided by defects near the area with the highest load.

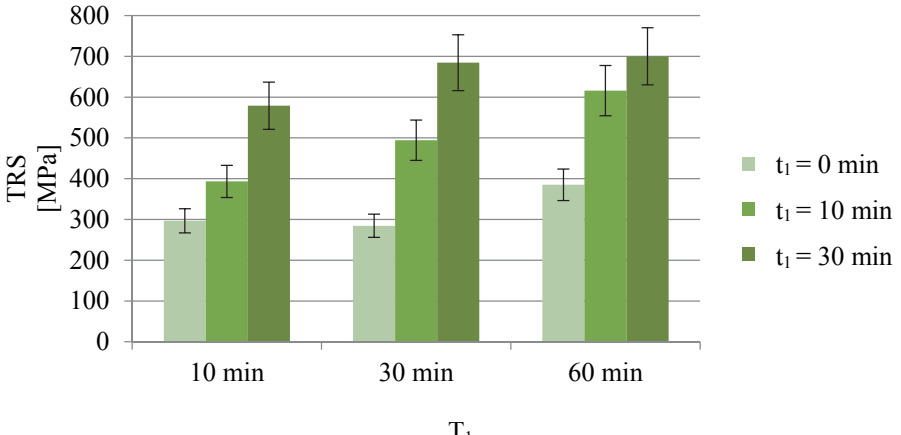

Figure 2.14. Tensile rupture strength influenced by dwell durations sintered at T_1=1270 °C and T_2=1500 °C [68]

Similar to the hardness results in the case of TRS, an increase in strength values was observed with elongated liquid state dwell duration, the highest being after 60 minutes. Additionally, a significant increase is due to longer dwell durations at 1270 °C.

With increased dwell duration at 1270 °C, the mechanical properties improved and an additional sintering cycle was done with both dwell durations (t_1 and t_2) for 60 minutes. Microstructures of both sintering regime samples are illustrated in Figure 2.15.

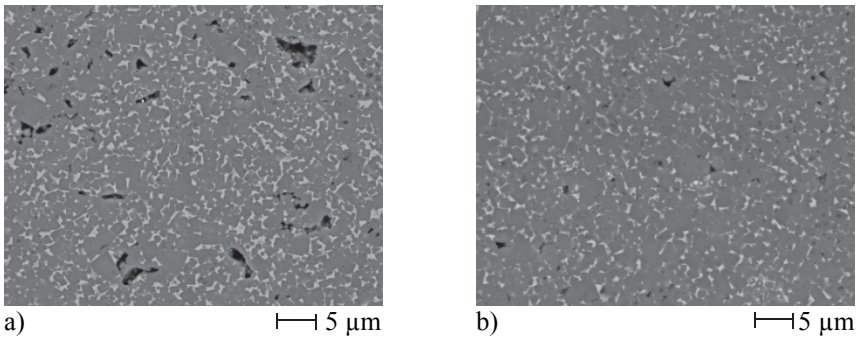

Figure 2.15. Microstructure images of reactive sintered Ti(Mo)C-Ni cermet at 1500 °C for 60 minutes: a) no dwell at 1270 °C; b) 60 min dwell at 1270 °C [68]

The difference in porosity is clear with additional dwell at 1270 °C for 60 minutes, which has substantially aided to densify the material. Similar indication can be observed from the mechanical properties, as the density has increased (Table 2.4).

Table 2.4. Mechanical properties of reactive sintered Ti(Mo)C-Ni cermet at 1500 °C for 60 minutes [68]

Sample	Sintering	Grain size [µm]	Density [g/cm^3]	HV10	TRS [MPa]
1	1500 °C for 60 min	0.98±0.43	5.17	1458	385
2	1500 °C for 60 min (1270 °C for 60 min)	1.10±0.49	5.35	1712	792

This change in porosity has a significant impact on the strength of the material since defects act as stress concentrators and inhibit both crack formation and propagation. An interesting observation was also made about grain size. With increased sintering duration, grain growth expected would be noticeable due to Ostwald ripening [49] but the change in average grain size is trivial considering the error margins. This, in turn, suggests that lower temperature dwell for carbide synthesis causes no aggressive grain growth.

Dwell temperature

The final temperature of 1500 °C for liquid phase sintering was chosen based on the sintering regime of a commercial TiC-NiMo cermet equivalent. The carbide synthesis temperature of 1270 °C was based on thermogravimetric analysis but as the endothermic peak has a range from 1200–1300 °C and microstructures of the XRD samples in this range differ significantly. Different temperatures were therefore tested in order to determine the optimal one. Temperatures of 1200 °C, 1270 °C and 1340 °C were investigated for carbide synthesis and 1470 °C, 1500 °C and 1530 °C for the liquid phase sintering. Hardness and strength values of samples with different carbide synthesis temperatures are illustrated in Figure 2.16.

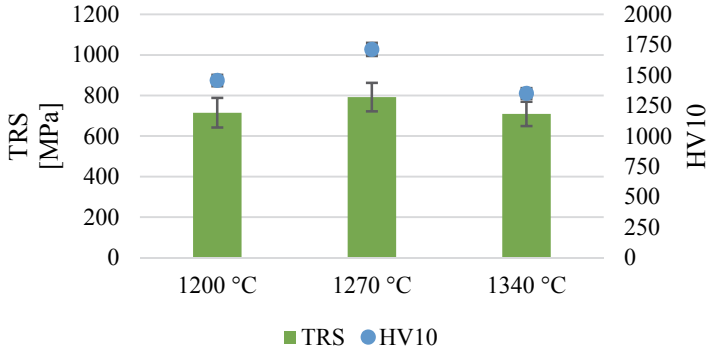

Figure 2.16. Mechanical properties of reactive sintered Ti(Mo)C-Ni cermets at different dwell temperatures (T_1) sintered to 1500 °C [68]

In both cases, the optimum temperature for carbide synthesis is at 1270 °C. The reason for inferior mechanical properties at lower temperatures may be related to the high viscosity of the liquid binder and still uneven melting, as illustrated previously in Figure 2.9c. As for dwell at 1340 °C, the reason for decreased values is unclear. Considering the TGA analysis at this temperature, the final exothermic peak appeared, which was believed to be due to metal oxide reduction. Furthermore, the difference in TGA analysis and sintered samples is the heating speed. During TGA, slower heating speed of 4 °/min throughout the cycle is used in order to detect the beginning of a thermal heat flow change more accurately. In this case, the heating rate was set to 10 °/C and also the volume of the samples was much larger compared to TGA samples. Considering those two factors of heating speed and sample volume, it is suggested that previous phase changes may be interfering with the metal oxide reduction.

Additional temperature influence on the properties of reactive sintered Ti(Mo)C-Ni cermets was conducted at the liquid phase temperature. At this point, the temperature was changed and a high-temperature AIP6-30H furnace mostly designed for high-pressure sintering regimes was used. Also, slower heating rates of 5 °/C are used during liquid phase. The sintering regimes used are illustrated in Figure 2.17.

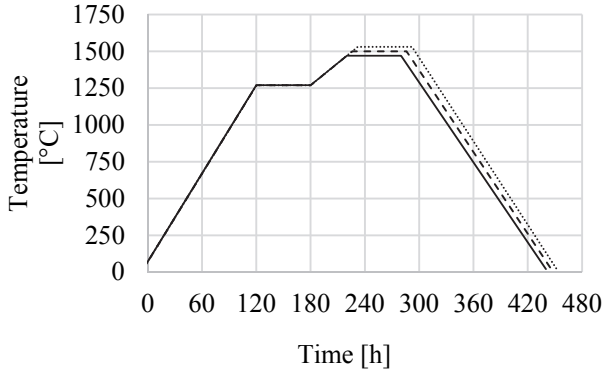

Figure 2.17. Sintering regimes with the final sintering temperature (T2) at 1470 °C, 1500 °C and 1530 °C [69]

Samples from all temperature ranges are illustrated in Figure 2.18. As the final temperature was under investigation, average grain size and grain size distributions were also measured.

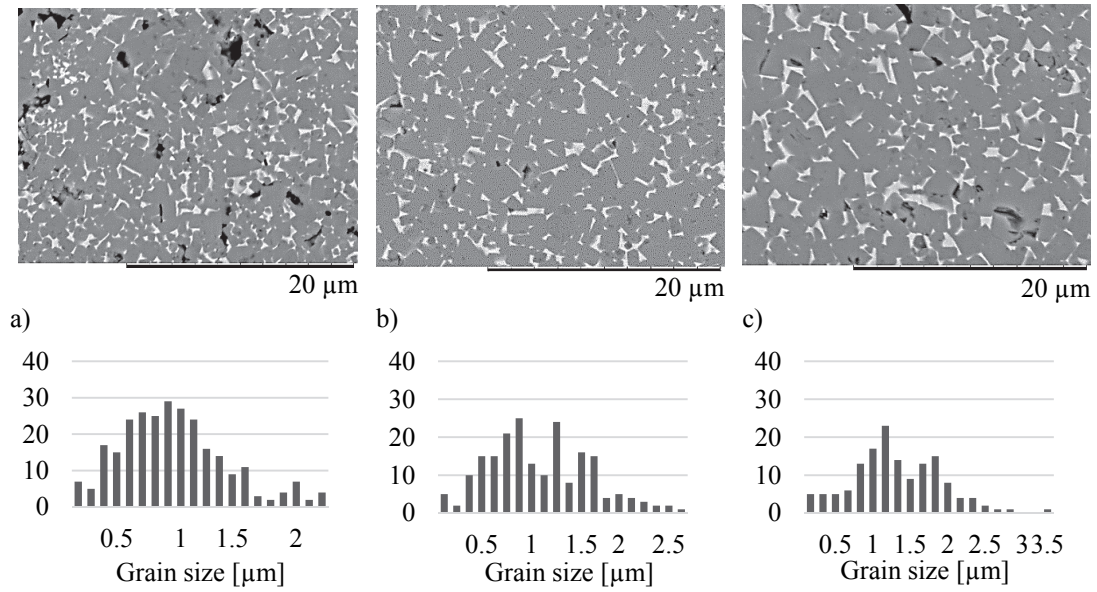

Figure 2.18. Microstructure images and corresponding grain size distribution of reactive sintered Ti(Mo)C-Ni cermets: a) at 1470 °C; b) at 1500 °C and c) at 1530 °C [70]

Microstructure images indicate that at 1470 °C a high amount of porosity is still present in the material. The optimum liquid state sintering temperature stays at 1500 °C with the least amount of porosity. Grain growth was also observed in the microstructure with increasing temperature as the number of larger grains increases and the grain size distribution graphs shift to the right. In all cases, the range of grain size was in between 0.5–3.5 µm. This is a relatively stable range of grain sizes considering the temperatures used and long dwell durations. However, this would not be the case for other cermet materials that would use, for example, tungsten or chromium carbides as their main hard phase [63]. The mechanical properties in Table 2.5 also suggest that the optimum liquid state sintering temperature is kept at 1500 °C.

Table 2.5. Mechanical properties of reactive sintered Ti(Mo)C-Ni cermets at different liquid phase sintering temperatures [70]

Temperature [°C]	**Grain size [µm]**	**HV10**	**TRS [MPa]**	**Toughness [MPa·m$^{1/2}$]**	**Density [g/cm^3]**
1470	1.04	1272 ±44	753 ±69	8.70 ±0.23	5.26 ±0.06
1500	1.25	1451 ±22	956 ±64	10.59 ±0.30	5.42 ±0.06
1530	1.43	1360 ±59	857 ±28	12.11 ±0.27	5.40 ±0.06

The calculated theoretical density of the cermet with $Ti_{0.94}Mo_{0.06}C_{0.77}$-0.167Ni is 5.42 g/cm^3. Comparing the density values obtained, the sample with 1500 °C

has the same density but this includes contamination from milling, which adds heavy WC (ρ = 15.63 g/cm^3) particles. According to Figure 2.19, contamination from WC of even 1 wt% increases the density of the final material over 5.50 g/cm^3.

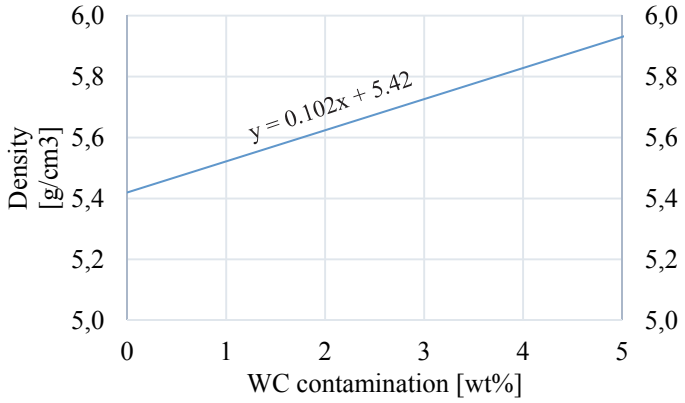

Figure 2.19. Density of Ti0.94Mo0.06C0.77-0.167Ni depending on WC contamination

Theoretical material density in g/cm^3 can be calculated using a linear function Eq. (2.5):

$$y(x) = 0.102x + 5.42\ , \tag{2.5}$$

where x is the amount of WC contamination in wt%.

Another observation can be made to compare the properties of samples sintered using the same sintering regimes but in different furnaces (Table 2.6). The sintering regimes were identical apart from the heating rate from 1270–1500 °C that was set at 10 °/min for the test series investigating dwell durations and temperatures and now set to 5 °/min in the temperature investigation test series. The second difference in the sintering of those test series is the pressure of the sintering chamber. The initial tests were conducted using a furnace built for high vacuum as the latter was designed for high pressures. The vacuum in R.D. Webb 107 furnace reaches 4 Pa during the dwell at the liquid phase sintering, which is considered high vacuum. The AIP6-30H hot isostatic pressing furnace uses vacuuming to remove atmosphere from the sintering chamber but purging with inert gas is recommended for removing residual oxygen and moisture from the system. The vacuum that can be reached with the AIP6-30H is about 10 times lower, at around 30 Pa. Pressure in the sintering environment can explain the possible difference in the mechanical properties of the samples.

Table 2.6. Comparison of reactive sintered Ti(Mo)C-Ni cermets in different furnaces

Furnace	Pressure [Pa]	Density [g/cm^3]	HV10	TRS [MPa]	Grain size [µm]
R.D. Webb 107	3–5	5.35	1712	792	1.10
AIP6-30H	30	5.42	1451	956	1.25

In terms of lower density and strength values together with higher hardness, it is similar to the decreased binder content of commercial cermets. In addition, taking into account the high vacuum in the R.D. Webb 107 it is plausible that some of the nickel evaporated during the 60-minute liquid phase sintering at 1500 °C. Binder evaporation is a known phenomenon and needs further investigation to be confirmed in this case.

Sintering pressure

Sintering under isostatic pressure using inert gases is an effective route for reducing residual porosity from the material. This method is referred to in the industry as hipping (hot isostatic pressure) or sinter-hipping [71]. It can be done during the same sintering cycle when the green bodies are sintered or as a separate cycle depending on the capabilities of available furnaces. Pressure is introduced during the main liquid state sintering cycle when inert gas is inserted into the furnace. Depending on the material being consolidated, it can be argon, nitrogen or some other gas. No possibility of undesired reaction between the gas and the sample material is allowed. In the case of TiC based cermets, argon gas is used since nitrogen can form nitrides. Gas is usually inserted into the sintering chamber after most of the microstructure formations have already occurred at liquid phase temperatures. If the gas is introduced before open porosity is closed, the gas fills the open pores in the material and no further consolidation is possible. Alternatively, post-hipping can be done after the liquid phase sintering is finished and in [72, 73] post-hipping of WC-Co samples was implemented at lower temperatures. The amount of pressure depends how prone the material is to pores and the viscosity of the binder. In [74, 75] the influence of hipping has been shown to improve the mechanical and tribological properties of TiC based cermets.

In the following experimental series, the same powder mixture was used in sintering regimes with carbide synthesis at 1270 °C for 60 minutes and liquid phase sintering at 1500 °C for 60 minutes. Argon gas pressure of 15 MPa was introduced at 30 minutes at 1500 °C and was kept for the remaining 30 minutes. The resulting microstructure of samples is shown in Figure 2.20 and mechanical properties in Table 2.7.

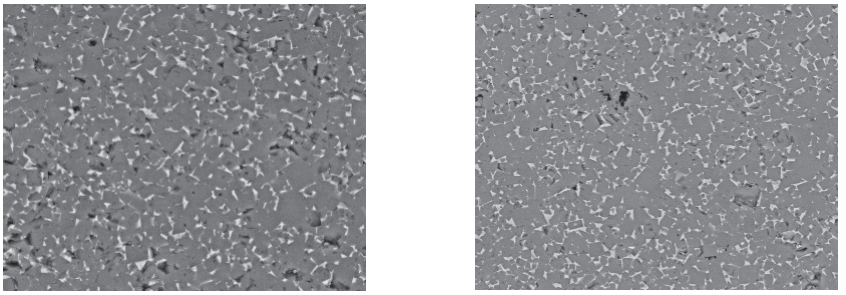

Figure 2.20. Microstructure images of reactive sintered Ti(Mo)C-Ni cermets: a) vacuum sintered; b) hip sintered with 15 MPa argon gas pressure [76]

A difference in visual porosity is clear from the microstructure and from the density values. A density value of 5.68 g/cm^3 of the hipped sample also suggests that a WC contamination could be just below 3 wt% (Figure 2.19), neglecting any remaining porosity, oxygen contamination and possible binder loss due to evaporation.

Table 2.7. Comparison of mechanical properties of vacuum and hip sintered Ti(Mo)C-Ni cermets [72]

Atmosphere	Pressure [MPa]	Density [g/cm^3]	HV10	TRS [MPa]
Vacuum	-	5.41	1547	632
Argon	15	5.68	1510	956

Otherwise, the hardness values of the samples remained on a similar level but a decrease in strength was observed in the samples sintered under vacuum. A drop of nearly 34 % in the strength values was present while the sintering regime and furnace stayed the same. On a closer investigation of the microstructures in Figure 2.18b and Figure 2.20a, an increase of defects is noticeable. Such defects are believed to be caused by the oxidation of the milled powder over a long period of time. The same patch of milled powder mixture was used for both experimental series but at different time periods. It is therefore possible that oxidation occurred even with the paraffin wax covering the powder. In essence, oxides are also ceramic compounds but in the case of titanium ceramics, oxides have poor mechanical properties (Table 2.3). The main issue with oxides and even oxy-carbides such as TiO_xC_y is the wetting angle. Wetting of possible oxide compounds is considerably worse than that of carbides, which would explain the increased porosity in the final material. Hipping in this case helped to reduce the amount of porosity, as suggested by microstructure images and density values but still some pores are visible in Figure 2.20b. In conclusion, sintering regime, including hipping, improved densification of samples made from the same

powder by 5 %. Additionally, it is required to consider oxidation of the powder over time when manufacturing reactive sintered titanium carbide based cermets.

2.3.3 Influence of milling duration on Ti(Mo)C-Ni cermet

Milling the powders serves multiple purposes. In general, the main goal of milling is to obtain a homogeneous mixture to prevent material with uneven microstructure such as binder “lakes” and grain agglomerates without any binder matrix. In addition, with reactive sintering, milling inputs energy into carbide forming elements by mechanically activating them, aiding with carbide synthesis both during milling and reactive sintering. Finally, milling grinds powder particles into smaller and finer powder even reaching nanoscale.

There are several methods for milling equipment and on an industrial scale, the most common ones are horizontal ball mills and high-energy attritor mills. Other types are vibration ball mills and planetary ball mills, the latter mostly used for very small volumes. In this research, an attritor mill was used to prepare powder mixtures because of the shorter milling durations. Conventionally, cermet powders and the reference material used in the project are milled for 72 hours in a horizontal ball mill with an inner diameter of Ø180 mm. The attritor mill used has a rotation speed of the rotor shaft fixed at 540 RPM. The inner diameter of the attritor is Ø140 mm. Maximum kinetic energy of the milling balls depends on the mass of the ball and the maximum speed that can be achieved in the mill. In both mills, the same hardmetal milling balls are used with an average mass of 14 g.

Many milling parameters, such as duration, size of the milling balls, ball to powder ratio, milling media, are alterable. Even atmosphere and temperature can be altered with specialised equipment. Both vacuum and gas can be used and attritor mills with liquid nitrogen cooling are used in some cases. In the current research, only milling duration was investigated. Ball to powder ratio in the attritor mill is kept at 10:1, respectively. Active water-cooling is necessary since considerable heat is produced during rotor blade impact with the milling balls and heptane as the wet milling agent can easily evaporate even at room temperature. As the previous powder mixture was milled for 10 hours and WC contamination was indicated by XRD results and confirmed by density measurements, shorter milling times were investigated. Milling durations used were 4, 6, 8 and 10 h. Scanning electron microscope images of milled powders are shown in Figure 2.21.

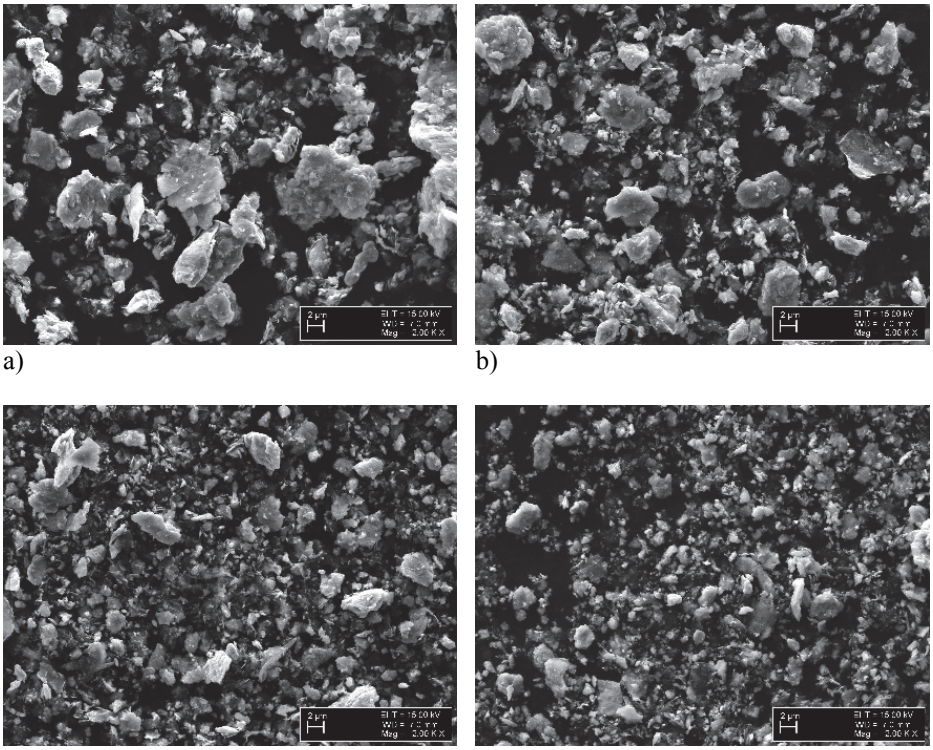

Figure 2.21. Microstructure images of powder mixtures after different milling durations: a) 4 h; b) 6 h; c) 8 h; d) 10 h [72]

Images indicate clearly that additional milling refines the powders in the mixture significantly. The largest particles in the mixture are titanium particles as the titanium starting powder has the largest particle size (Figure 2.22).

Drawbacks of longer milling durations include contamination and slower production output. Contamination includes two sources, as concluded from previous discussions. First contamination source is the wear of milling equipment and balls. Both are manufactured using WC-Co hardmetal, which is shown in the XRD analysis of powder mixtures (Figure 2.23).

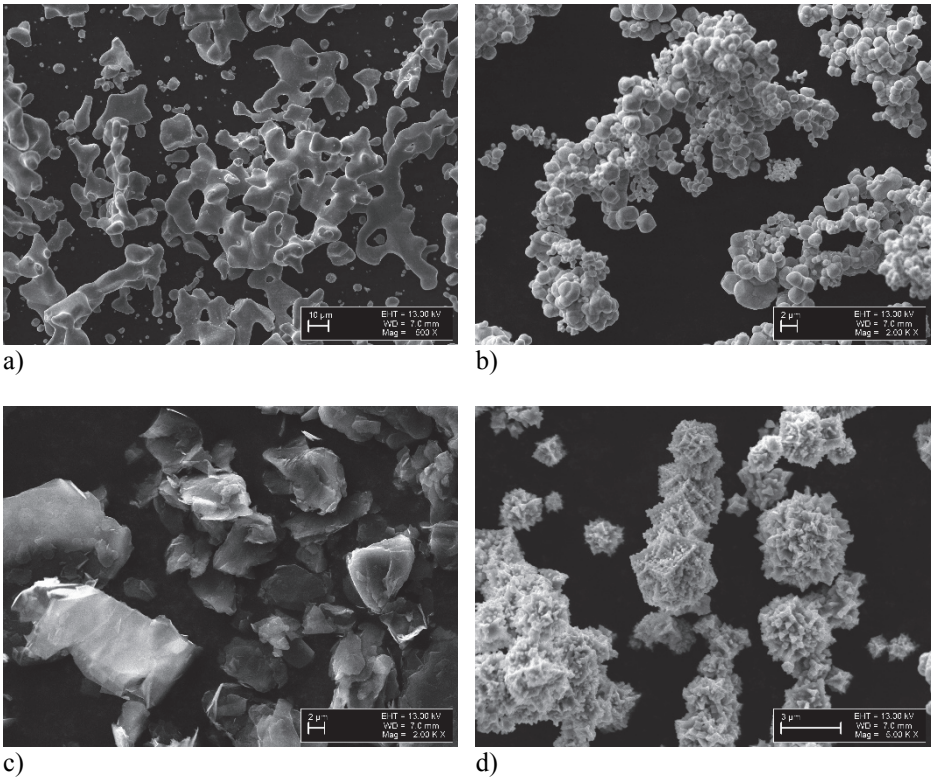

Figure 2.22. Microstructure images of starting powders with different magnifications and average particle sizes: a) titanium at 500x; b) molybdenum at 2000x; c) carbon at 2000x, nickel at 5000x

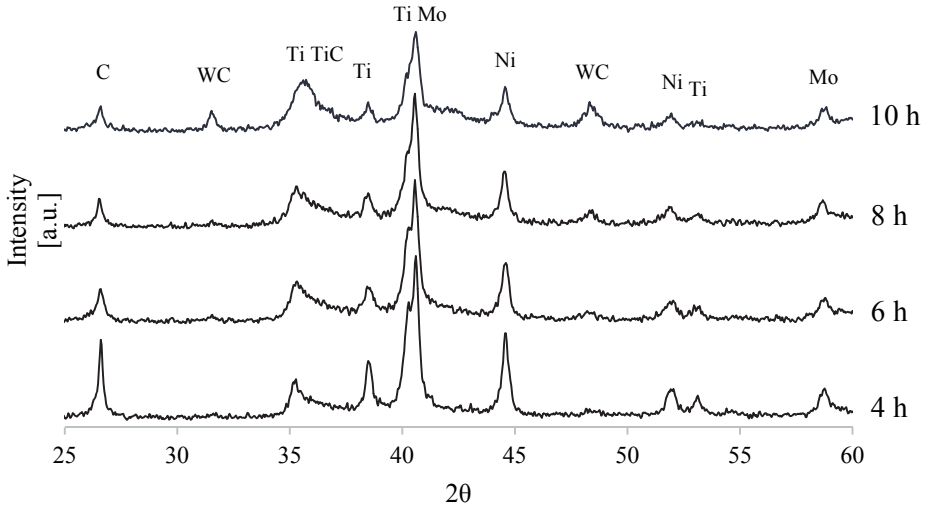

Figure 2.23. XRD patterns of powder mixtures with different milling durations [72]

The WC peaks are almost non-existent after 4 hours of milling but further milling indicates increasing peak intensities at 31.7° and 48.2° that are representing tungsten carbide. The exact amount of WC contamination is difficult to assess with the available equipment but was previously estimated around 2.7 wt% by density values for the powder mixture with 10 hours of milling. WC contamination is a result of mechanical wear and can therefore be estimated to have a liner correlation in time. Therefore, an amount of 0.27 wt% per hour of WC contamination can be expected from high energy attritor milling. This relation of WC contamination in wt% can be represented as a simple linear function over time as Eq. (2.6):

$$y(t) = 0.27t\ , \tag{2.6}$$

where t is the milling duration in the attritor mill in h.

At some point with prolonged milling durations, WC contamination speed would increase because of the increased amount of TiC synthesised during the milling process. With high hardness, TiC will act as an abrasive particle eroding the milling equipment and balls. One benefit of reactive sintering compared to conventional cermet production is the wear on the milling equipment. The materials milled have low hardness values since pure metals and carbon are soft compared to the WC-Co hardmetal.

The second contamination during milling is oxidation. All of the starting powders had an average of 0.2 wt% initial contamination and most of it due to oxygen. The level of oxygen was determined for the milled powders using Eltra ONH 2000. As the equipment allows both oxygen and nitrogen to be measured simultaneously, values for both elements are presented in Figure 2.24.

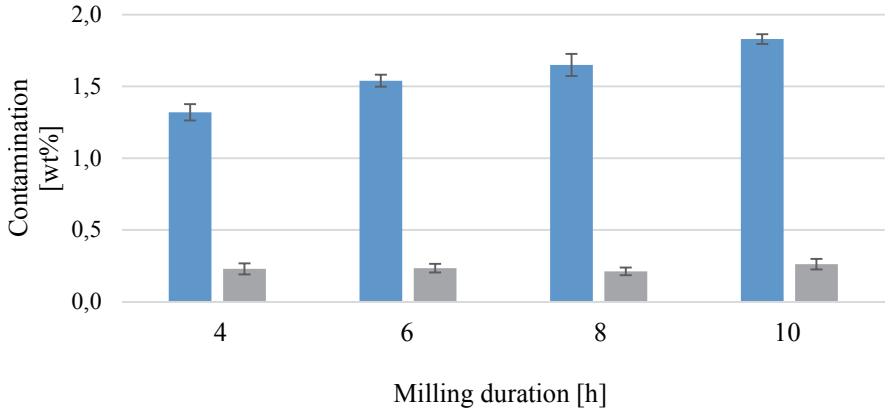

Figure 2.24. Oxygen and nitrogen contamination after different milling durations [72]

Nitrogen seems to be unaffected by milling duration and if it is used in the system to form carbonitride, it would not be considered as a contaminant. TiCN ceramic has high mechanical properties similar to TiC and TiCN cermets have good mechanical properties [3, 28]. Still, the amount of nitrogen in the system is minimal and the possible increase in the overall cermet properties negligible. On the other hand, oxygen contamination is unexpectedly large, linearly increasing with milling duration. As concluded in section 2.3.1, during the sintering cycle, an exothermic peak at 1353 °C was accounted for oxide reduction. With 1.83 wt% of oxygen in the powder mixture, a similar amount of carbon would be needed to fully remove all of the oxygen in the material. The exact amount of required carbon would be difficult to calculate since gas emission analyser detected both CO and CO_2 gases. Samples are sintered in a graphite container and heating elements are made from carbon, which means that additional carbon can be absorbed on the surface for both carbide synthesis and oxygen reduction but the inside of the material is most likely unaffected. Adding additional carbon to the powder mixture could be an option but would require very fine tuning since it would also increase chances of porosity due to free carbon clusters that have not reacted in carbide synthesis or oxide reduction.

The milled powder mixtures were sintered using both vacuum and hip sintering regimes described in section 2.3.2. In Figure 2.25, microstructure images of samples sintered in vacuum are compared with respective samples sintered using hip sintering cycles.

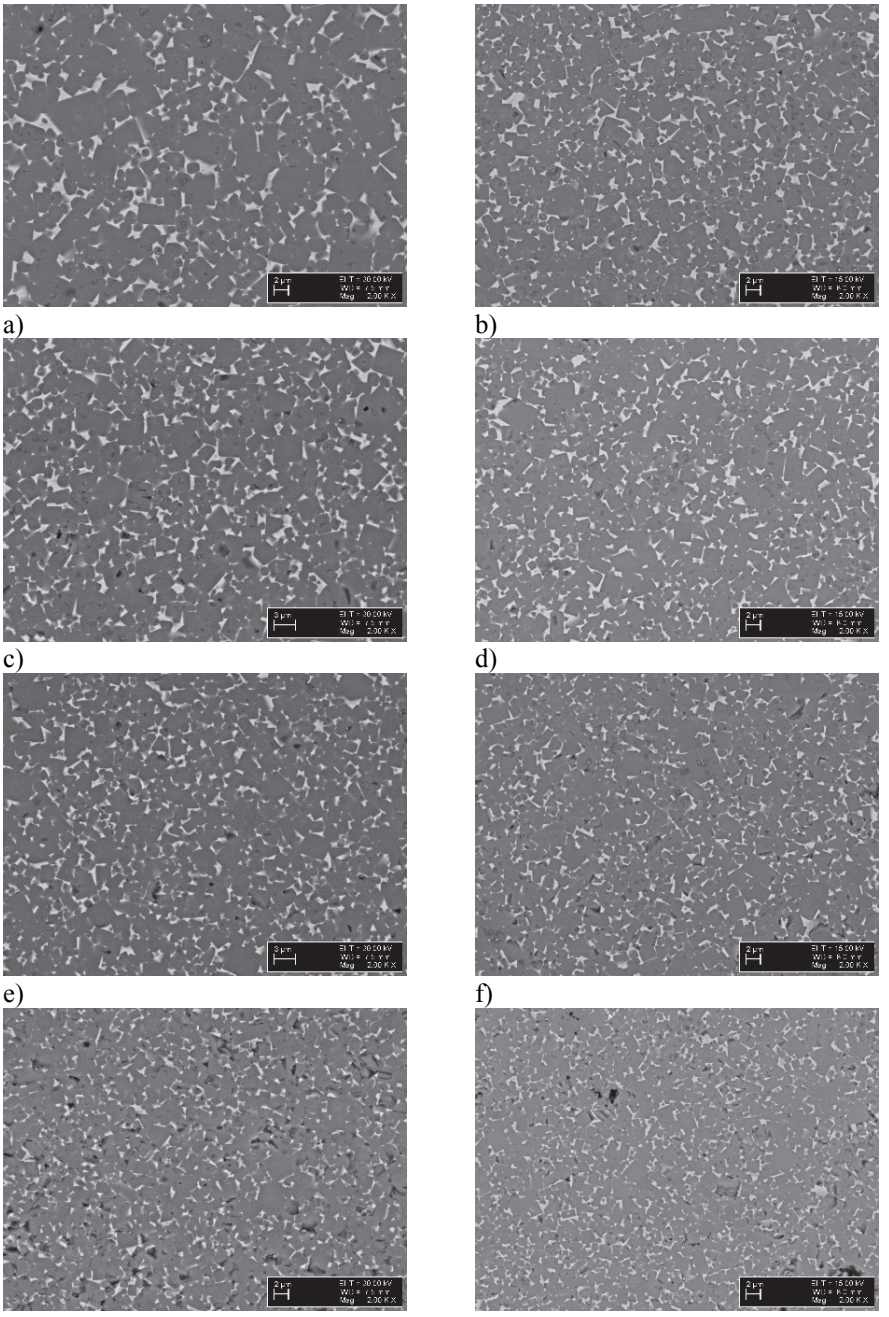

Figure 2.25. Microstructure images of samples with different milling durations sintered at 1500 °C under vacuum and hip conditions: a) 4 h vacuum; b) 4 h HIP; c) 6 h vacuum; d) 6 h HIP; e) 8 h vacuum; f) 8 h HIP; g) 10 h vacuum; h) 10 h HIP [76]

The microstructure images indicate that it is possible to lower milling durations to achieve homogeneous materials. Interestingly, with 4 hours of milling, the vacuum sintered sample (Figure 2.25a) exhibits larger grains. As compared to the milled powder (Figure 2.22a), similar large particles of titanium are present with particle sizes of ~10 µm. With the hipping cycle, these larger carbide grains are missing or at least reduced in number. Density of sintered samples is presented in Figure 2.26.

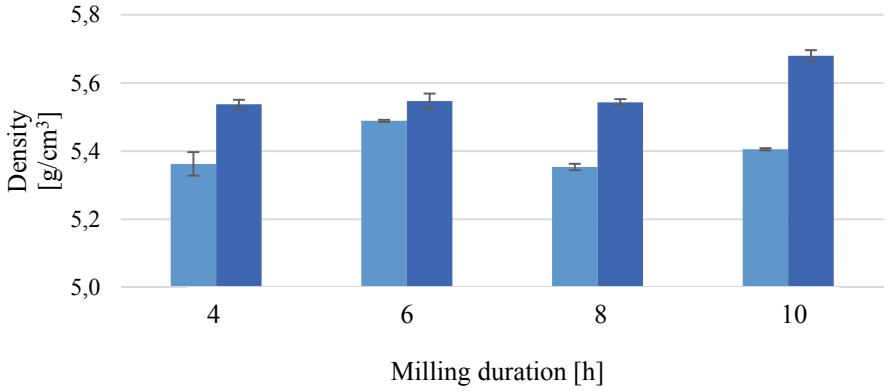

Figure 2.26. Density of samples with different milling durations sintered in vacuum and hipping regimes at 1500°C [76]

Density values indicate no strong correlation with the milling duration, suggesting that some other unaccounted factor has influenced the results. This influence can be material powder preparation related, sintering related or some other unknown cause. On the other hand, in all cases, an increase in density was observed when comparing vacuum sintering with hipping. In order to give further meaning to the density values, using Eqs. (2.6) and (2.7), corresponding theoretical densities were calculated for each milling duration considering WC contamination. The theoretical densities are presented in Table 2.8.

Table 2.8. Calculated densities of samples with different milling durations

Milling duration [h]	**4**	**6**	**8**	**10**
WC contamination [wt%]	1.08	1.62	2.16	2.70
Theoretical density [g/cm³]	5.53	5.59	5.64	5.70
RD vacuum sintered [%]	96.9	98.2	94.9	94.9
RD hip sintered [%]	100.1	99.3	98.2	99.6

Relative densities of hipped samples can be considered at acceptable levels apart from samples made from powder mixture with 8 hours of milling. The relative density value of over 100 % in the case of 4-hour milling means that at one point the sample is near full density but on the other hand, the suggested formulas are considered to be under ideal conditions and do not fully integrate all measured parameters and unaccounted ones.

The hardness and strength values of samples with different milling durations are presented in Figure 2.27 and Figure 2.28, respectively. There is a minor tendency of increased hardness with prolonged milling. As the composition of carbide synthesising materials should not change during milling, the most likely conclusion includes the WC "contamination". The term "contamination" is used since WC addition is not designed into material development. In reality, tungsten carbide cermets are widely used also with nickel binder and titanium carbide as hardening additive. This, in turn, means that in reactive sintered Ti(Mo)C-Ni cermet, WC also acts as a hardening additive while not disturbing microstructure formation. The main drawback of WC addition in this project is the added specific weight of WC, which increases the density of the potential armour tile material.

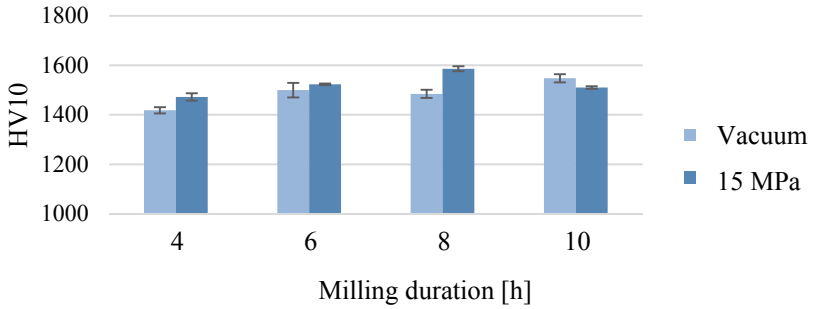

Figure 2.27. Hardness of samples with different milling durations sintered in vacuum and hipping regimes at 1500 °C [76]

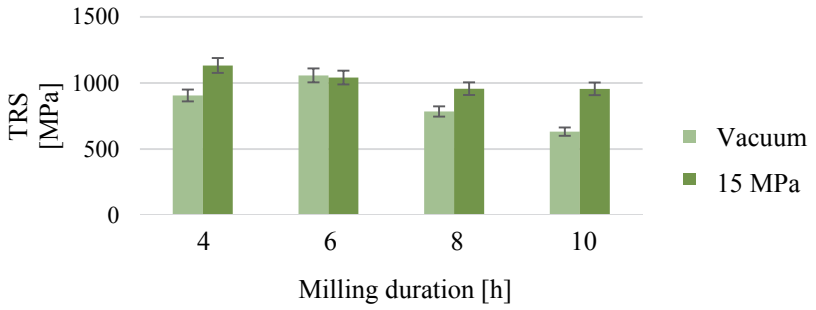

Figure 2.28. Strength of samples with different milling durations sintered in vacuum and hipping regimes at 1500 °C [76]

Strength values correlate well with the previous analysis with hardness values and densities. A general decrease in strength is observed as WC content with longer milling durations increases, leaving less binder in the system. The highest strength values under vacuum conditions for a mixture with 6-hour milling also resulted in the highest relative density, considering vacuum samples. Samples with the highest density of 100.1 % also have the highest strength value of 1133 MPa for the mixture at 4 hours of milling.

The results suggest that the final microstructure and mechanical properties of the reactive sintered Ti(Mo)C-Ni cermet highly depend on the milling characteristics. Materials with longer high energy milling contain more WC from the milling equipment and result in higher hardness and density values while the balance of hard phase to binder shifts. As a result, the strength values decrease with extended milling. Considering the application, a milling time of 6 hours was chosen with optimal mechanical properties while indicating the highest stability in properties.

2.3.4 Chemical composition of reactive sintered titanium carbide cermets

Possible variations of TiC based cermets are plentiful. As a composite material, the properties of the final material depend on the selection of the ceramic phase (e.g. TiC, TiCN, Ti(W)C, Ti(Mo)C etc.) and the binder matrix (e.g. pure Ni, Co, Fe or their combinations) as well as on the ratio between them. Any additional alloying elements (Cr_3C_2, VC, Al, B etc.) are usually aimed at engineering a specific set of mechanical properties or an ability to function in certain environmental conditions such as high temperature, corrosion etc. In the case of reactive sintering, another factor is introduced as carbon content to form the closest ratio of 1:1 between metal atoms to carbon atoms in carbide, without resulting in excess free carbon in the system as pores. The main focuse in the current research was on adjusting the chemical composition of the reactive sintered cermet with optimal mechanical properties most suitable from a ballistic performance perspective but also considering the availability and affordability of the materials regarding possible manufacturing.

2.3.4.1 Influence of Cr addition and C content

Chromium is a well-known alloying element for TiC based cermets next to molybdenum and vanadium. Usually, chromium is added in the form of carbides (Cr_3C_2), and it has been reported in [77, 78] that chromium has a positive effect on TiC cermets. As all the other elements in this research have been added in elemental form, it was decided that chromium will also be added as elemental Cr powder. The amount of chromium added was chosen to be 3 wt% of which 2 wt%

was at the expense of Ti and C powders and 1 wt% from Ni and Mo. With the addition of chromium, carbon content was also investigated since the behaviour of Cr in the reactive sintered TiC cermet was unknown. Chromium can form carbides on its own but can also solve in nickel. According to carbide enthalpies, titanium is more reactive in all temperature ranges than any form of chromium carbides. This would suggest that free carbon in the system would be first used by titanium, leaving any possible residual carbon for chromium. With 16 wt% of nickel and 3 wt% of chromium in the starting powders, the ratio between Ni and Cr is 15.8 wt% of Cr. According to Ni-Cr phase diagram (Figure 2.29), at sintering temperature, both elements should be in liquid form if unaffected by other elements and compounds in the system and below solidus line, chromium would be dissolved in the face-centred cubic crystal structure of nickel. Carbon content was altered in the range of 16 to 18 wt% out of Ti and C.

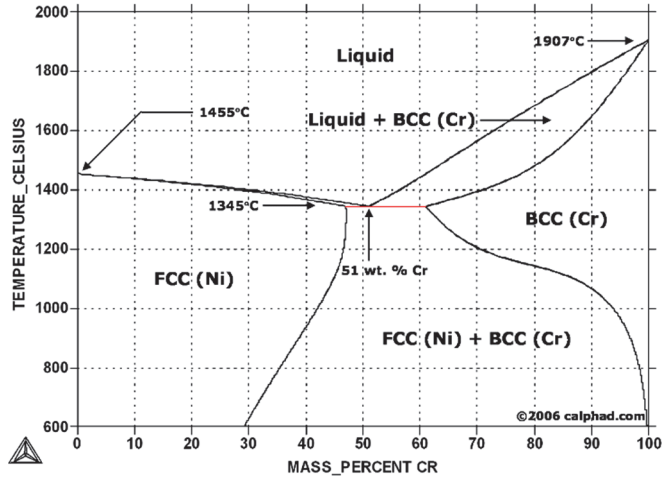

Figure 2.29. Ni-Cr phase diagram by Calphad [79]

The compositions of the milled powder mixtures are presented in Table 2.9. Milling duration of the powders was set at 6 hours in a high energy attritor mill and sintering regime of 60 minutes of dwell at 1270 °C and 1500 °C was applied under vacuum.

Table 2.9. Powder mixture compositions with Cr additions and different C contents in wt% [80]

Powder ratios	Ti	C	Ni	Mo	Cr
73(Ti+16C)-24NiMo(2:1)-3Cr	61.3	11.7	16.0	8.0	3.0
73(Ti+17C)-24NiMo(2:1)-3Cr	60.6	12.4	16.0	8.0	3.0
73(Ti+18C)-24NiMo(2:1)-3Cr	59.9	13.1	16.0	8.0	3.0

Microstructure images of sintered samples are presented in Figure 2.30.

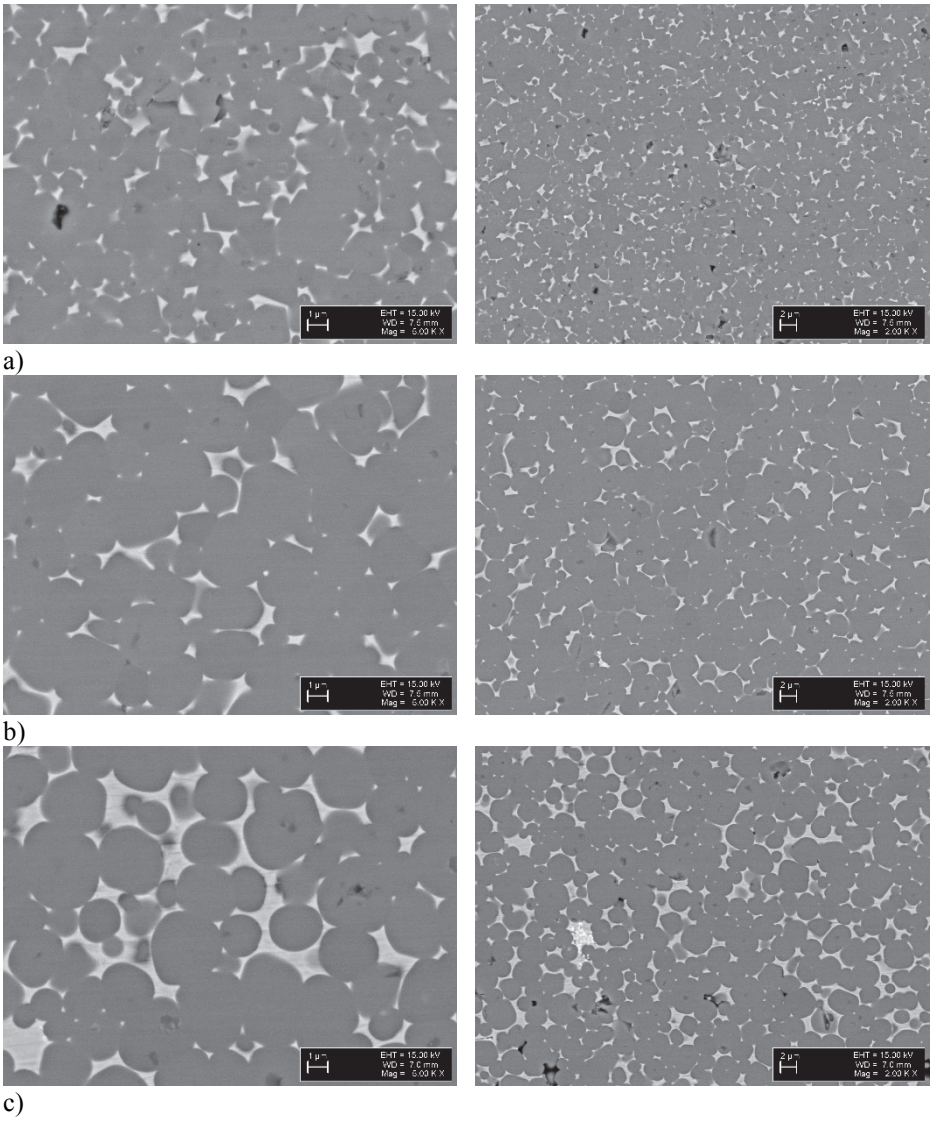

Figure 2.30. Microstructure images of samples with Cr addition and different C content: a) 16 wt% C; b) 17 wt% C; c) 18 wt% C [80]

The first initial change in the microstructure with added chromium is the shape of the carbide grains. Wetting of the more spherical grains is excellent and microporosity is low. The remaining porosity in 16 wt% and 18 wt% of carbon is slightly higher, suggesting that even with added Cr additive, the optimal carbon ratio to titanium is 17 wt% of C. Most of the chromium is in the binder (Figure 2.31) but EDS mapping also indicates that Cr is unevenly distributed.

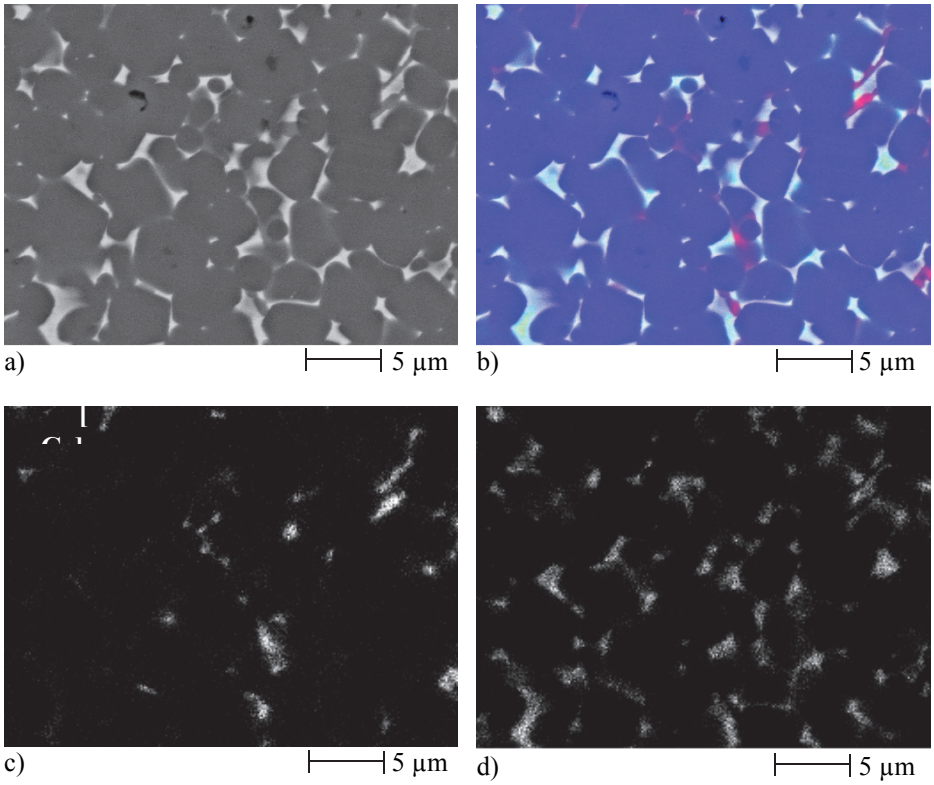

Figure 2.31. EDS mapping of reactive sintered Ti(Mo)C-NiCr cermet: a) SEM microstructure; b) EDS map with Ti-blue, Cr-purple, Ni-light blue; c) Cr mapping; d) Ni mapping

Chromium dissolves in nickel, increasing the hardness of the binder phase, which increases the overall hardness of the cermet. As chromium dissolves in nickel, chromium atoms replace some of the atoms in nickel's crystal structure and because of slightly larger atomic radius, it creates distortions in the crystal planes within the nickel grain. These distortions increase the resistance to dislocations along the crystalline planes and therefore hardness. On the other hand, these distortions can accumulate and concentrate, causing regions prone to inhibiting crack formation.

Adding chromium into the system has a positive impact on the mechanical properties, considering the application in Table 2.10. Strength of the samples has decreased from 1058 MPa to 862 MPa while comparing mixtures with 6-hour milling and 17 wt% of C after vacuum sintering. This may be caused by the increase in concentrated distortions by dissolved Cr atoms in the Ni crystal structure. The hardness value has increased from HV10 1500 to HV10 1748 with a high fracture toughness of 11.57 $MPa \cdot m^{1/2}$.

Table 2.10. Mechanical properties of reactive sintered Ti(Mo)C-NiCr cermets with different C content [80]

Relative carbon content [wt%]	**16**	**17**	**18**
HV10	1684	1748	1454
Toughness [MPa·m$^{1/2}$]	8.15	11.57	11.43
TRS [MPa]	829	862	879

2.3.4.2 Influence of Mo content

Molybdenum is the most widely used alloying element in TiC cermets due to its effect on the wettability of the two phases, therefore increasing the mechanical properties of the final material [33, 38]. Conventional indication of Mo in the cermet material is expressed as Ni to Mo ratio in weight. As the ratio of TiC to binder in the cermet influences the mechanical properties of the final material, it influences also the ratio of Ni to Mo. Additional molybdenum increases the volume of the hard ceramic phase in the system, resulting in increased hardness with decreased strength. Typical Ni to Mo ratios are 1:1, 2:1, 3:1 and 4:1 of nickel and molybdenum, respectively. As the hardness value of the cermet with 2:1 ratio is sufficient, ratios 3:1 and 4:1 were chosen. The composition of mixtures is presented in Table 2.11.

Table 2.11. Composition of reactive sintered Ti(Mo)C-NiCr with different Ni-Mo ratios [80]

Mixture	**Ti**	**C**	**Ni**	**Mo**	**Cr**
73(Ti+17C)-24(NiMo 2:1)-3Cr	60.6	12.4	16.0	8.0	3.0
73(Ti+17C)-24(NiMo 3:1)-3Cr	60.6	12.4	18.0	6.0	3.0
73(Ti+17C)-24(NiMo 4:1)-3Cr	60.6	12.4	19.2	4.8	3.0

With these sets of ratios, strength values are expected to increase; however, as Mo powder is the most expensive component of the starting powders, lower volume of Mo would reduce the financial costs of the cermet. The microstructure images of these samples are presented in Figure 2.32.

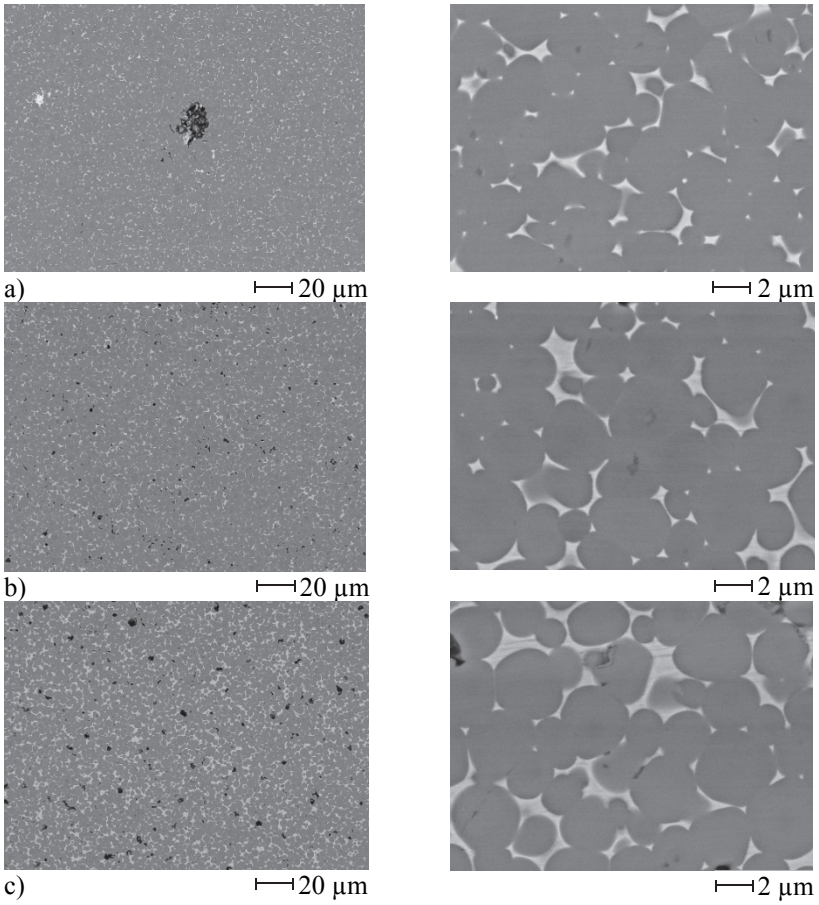

Figure 2.32. Microstructure images of reactive sintered Ti(Mo)C-NiCr cermets with different Ni to Mo ratios: a) 2:1; b) 3:1; c) 4:1 [80]

In all cases, the spherical shape of carbide grains remained present. From the 500x magnification, there is a clear indication of increased porosity in the system with less Mo. These results suggest that at a decreased Mo content, the carbide composition does not include enough Mo atoms to fully wet the binder metal. With the change in Ni to Mo ratio, the initial carbide formula of $Ti_{0.94}Mo_{0.06}C_{0.77}$ changed to $Ti_{0.95}Mo_{0.05}C_{0.78}$ for Ni-Mo ratio of 3:1 and $Ti_{0.96}Mo_{0.04}C_{0.78}$ for Ni-Mo ratio of 4:1. The porosity visible on the microstructure suggests that a minimum recommended amount of 6 % of the metal atoms in the Ti(Mo)C carbide should be molybdenum for wetting purposes. In a conventional TiC-NiMo cermet, the nickel and molybdenum ratio can be more heavily modified with less Mo since molybdenum atoms are present only in the carbide rim as they unable to infuse deeper into the larger grains (Figure 2.33).

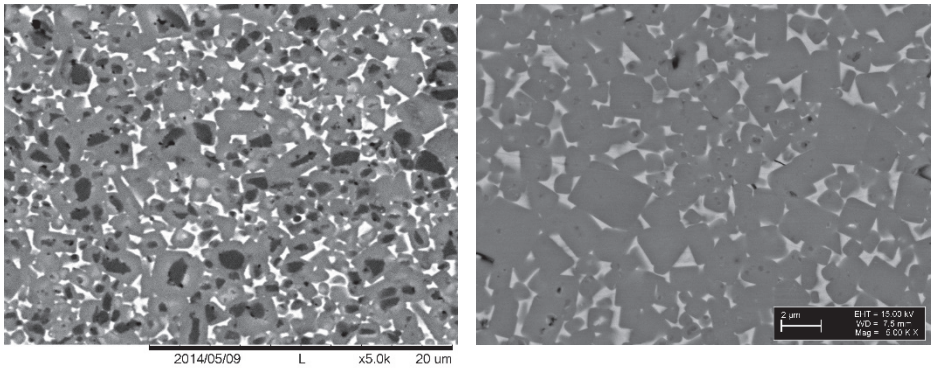

a) b)

Figure 2.33. Comparison of three phased and two phased TiC cermets with different technological routes: a) conventional three phased cermet; b) reactive sintered two phased cermet [70]

As the dual-carbide synthesis occurs *in situ* during reactive sintering, the grains are more homogeneous in metal atom distribution, leaving a smaller overall Mo content (Figure 2.33b). With a typical conventional TiC-NiMo cermet (Figure 2.33a), the inner core of the carbide is pure TiC and the molybdenum dual-carbide only on the outer ring of the carbide grain.

Theoretical density of the material depending on the nickel content is illustrated in Figure 2.34 without WC contamination from milling.

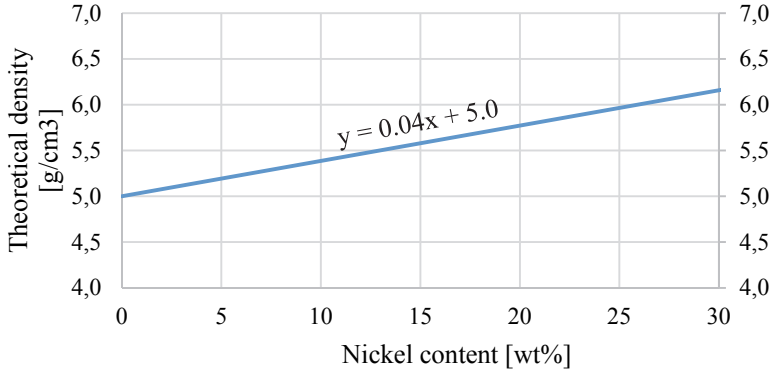

Figure 2.34. Density of reactive sintered Ti(Mo)C-NiCr depending on the Ni content

In addition, factoring in the WC contamination on the theoretical densities of the mechanical properties of the samples is presented in Table 2.12.

Table 2.12. Mechanical properties of reactive sintered Ti(Mo)C-NiCr cermets with different Ni-Mo ratios [80]

Ni-Mo ratio	2:1	3:1	4:1
Density [g/cm^3]	5.52±0.05	5.60±0.06	5.52±0.06
Relative density [g/cm^3]	95.5	95.6	93.5
HV10	1748±48	1696±28	1484±26
Toughness [MPa·m$^{1/2}$]	11.6±0.8	11.6±0.8	13.0±0.6
TRS [MPa]	862±190	993±104	933±13

The density values correlate with the microstructure images when also considering the relative densities with the increased binder content with higher density. The mixture with 2:1 Ni-Mo ratio has no visible wetting issues between the two phases but relative density is lowered by the presence of larger defects in the material, also visible in Figure 2.32a. Mixture with 3:1 Ni-Mo ratio exhibits microporosity between the carbide grains and the binder but larger defects are not present. Finally, neither does the material with most nickel metal (Ni-Mo ratio 4:1) exhibit large defects, but rather the highest microporosity with the lowest relative density. The hardness values are decreasing together with the molybdenum content, which is to be expected but still stayed at a high level for the Ni-Mo ratio of 3:1 compared to 2:1. Fracture toughness also remained the same for Ni-Mo ratios of 2:1 and 3:1 but increased for 4:1. This was expected, as the binder content increases but considering the high porosity in the system, it is a somewhat unusual since the strength value decreased from 3:1 to 4:1. One reason may lie in the strength, for the increased binder content is unable to overcome the high amount of porosity of 6.5% (mixture with 4:1 ratio of Ni-Mo) but fracture toughness is not as sensitive to microporosity as small pores can in some circumstances interfere crack propagation. Possibly, the properties of these samples with higher Ni to Mo ratios can be improved with the hipping process, as previously the densities increased an average of 3 % from vacuum sintering to hip regime.

2.4 Conclusions on material development

Titanium carbide cermet material was chosen as an option for an alternative ballistic protection material against armour piercing rounds. A standard industrial grade material of 80TiC-20NiMo(2:1) was used as reference and reactive sintered materials were developed in order to achieve material properties of equal or better mechanical properties. During the studies, several aspects of reactive sintered Ti(Mo)C based cermets with nickel as the main binder and with optional

chromium additive were investigated. Understanding the microstructure formation was the basis for engineering the composition of reactive sintered Ti(Mo)C based cermets. In addition, experiments for optimising powder preparation and sintering regimes were conducted.

The main conclusion made from developing reactive sintered Ti(Mo)C based cermets are as follows:

- Carbide synthesis occurs in three phases and before nickel binder enters the liquid state. Initial carbide synthesis of TiC begins during high energy milling. TiC and MoC are synthesised during lower temperatures under 800 ˚C, followed by the final formation of uniform Ti(Mo)C dual-carbide. The final microstructure is a two phased composite material with Ti(Mo)C carbide grains with nickel binder as matrix, unlike commercial three phased materials with TiC grain cores surrounded by Ti(Mo)C dual-carbide rims in a nickel matrix.
- With homogeneous distribution of Mo in the carbide grains, a minimum amount of molybdenum content of 6 % from the carbide metal atoms is present to ensure sufficient wetting between carbide grains and binder without microporosity.
- Chromium metal is responsible for more spherical carbide grains in the material, resulting in an increased hardness of the material by 10 %.
- An optimal sintering regime implements an additional dwell step at 1270 ˚C to ensure homogeneous microstructure with less porosity. With the test samples prepared, the most suitable dwell duration at 1270 ˚C and 1500 ˚C was 60 minutes.
- The depth of vacuum can affect the material properties as high vacuum can result in binder evaporation. Applying hot isostatic pressure during liquid phase sintering can result in an increase of density as high as 3 % depending on the relative density of the material before hipping.
- Milling duration of 6 hours using high energy milling equipment resulted in the best combination of mechanical properties. Contamination with WC was at a rate of 0.27 wt% per hour, which significantly increases the theoretical density of the final material.

An overview of the main mechanical properties that are of interest from a ballistic protection perspective is presented in Table 2.13.

Table 2.13. Comparison of material properties between commercial and reactive sintered TiC based cermets

Mixture	TiC-NiMo	Ti(Mo)C-Ni	Ti(Mo)C-NiCr
Carbide to binder ratio [wt%]	86.7-13.3	83.3-16.7	79.0-21.0
Density [g/cm^3]	5.59±0.06	5.55±0.05	5.60±0.06
HV10]	1579±56	1523±34	1696±28
Toughness [MPa·m$^{1/2}$]	11.0±0.6	9.83±0.7	11.6±0.8
TRS [MPa]	990±73	1042±51	993±104

The results indicate that it is possible to obtain reactive sintered Ti(Mo)C based cermets with mechanical properties that are equivalent or even superior to commercial TiC based cermets. The sintering regime of reactive sintered cermets requires specific steps and modifications but can be produced using the same furnaces.

3 ARMOUR TILE DEVELOPMENT

In this chapter, the experimental tests of armour tiles are investigated. Materials under consideration are the *in house* developed TiC based cermets, Al_2O_3 tiles from an armour panel solution certified against 7.62x51 AP (WC core) round with multi-hit capability and SiC tiles with different thicknesses by a ceramic manufacturer. Testing of single armour tiles is not yet standardised since the influences of experimental setup are under investigation. This, in turn, results in a number of alternatives in which the ballistic tests can be prepared and conducted. In general, an armour tile is glued with an adhesive on to a semi-infinite backing. The backing material is usually either aluminium alloy (e.g. Al60xx) or various steels [81–85]. The backing or also named reference material can be different but has to remain constant throughout the test series [8]. For the bullet propulsion, different options have been used. Depending on the testing facility and available equipment, testing setup may include firing from a sniper rifle [86], single stage gas propelled gun [85] or a reverse impact two stage gas gun [87, 88]. A common quantifiable measure for evaluating the ballistic performance of armour tile materials is the depth of penetration (DoP) created by fragments from the bullet and the armour tile. These can be measured by mechanically cutting the specimen and visually determining the length of the deformation. Alternatively, X-ray analysis is used to assess DoP on the specimens but also the ballistic interaction can be recorded during impact with high speed X-ray detectors.

The main armour tile currently on the market is Al_2O_3, mostly due to its cost efficiency. Silicon carbide has superior mechanical properties, including lower density but due to more complex manufacturing can be several times more expensive (Table 3.1). Commercial TiC cermet with 80 wt% of TiC has higher density than ceramic materials but sufficient hardness against the bullet core material and increased fracture toughness and strength compared to ceramics.

Table 3.1. Material properties of armour tiles under investigation [8, 89–91]

Material	TiC-20NiMo(2:1)	Al_2O_3	SiC
Density [g/cm^3]	5.60±0.06	3.84±0.01	3.15±0.03
HV10	1510±30	1580±20	2420±30
Toughness [MPa·m$^{1/2}$]	11±1	4±1	4±1
TRS [MPa]	990±50	379±30	550±40
Young's modulus [GPa]	415±15	370±20	405±25
Relative cost [a.u.]	1.0	1.0	2.5–4.5

With a unique set of densities and other mechanical properties, the final armour tile thickness and resulting areal mass density vary. The areal mass

densities of the materials under investigation depending on the thicknesses are illustrated in Figure 3.1.

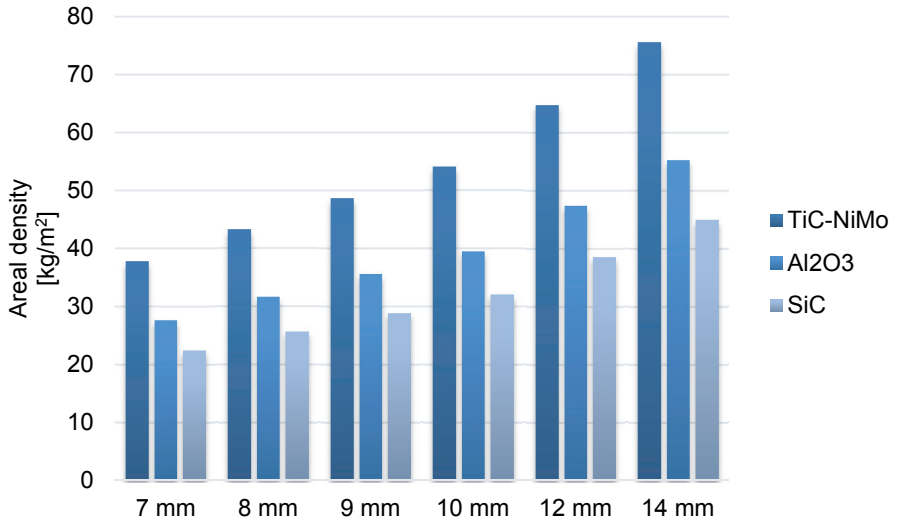

Figure 3.1. Areal mass densities of armour tile materials with different thicknesses

According to data for TiC-NiMo from the previous project, the minimum tile thickness in the configuration developed was 10 mm, resulting in an areal mass density of 54.0 kg/m^2. The market solution against the same threat level using Al_2O_3 applied 14 mm thick tiles with an areal mass density of 55.3 kg/m^2. With SiC, no solutions on the market were obtained during the project but tiles with different thicknesses were acquired for testing purposes.

The main goal of armour tile testing was to assess the required areal mass density (shape and thickness) of TiC-NiMo cermet against 7.62x51 AP (WC core) round and to compare it to competing ceramic materials most common on the market. Throughout this project, aluminium alloy 6082 backing was used to assess the depth of penetration values. Test shooting was conducted in EDF laboratory and sniper rifle Steyr SSG was used by EDF personnel from a 30 m distance. Nammo 7.62x51 AP8 (WC core) rounds were used with measured speeds of 955±7 m/s. The test sample setup is presented in Figure 3.2 where the armour tile with confinement and aluminium block backing is clamped to a steel frame. Both X-ray analysis and visual measurement of cut samples were implemented for DoP measurements. During the ballistic impact tests, several influencers were investigated. The geometry of the armour (area and thickness), material (TiC cermets, SiC and Al_2O_3) and confinement of tiles were considered.

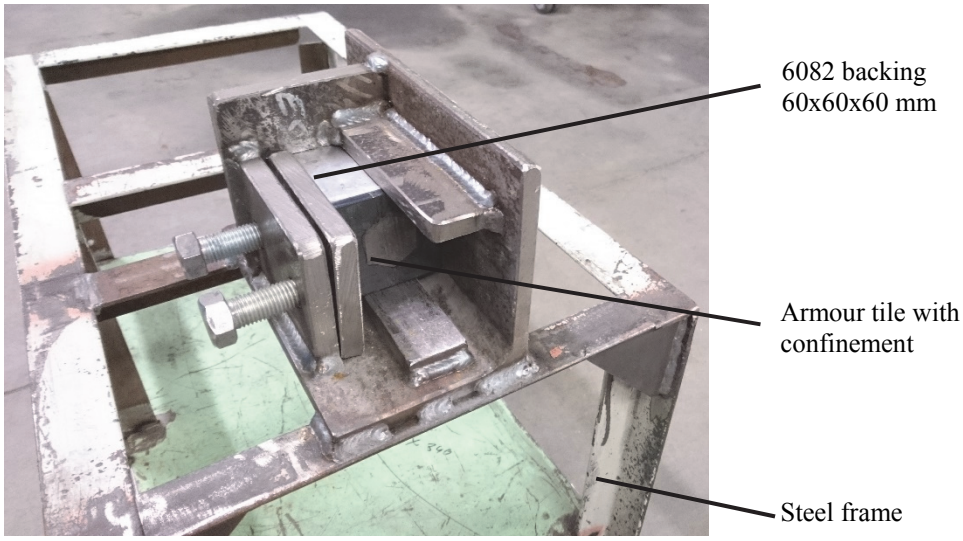

Figure 3.2. Experimental setup of single armour tile testing on aluminium block backing

3.1 Armour tile geometry

The simplest shape in the form of a square has been used in market solutions and also at an early stage of the project. But the most common shape currently offered is a hexagonal shape. During the course of the project, it was decided to change the shape of the tile from square to hexagonal because of two drawbacks accompanied by the square shape.

Firstly, adjacent tiles can be damaged by the expanding tile fragments. As the tile is hit by the projectile and fragmentation is occurring, the volume the tile occupies expands in all directions (Figure 3.3). Expansion towards the impact location (yellow) has minimal resistance by mostly packing and covering layers. Expansion in the same direction of the bullet trajectory (red) is expected and has to be withstood by the backing material. Radial expansion (Figure 3.3 green) is distributed to adjacent armour tiles.

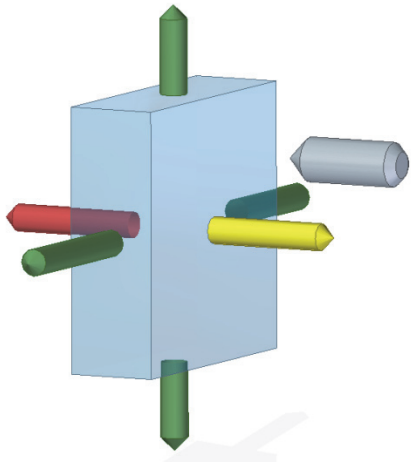

Figure 3.3. Armour tile expansion vectors

The dynamic radial pressure by the created fragments has been found to damage tiles that are not otherwise directly hit by the projectile. Figure 3.4 shows clearly that two tiles away from the actual impact points were cracked due to the corners of expanding tiles.

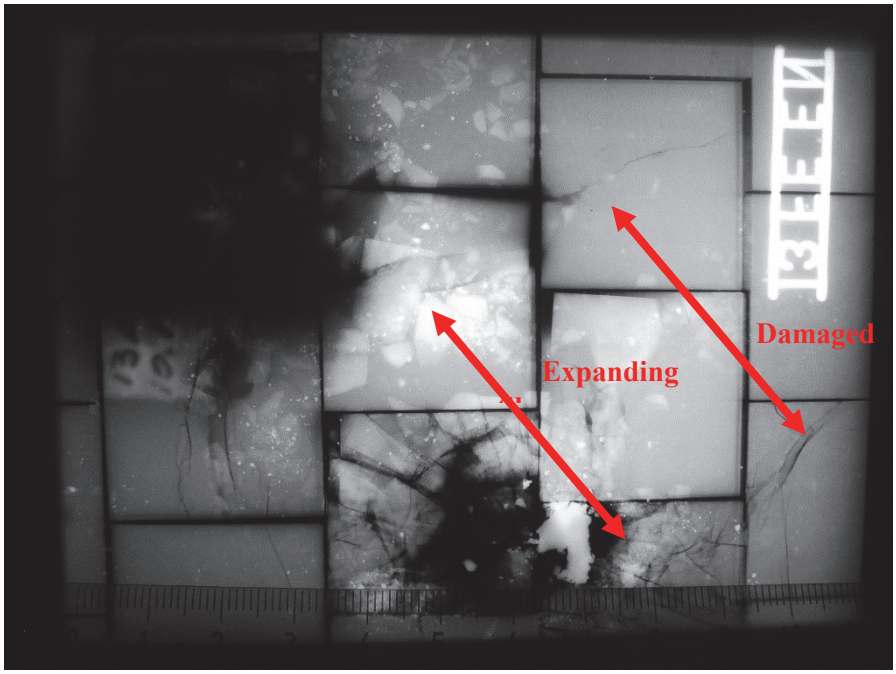

Figure 3.4. X-ray analysis of an armour panel with 30x30x10 mm TiC-NiMo tiles

Secondly, adjacent tiles can dislocate due to expanding tiles. As the armour tiles can be arranged in a simple grid or "brick-wall" patterns (Figure 3.5), in both cases, dislocation of armour tiles can occur within the aligned rows/columns, indicated with blue arrows. With a simple grid arrangement, dislocation can arise in two directions (x, y). With the "brick-wall" pattern, one direction (y) is eliminated but as discussed previously, with this pattern, additional tiles can be damaged by the radially moving fragments.

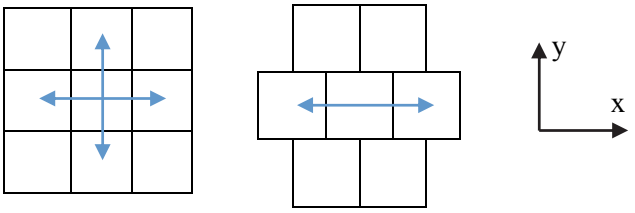

a) b)

Figure 3.5. Armour tile configuration patterns: a) simple grid; b) "brick wall"

An example of tile dislocation is illustrated in Figure 3.6. The gap introduced between the tiles can be up to 2 mm and with a multi-hit testing pattern, the second round can be located in the gap area. In this case, since the tiles have already moved in the radial direction, it is likely that the bullet core can push the tiles away from their path instead of ballistic impact where the tile and projectile would be mutually destroyed by fragmentation.

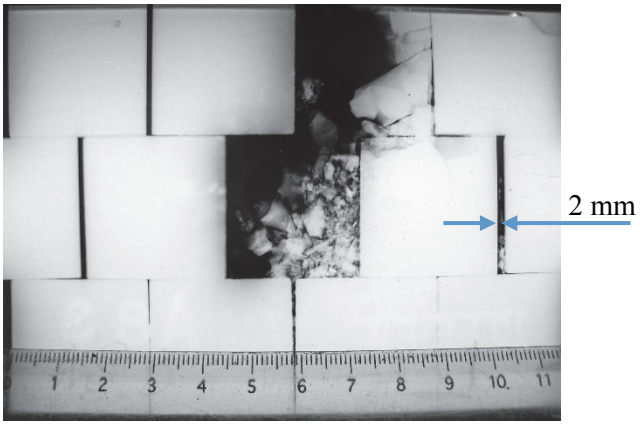

Figure 3.6. Example of tile dislocation after impact with 30x30x10 mm TiC-NiMo tiles

An alternative tile shape design was therefore implemented in the form of hexagonal tiles. The expansion of a tile hit is expanding in six radial directions trying to dislocate six different adjacent tiles (Figure 3.7 blue). The tile on the left forced to move left, indicated by green arrow is stopped geometrically by three

other tiles (indicated with red arrow). This configuration offers increased rigidity of the system.

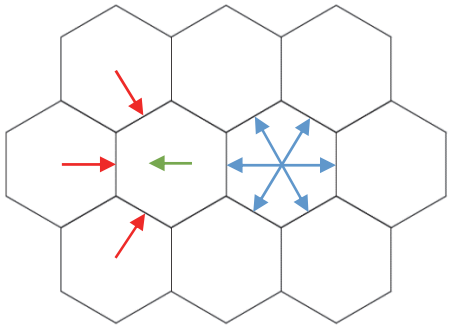

Figure 3.7. Hexagonal pattern with radial movement vectors: blue, expansion vectors of the tile hit; green, displacement vector of the adjacent tile; red, pressure from other tiles preventing the movement of the adjacent tile

The new hexagon tile design has a height of 30 mm, i.e. the total side area is slightly smaller (Table 3.2), suggesting higher dynamical radial pressures. The upside of hexagon design shows when a tile hit is expanding or a tile is introduced to radial dislocation; the interaction between any two tiles is through the whole area of the tile's side areas. In the case of the "brick-wall" design, in the x-axis (Figure 3.5) the full area of the side is used in the interaction but in the y-axis, the moving tile introduces pressure on two individual tiles. This will result in an uneven loading on the tile indicated with the green displacement vector (Figure 3.8) and a stress concentrator inhibiting crack formation, as shown in Figure 3.4.

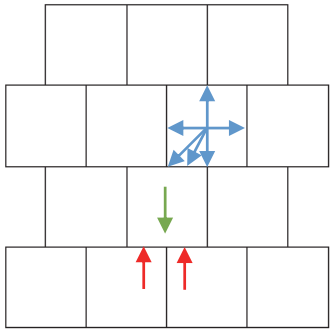

Figure 3.8. Radial loading of tiles in "brick-wall" pattern: blue, expansion vectors of the tile hit; green, displacement vector of the adjacent tile; red, pressure from other tiles preventing the movement of the adjacent tile

In a honeycomb pattern, all of the corners of the tiles meet and a more evenly distributed loading of dynamic radial pressure occurs between the whole side area

of the tiles. Any dislocation, e.g. in the x-axis of the adjacent tiles, is also disallowed geometrically by tiles in the upper and lower rows. An example of a honeycomb pattern armour panel after test firing with hexagon tiles of 30 mm height and 10 mm thickness is presented in Figure 3.9 with no cracks in adjacent tiles and dislocation. Adjacent damaged tiles can certainly still occur with hexagon tile design, as reported earlier at the beginning of section 2.1 and illustrated in Figure 2.1 but are reduced by tile shape design.

Table 3.2.Comparison of geometrical values between square and hexagon tile design

Geometry	Square	Hexagon
Length/height [mm]	30	30
Bottom surface area [mm^2]	900	852
Perimeter [mm]	120	109
Single side area with 10 mm thickness [mm^2]	300	182
Total side area with 10 mm thickness [mm^2]	1200	1090

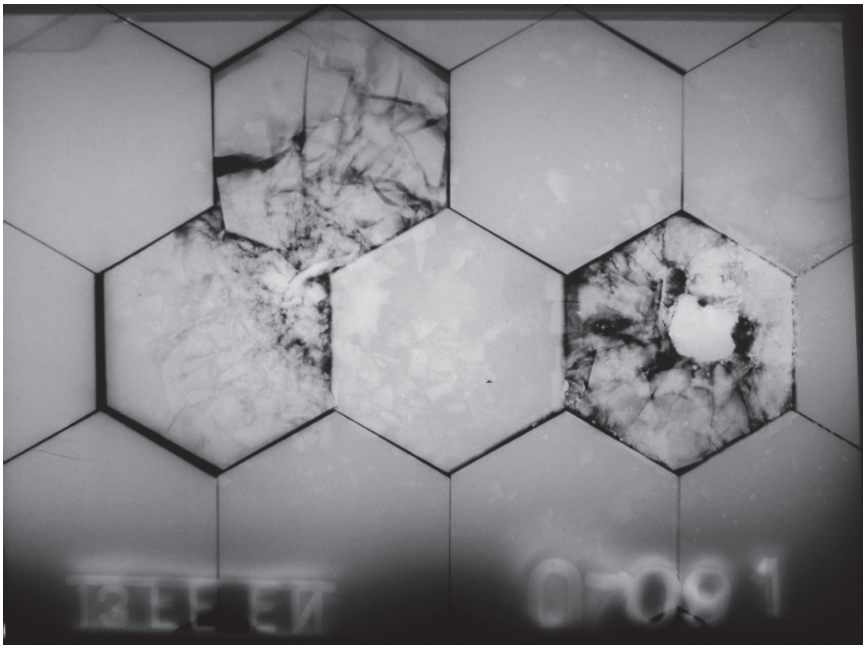

Figure 3.9. Honeycomb pattern of hexagonal tiles after firing tests

3.2 Depth of penetration testing of armour plates

Depth of penetration is a common technique for comparing armour tile materials and thicknesses due to its simple and inexpensive setup compared to other methods. The reference or i.e. backing material chosen was aluminium alloy 6082. Initially, the stock material heat treated and artificially aged was defined as T6. A baseline firing with the 7.62x51 AP (WC core) firing without any armour tile was done with a DoP of 53 mm. It was then decided to anneal the aluminium alloy in order to obtain larger penetration values to better evaluate the differences in small changes in tile thicknesses. The resulting DoP was twice the length at 110 mm. X-ray images of baseline test firing with 7.62x51 AP (WC core) into aluminium alloy semi-infinite blocks with different heat treatments are illustrated in Figure 3.10.

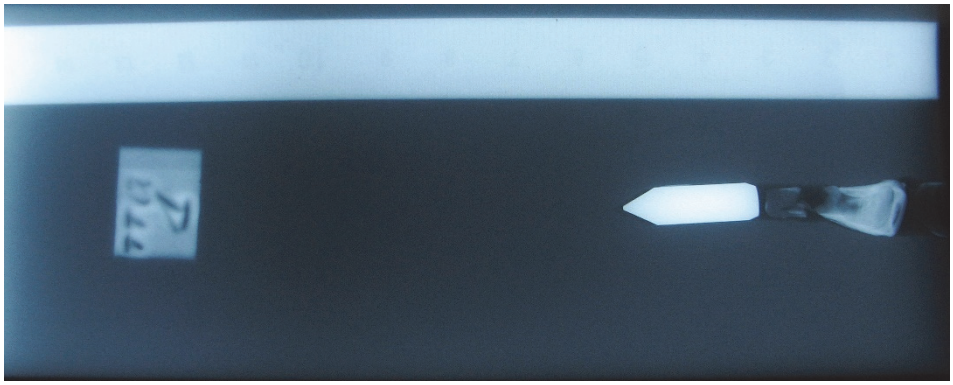

a)

b)

Figure 3.10. X-ray analysis of DoP baseline testing with 7.62x51 AP (WC core) rounds into aluminium alloy 6082 blocks: a) heat treated and artificially aged (T6); b) annealed (O)

The mechanical properties of aluminium alloy with different heat treatment states and resulting DoP values are presented in Table 3.3.

.

Table 3.3. Mechanical properties of aluminium alloy 6082 with different heat treatments [92]

Backing material	6082-T6	6082-O
HBS	104	33
Elongation [%]	10	27
Tensile strength [MPa]	290	130
DoP [mm]	53	110

When the Al_2O_3 tiles from a certified armour panel solution according to NATO STANAG 4569 level III (WC core) manufactured Scanfiber were obtained, these were also considered to act as a benchmark armour tile. The hexagon tiles had a height of 26 mm and thickness of 14 mm with an areal mass density of 55.3 kg/m^2. Test firing of the entire panel was conducted by EDF, following the shot pattern described in AEP-55. The armour panel withstood all four shots (Figure 3.11) with some damage to the backing material and the protective cover. These cutting lines in the protective cover and backing fibres were mostly due to the firing setup since the panel was fastened between two steel plates with openings in the middle. On the front, the window allows the shooter to aim and the back window allows possible penetrated fragments to be caught by a witness plate (Figure 3.16). The witness plate is designed to assess the remaining energy of the fragments. Tight fastening of the panel between the steel plates and flexible nature of the backing cut the protective cover and a few layers of the backing due to the sharp edges of the steel window. Nevertheless, the armour panel has no penetration of bullet or armour tile fragments.

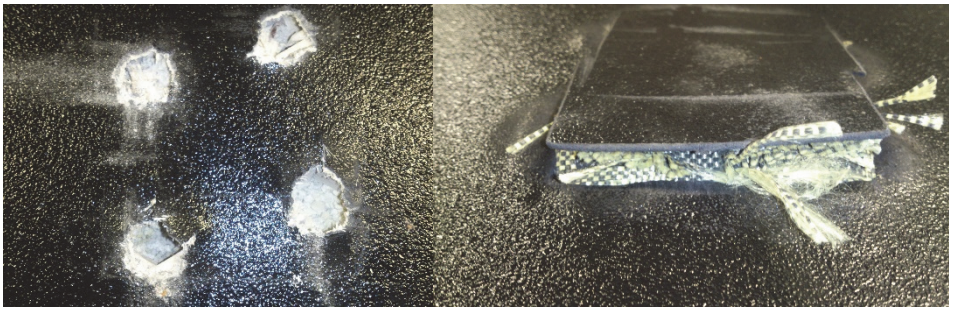

a) b)

Figure 3.11. Certified armour panel according to NATO STANAG 4569 level 3 (WC core) after test firing according to AEP-55: a) front side; b) back side

Therefore, test firings of the 14 mm thick Al_2O_3 tile on aluminium alloy 6082-O semi-infinite backing can also be considered as a benchmark armour tile design with sufficient ballistic protection capabilities against the 7.62x51 AP (WC core) round. The generated deformations or DoP into the backing block can be regarded as acceptable and baseline deformations on the semi-infinite aluminium alloy 6082-O backing. The test firing resulted in no penetration by fragments but an imprint of 3 mm of the entire tile into the aluminium (Figure 3.12.

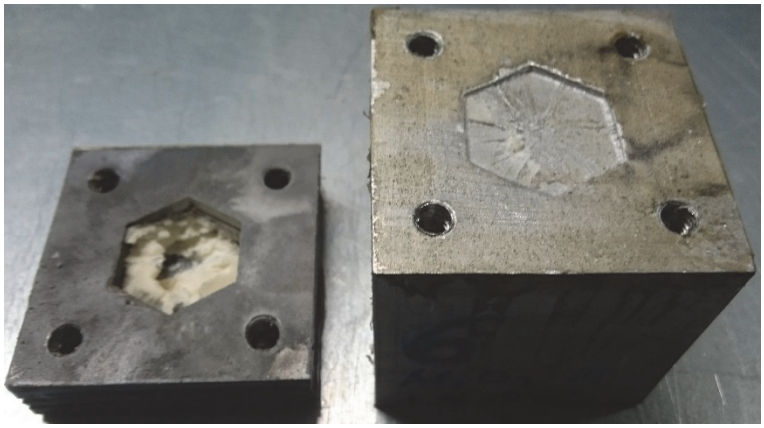

Figure 3.12. Al_2O_3 tile on aluminium alloy 6082-O backing test firing with 7.62x51 AP (WC core) round

Test series with TiC-NiMo cermets and SiC ceramics were conducted using hexagon tiles with 30 mm height and thicknesses from 6 mm to 12 mm. Titanium carbide cermets were manufactured in TUT but silicon carbide tiles were provided by Saint-Gobain.4. Tiles were glued on the aluminium alloy 6082-O semi-infinite blocks with 60x60x60 mm using purethane adhesive. Mild steel frames were used for confinement purposes in order to simulate the loading conditions in an armour panel. The results of firing tests are illustrated in Figure 3.13 and Figure 3.14.

DoP values obtained for TiC-NiMo and SiC have similar functions. Using these functions, the required thicknesses for absolutely no deformation on the aluminium backing would require tile thicknesses of 11.9 mm for TiC-NiMo and 12.3 mm for SiC. Considering the baseline deformations with Al_2O_3, a deformation of 3 mm in the backing as acceptable, the recalculated tile thicknesses would be 11.3 mm for TiC-NiMo and 11.6 mm for SiC. The tile thickness is usually rounded up to the closest round number in which case with both materials, the recommended tile thickness is 12 mm. The areal mass densities with these tiles would be then 64.8 kg/m^2 for TiC-NiMo and 38.5 kg/m^2 for SiC. In this case, the test setup suggests that the same volume of material is needed against the same ballistic threat and due to the differences in the specific

weight, SiC has an advantage over TiC-NiMo cermet in terms of armour system weight.

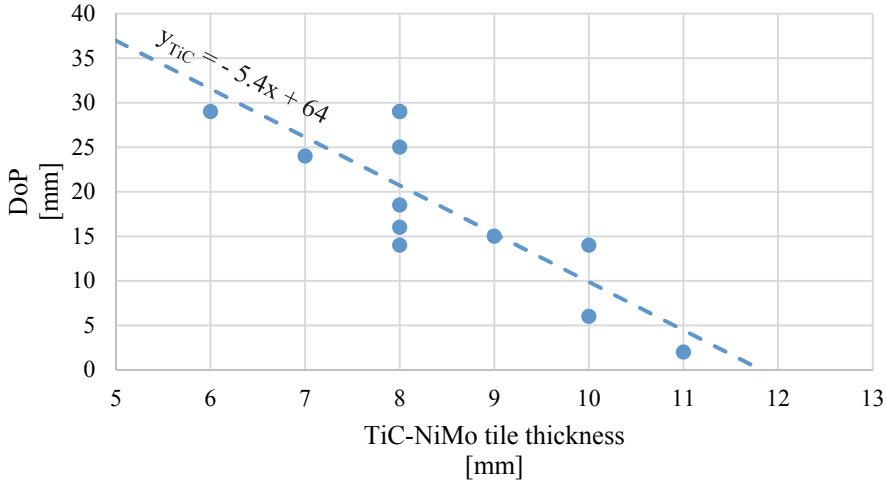

Figure 3.13. DoP of TiC-NiMo tiles with hexagon height of 30 mm shot by 7.62x51 AP (WC core) round

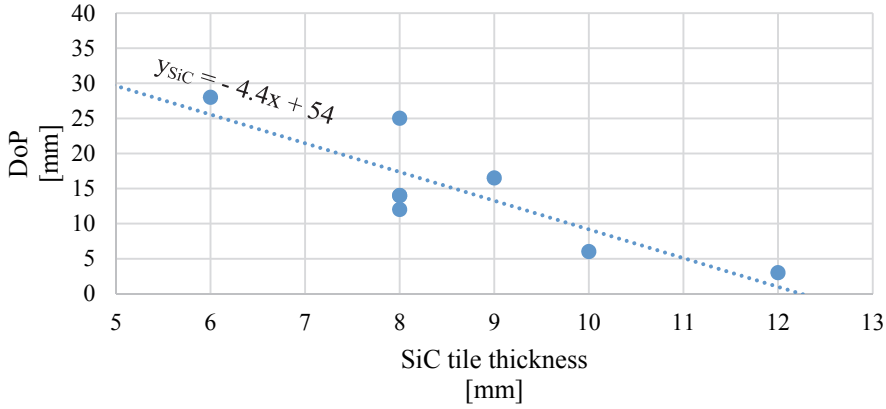

Figure 3.14. DoP of SiC tiles with 30 mm height shot by 7.62x51 AP (WC core) round

Still, the estimated tile thickness suggested by DoP testing should not be directly transferred to the armour panel system mostly because of the different backing material in the panel. Static and dynamic mechanical properties of DoP backing and panel backing are very different, resulting in different tile-backing interaction.

The most important influencers in an armour tile/backing combinations are still under investigation and debate but a recent analysis in [93] provides a hierarchic order of influences on the ballistic resistance of armour ceramics. The first priority is defined there as the mode of armour material fragmentation which

governs the dwell duration during the projectile/armour interaction and also the abrasive efficiency of the armour material debris. Mode of fragmentation is reported not to affect crack length that can be represented by fracture toughness but instead, the number and spacing of cracks. Comparison of TiC-NiMo cermet and SiC ceramic tiles clearly reveals that the mode of fragmentation of these materials is different (Figure 3.15). The spacing between cracks is clearly denser with SiC. This, in turn, means that the abrasive efficiency of the finer debris causes less damage to the projectile than to larger debris. TiC-NiMo fragments are larger, suggesting increased abrasive efficiency. Considering the abrasive erosion interaction between the projectile and armour material fragments, it should be noted that the target to be eroded is the hardmetal bullet core. In this case, SiC has the advantage as a material with higher hardness that erodes softer materials more efficiently. Taking both of these factors into account, similar ballistic performance in terms of armour tile thickness may have evened out but the mass efficiency is still strongly in favour of SiC.

Figure 3.15. Comparison of the mode of fragmentation between TiC-NiMo tile on the left and SiC tile on the right

Another important factor is the backing material's dynamic stiffness. It is argued that the Young's modulus of the backing material is not the most important factor, as glass with Young's modulus of 70 GPa yielded better ballistic performance for the armour ceramic than aluminium alloy with Young's modulus of 85 GPa [93]. In fact, glass backing resulted in similar results to steel backing with Young's modulus of 210 GPa. The positive effect of glass is believed to be caused by an increase in the abrasive efficiency of the larger armour material debris compared to using aluminium alloy backing. It is therefore argued that

dynamic parameters of the backing material are responsible for altering the mode of fragmentation of the armour material.

3.3 Armour tile optimisation within armour panel configuration

The materials used as backing in the armour panel are composite and fibre materials, which have different static and dynamic properties compared to metal alloys such as aluminium alloy 6082. This, in turn, means that the armour tile/backing interaction and wave propagation are very different. The backing materials investigated for the armour panels are S2-fibreglass, rubberised aramid and ultra-high-molecular-weight-polyethylene (UHMWPE) composite. On the market, both rubberised aramid and UHMWPE backings are mostly used due to their lower mass efficiency (Table 3.4).

Table 3.4. Mechanical properties of armour panel backing composites

Material	Density [g/cm^3]	Tensile strength [MPa]	Young's modulus [GPa]	Compressive strength [MPa]	Relative cost [a.u.]
S2-fibreglass	2.48	3300	85	1600	1
Aramid	1.44	2800	90	300	2
UHMWPE	0.97	2900	140	200	3

Armour panels were tested using the setup in Figure 3.16. Larger armour panels (400x400 mm) to be tested are placed between steel frames and fixed in the construction frame in front of the reference panel. When testing smaller panels (200x200 mm), the panel is fixed using two steel sheets with windows on both sides.

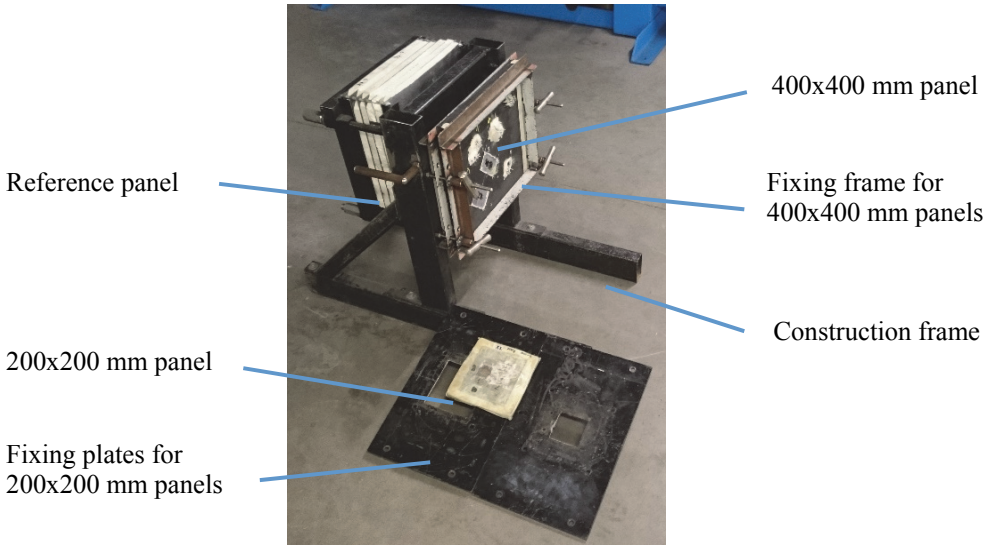

Figure 3.16. Experimental setup of 400x400 mm and 200x200 mm armour panel ballistic testing

3.3.1 Armour panels with TiC-NiMo tiles

Initial testing of TiC-NiMo tiles was conducted with S2-fiberglass backing since this was used in the previous project and the know-how of producing composite backing plates with specific thicknesses (nr. of layers) was available *in-house*. Test series using a single confined armour tile on aluminium alloy 6082-O block suggested a thickness of 12 mm. As the backing materials used differed in their properties and an armour tile with 10 mm thickness was available from the previous project, for a start, a 10-mm tile thickness with 2 mm steps at 8 mm and finally, that of 6 mm were selected. Each panel configuration was tested with two panels.

The first small panel with 10 mm tiles stopped both shots but with the second panel, the second shot penetrated slightly with only minor dents in the first 1 mm aluminium sheet reference plate (Figure 3.17). Panels with 8 mm TiC-NiMo tiles both were able to stop the initial shot but the second hit was able to penetrate the armour panel. A closer investigation revealed that the second shot in the case of the two panels with 8 mm TiC-NiMo tiles and the 10 mm panel with slight penetration had the impact near the edge of the window of the steel plate used to hold the panel in place. As a result, the fibres in the backing composite were pressed against the steel's edge, creating a cutting effect between the steel plate and the armour tile. From Figure 3.18b, the cut fibres can be seen along a straight line on the right. This might be the main cause of a resulting penetration since fibre composites are designed to perform best with tension along the fibres.

a) b)

Figure 3.17. Armour panel (200x200 mm) with 10 mm thick TiC-NiMo tiles on S2-fiberglass composite after two shots with 7.62x51 AP (WC core) with 30 mm between impacts: a) front side; b) back side

a) b)

Figure 3.18. Armour panel (200x200 mm) with 8 mm thick TiC-NiMo tiles on S2-fiberglass composite after two shots with 7.62x51 AP (WC core) with 30 mm between impacts: a) front side; b) back side

The analysis of these results suggests that TiC-NiMo tiles with 10 mm thickness are suitable against 7.62x51 AP (WC core). 8 mm tiles are promising but the test setup needs adjustment to eliminate the possibility of cutting forces to the backing material. As the S2-fibreglass composite backing is the heaviest compared to aramid and polyethylene, the areal mass densities of armour panels with 10 mm and 8 mm TiC-NiMo tiles are 74.0 kg/m^2 and 63.2 kg/m^2, respectively.

With the next test firing, the window in the steel plate for fixing the small panels in place was made larger to prevent cutting forces near the impact area. 8 mm TiC-NiMo tiles were applied with rubberized aramid, which is widely used on the market as a backing material. The aramid composite allows flexibility compared to S2-fibreglass and is lighter in density. Two shots in adjacent tiles were both stopped by the panel but some delamination and deformation occurred in the backing (Figure 3.19). It is estimated that with larger panels, these effects are reduced. The second panel unfortunately did not stop the first shot and the exact cause is still unclear (Figure 3.20). The number of damaged adjacent tiles with TiC-NiMo is minimal, with only one damaged tile per three shots that was not directly hit. The areal mass density of 8 mm TiC-NiMo tiles with aramid backing is 54.7 kg/m^2.

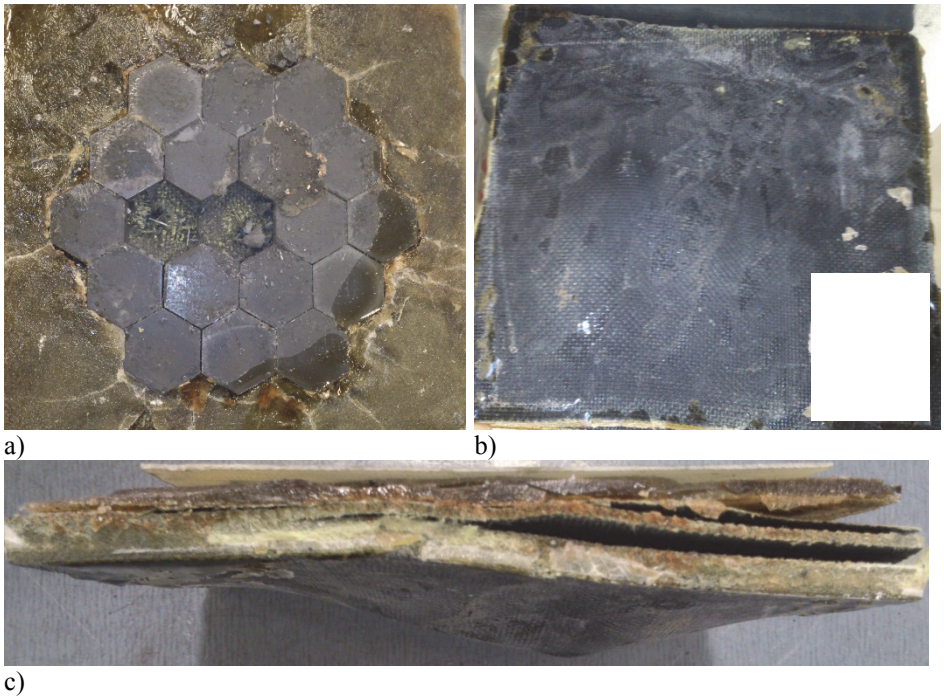

Figure 3.19. Armour panel (200x200 mm) with 8 mm thick TiC-NiMo tiles on rubberised aramid composite after two shots with 7.62x51 AP (WC core) with 30 mm between impacts: a) front side; b) back side; c) side view

Therefore, it was decided that in preparation for testing by an independent laboratory, 9 mm TiC-NiMo tiles would be used. In this case, UHMWPE backing was received, which is considered the lightest backing material for ballistic protection for light weight vehicles (Figure 3.21). With a product name of HB26, it has higher stiffness than rubberised aramid, which should increase the armour tile's abrasive effectiveness. The areal mass density of 9 mm TiC-NiMo tiles with HB26 polyethylene backing is 60.4 kg/m^2.

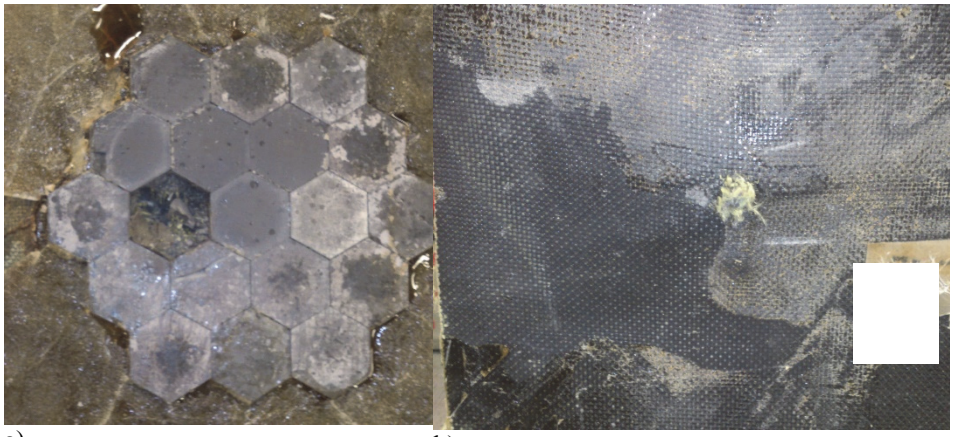

a) b)

Figure 3.20. Armour panel (200x200 mm) with 8 mm thick TiC-NiMo tiles on rubberised aramid composite after one shot with 7.62x51 AP (WC core): a) front side; b) back side

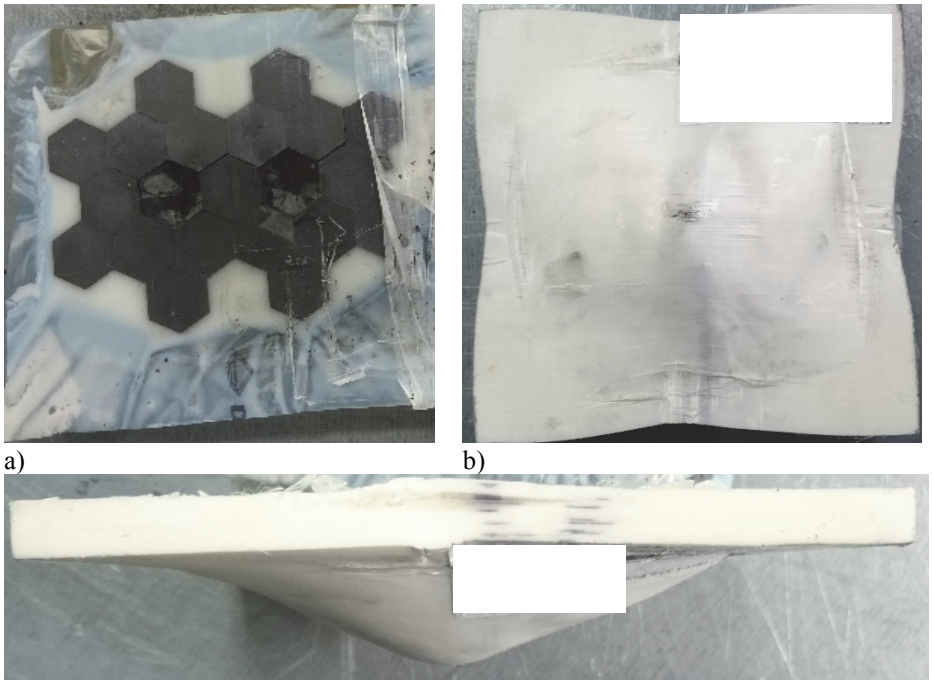

a) b)

c)

Figure 3.21. Armour panel (200x200 mm) with 9 mm thick TiC-NiMo tiles on polyethylene HB26 after two shots with 7.62x51 AP (WC core): a) front side; b) back side; c) side view

In conclusion, considering both a single armour tile and in armour panel configurations, TiC-NiMo cermets can be used against 7.62x51 AP (WC core) rounds for armouring material. The thickness of TiC-NiMo tiles was first

estimated at 12 mm from the depth-of-penetration tests, which was successfully reduced to 9 mm tile thickness with areal mass density of 48.6 kg/m^2. In addition, preliminary testing has indicated that with proper backing configuration, the tile thickness could be reduced to 8 mm with areal mass density of 43.2 kg/m^2 but it requires additional investigation.

3.3.2 Armour panels with SiC tiles

Testing of single armour tiles recommended a tile thickness of 12 mm for SiC tiles. In the following test series, different tile thicknesses were tested in order to optimise the areal mass density of the armour panel. A decrease of 1 mm of SiC tile thickness reduces the areal weight of the armour 3.2 kg/m^2. Backing material used was UMHWPE with a product name of HB26. Smaller panels for two shots were made with dimensions 200x200 mm and larger panels had dimensions of 400x400 mm for testing according to AEP-55 four shot pattern. Precise assembly and confinement information is considered confidential.

Small panels with 12 mm thick SiC tiles withstood both shots with a distance of 30±5 mm. Deformations to the backing material are significant (Figure 3.22). A panel with 10 mm thick SiC tiles was also able to withstand both shots but in this case, the deformations in the backing were already causing delamination of UHMWPE layers (Figure 3.23). Still, the panel illustrated that the 10 mm tiles are able to cause sufficient damage to the bullet core for the backing to absorb the debris and fragments. The resulting backing delamination and deformation suggest that the construction needs redesigning regarding stiffness. With these configurations, the total areal mass density of the panels would be 50.3 kg/m^2 and 43.9 kg/m^2 with 12 mm and 10 mm of SiC tile thickness, respectively.

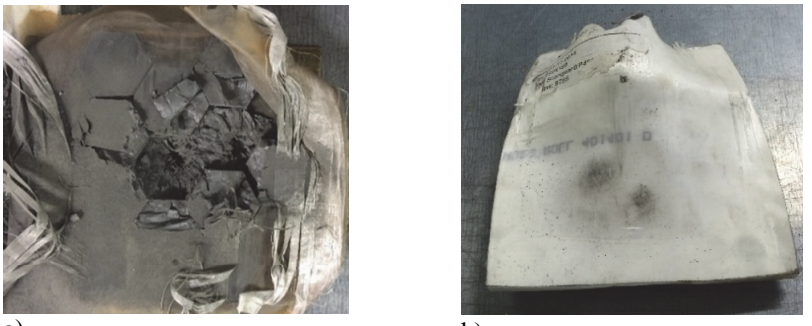

a) b)

Figure 3.22. Armour panel (200x200 mm) with 12 mm thick SiC tiles on BT26 after two shots with 7.62x51 AP (WC core) with 30 mm between impacts: a) front side; b) back side

a) b)

Figure 3.23. Armour panel (200x200 mm) with 10 mm thick SiC tiles on BT26 after two shots with 7.62x51 AP (WC core) with 30 mm between impacts: a) front side; b) back side

9 mm thick SiC tiles were also tested but in this case it was decided to use the large panel setup to ensure higher stiffness of the backing material. With a larger area, individual layers have more contact with fibres in connecting layers and it takes more energy to delaminate. In this case, the backing deformations considerably decreased but the second and fourth impact was not stopped by the panel. This suggests that initial shots (first and third) damaged adjacent tiles and the next shot of 30 mm radius impacted an already damaged tile (Figure 3.24). Therefore, 9 mm SiC tiles are unable to withstand the high loading of tensile and compressive stresses created by the elastic shock wave front. The areal mass density of an armour panel configuration of 9 mm SiC and BT26 is about 40.7 kg/m^2, not considering additional weight from assembly. It may be possible to use 9 mm SiC tiles if the armour configuration can be adjusted to make sure that adjacent tiles remain intact. One option could be to add a small gap between the tiles that is filled with the adhesive used to glue the tiles on the backing. With this option, it needs to be tested if the bullet core can still be sufficiently destroyed if it impacts directly the gap. Existence of gaps has been used with ceramic Al_2O_3 armour tiles with cylindrical shape in [88]. The same tile design is provided by TenCate LIBA who offers solutions against NATO STANAG levels I–V, implementing Al_2O_3 pellets with the same composite armour backings as investigated in this project [94]. Similar composite armour panel design is described in a patent [95], which also indicates that gaps can be used to design armour panels.

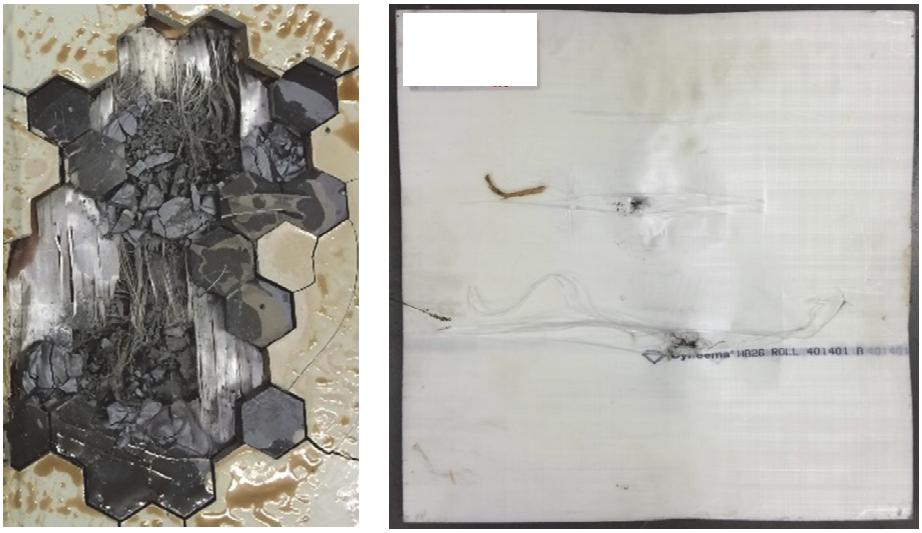

a) b)

Figure 3.24. Armour panel (400x400 mm) with 9 mm thick SiC tiles on BT26 after four shots with 7.62x51 AP (WC core) with 30 mm between two impacts: a) front side; b) back side

In conclusion, considering both a single armour tile and in armour panel configurations, SiC ceramic can be used against 7.62x51 AP (WC core) rounds for an armouring material. The thickness of SiC tiles was initially estimated at 12 mm from depth-of-penetration tests, which was successfully reduced to 10 mm tile thickness with an areal mass density of 32.1 kg/m^2. Tile thickness of 9 mm with an areal mass density of 28.9 kg/m^2 is also plausible but requires additional investigation to assure multi-hit capability.

3.4 Financial comparison

In the financial analysis of the armour solutions indicated above, the armour tile costs were combined with the backing material cost. In this case, a functional unit for comparison purposes was chosen 1 m^2. The armour tile costs of titanium carbide cermets are based on the powders acquired in 2012 and figurative production cost estimations. In all cases, the final armour panel solution uses the same UHMWPE backing. Comparison of the main armour panel components (armour tile and backing material) with different armour tile materials is presented in Table 3.5. In these armour panel cost estimations, no adhesive and protective cover material costs and fabrication costs of the full armour panel system are included, as they are outside the field of expertise of the author.

Table 3.5. Estimated armour panel solution costs with silicon carbide and titanium carbide cermet armour tiles manufactured with conventional and reactive sintering technologies

	TiC-NiMo*	**TiMoC-NiCr**	**SiC**
Panel weight [kg/m^2]	60.1	60.1	43.6
Starting powders [€/m^2]	1382	649	-
Armour tiles [€/m^2]	2367	1634	3592
Backing panel [€/m^2]	1715	1715	1715
Armour panel [€/m^2]	**4082**	**3349**	**5307**

* Reference material

In both cases, titanium carbide cermet armour tiles are more cost efficient than silicon carbide armour tiles. Comparing reactive sintering to conventional powder metallurgy, a 53 % cost reduction can be achieved with the starting powders, which reduces the cost of the main components by 18 % in the armour panel. On the market, solutions offered with aluminium oxide ceramic armour tiles and either UHMWPE or rubberised aramid backing are around 6000 €/m^2. However, those values include a full armour panel solution (with assembly costs, profit and taxes) and are made for test samples, which may be reduced for large scale orders.

3.5 Conclusions on optimising armour tile areal mass density

Aluminium oxide ceramic is a very common armour tile material with its relatively low density and manufacturing costs. Silicon carbide is known to have superior ballistic performance with higher mass efficiency but is not widely used for ground vehicle protection due expensive manufacturing costs. As vehicles have high surface area to be protected and the number of vehicles for personnel transportation in defence forces is large, Al_2O_3 is often preferred even with increased total weight. In this research, TiC based cermets were both developed and geometry optimised as an alternative armour tile material. It was found that TiC-NiMo cermet offers a solution in between SiC and Al_2O_3 in terms of areal mass density even as the material with the highest density. A decrease in the areal mass density was obtained by reducing the thickness of the armour tile, resulting in a higher mass efficiency compared to Al_2O_3 (Figure 3.25). Manufacturing costs have not been evaluated for TiC-NiMo but are estimated to be between those of SiC and Al_2O_3.

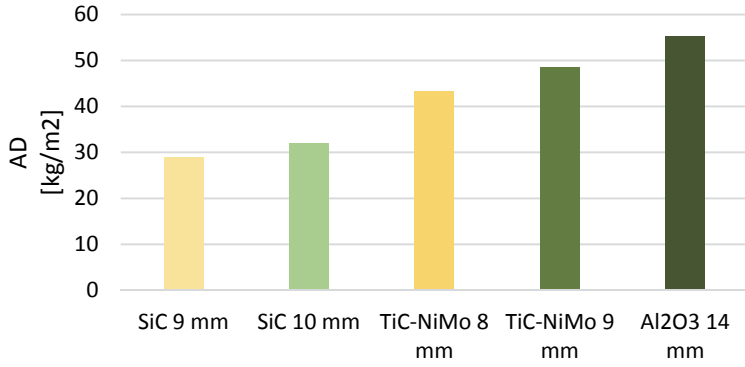

Figure 3.25. Areal mass densities of armour tile materials. Shades of green indicate tile thicknesses that have stopped 7.62x51 AP (WC core) rounds successfully and shades of yellow indicate tile thicknesses that may stop the same threat with additional investigation in panel construction

4 CONCLUSIONS

Conclusions of the dissertation are divided into two groups. The first group focuses on the material development of the reactive sintered TiC based cermets and the second group on the evaluation of TiC-NiMo cermets as armour material against 7.62x51 armour piercing rounds with hardmetal core. After the conclusions, answers to the postulated hypotheses are addressed.

Conclusions on the development of reactive sintered TiC based cermets:

1. Carbide synthesis occurs during high energy milling and sintering of the final part. The final hard phase consists of Ti(Mo)C dual-carbide where a minimum amount of 6 % of metal atoms need to be Mo in order to result in a dense material with minimum porosity. The final microstructure is a two phased composite material with Ti(Mo)C carbide grains with nickel binder as matrix unlike commercial three phased materials with TiC grain cores surrounded by Ti(Mo)C dual-carbide rims in a nickel matrix.
2. Chromium dissolves in the binder, increasing the hardness of the binder matrix and the cermet. With uneven distribution of chromium, it is believed to concentrate to increased crack inhibition, decreasing the strength of the material.
3. An optimal sintering regime implements an additional dwell step at 1270 ˚C to ensure homogeneous microstructure. With the test samples prepared, the most suitable dwell duration at 1270 ˚C and 1500 ˚C was 60 minutes. Applying hot isostatic pressure during liquid phase sintering can result in an increase of density by 3 %.
4. Milling duration of 6 hours using high energy milling equipment resulted in the best combination of mechanical properties. Contamination with WC was at a rate of 0.27 wt% per hour, which significantly increases the theoretical density of the final material.

Conclusions on the development of TiC-NiMo armour tiles are as follows:

1. TiC-NiMo cermet has sufficient ballistic properties to defeat WC-Ni hardmetal projectiles. The mode of fragmentation of a cermet material results in a larger fraction of fragmentation debris compared to ceramic materials. Ceramic fragments of SiC are finer but have significantly higher hardness or HV10 2420 compared to HV10 1510 of TiC-NiMo cermet, suggesting a similar abrasive effectiveness between the two materials. Compared to Al_2O_3 ceramic, the hardness values are similar (HV10 1580 for alumina) but with finer fragmentation debris TiC-NiMo has increased abrasive effectiveness, which results in higher mass efficiency for TiC-NiMo compared to Al_2O_3.
2. Initial indication of armour tile thicknesses of TiC-NiMo cermet and SiC ceramic according to the depth of penetration tests were in both cases 12 mm

for hexagonal tiles with 30 mm height. Due to complex interaction under dynamic loads between the armour tile and the backing material, the final thicknesses of TiC-NiMo cermet is 9 mm and 10 mm for SiC, which stand for areal mass densities of 48.6 kg/m^2 and 32.1 kg/m^2, respectively. It is suggested that these tile thicknesses can be both reduced by 1 mm with further engineering of armour panel configuration.

3. Comparison of TiC-NiMo cermets and the ceramics on the market revealed that titanium carbide cermets have increased multi-hit capability due to higher strength values. Mass efficiency of TiC-NiMo cermets is between SiC and Al_2O_3, with silicon carbide being the lightest option. Compared to silicon carbide armour tiles, titanium carbide cermet tiles are 37 % more cost efficient under reactive sintering technology.

Main conclusions to the postulated hypotheses:

I. *Reactive sintering technology is able to produce TiC based cermets with similar and in some cases, with superior mechanical properties compared to equivalent cermet compositions manufactured with conventional route.*

II. *TiC based cermets with sufficient hard phase content are able to destroy the hardmetal core of 7.62x51 armour piercing rounds.*

III. *TiC based cermets have a mass efficiency for ballistic protection between SiC and Al_2O_3 ceramic armour materials.*

Scientific novelty

Main novelty aspects from the research presented in the current dissertation are as follows:

1. Fast high energy milling process was implemented for preparing elemental powder mixtures to be reactively sintered. It was shown that a milling duration of 6 hours is sufficient to mechanically activate powders that are later synthesising carbides before the liquid phase of the binder occurs.
2. A sintering regime for producing high density cermets was developed for reactive sintering of titanium carbide based cermets. It was found that additional dwell at 1270 ˚C is needed to improve dense microstructure formation.
3. The effect of chromium and molybdenum on the mechanical properties of reactive sintered TiC cermets was analysed and suggestions are made for material design with a tailored set of properties.
4. Comparison on the mass efficiency of TiC cermet to SiC and Al_2O_3 armour ceramics is illustrated for armour tiles engineered against 7.62x51 armour piercing rounds with WC hardmetal cores according to NATO STANAG 4569 level 3 with multi-hit capability described in AEP-55.

Recommendations for future work

Concerning material development of reactive sintering technology, the following recommendations for further research are proposed:

- For other applications, it is required to expand the range of properties by changing the ceramic and binder phase ratio;
- Additional alloying elements can be investigated for enhanced mechanical properties, e.g. those of vanadium;
- Possible effect of sintering in nitrogen to synthesise TiCN *in situ* during reactive sintering could improve mechanical properties of the cermets.

Concerning TiC based cermets as armour material, the following recommendations for further research are proposed:

- Scaling up production of reactive sintering technology needs to addressed;
- Testing of reactive sintered cermet's ballistic capability needs numerous experiments to validate their ballistic performance;
- Reducing the binder content in TiC based cermets could potentially increase their mass efficiency as the hardness increases, which aids in projectile erosion and lowers the density of the cermet.

REFERENCES

[1] Eesti Kaitsevägi. [WWW] http://www.mil.ee/et/kaitsevagi/tehnika/transport/Transportoorid (09.12.2015)

[2] Protection levels for Occupants of Logistic and Light Armoured Vehicles : STANAG 4569. Brussels : NATO Stantardization Agency, 2012.

[3] Brookes, J.K. World Directory and Handbook of Hardmetals and Hard Materlials Sixth Edition. Hertfordshire : International Carbide Data, 1996.

[4] Sarin, V.K. Comprehensive Hard Materials, Hardmetals. Oxford : Elsevier, 2014.

[5] Villareco. [WWW] http://www.villacero.com/images/pdf/en/ArmourSteel.pdf (20.01.2016)

[6] Brown MacFarlane. http://www.brownmac.com/UserFiles/Docs/Products%20Brochures/armour_steel_plate.pdf (20.01.2016)

[7] Hazell, P.J. Armour: Materials, Theory, and Design. Boca Raton : Taylor & Francis, 2015.

[8] Hazell, P.J. Ceramic armour : design and defeat mechanisms. Canberra : Argos Press, 2006.

[9] Den Reijer, P.C. Impact on Ceramic Faced Armour : PhD dissertation. Delft, Delft University of Technology, 1991.

[10] Lundberg, P., Renström, R., Lundberg, B. Impact of metallic projectiles on ceramic targets: transition between interface defeat and penetration. – *International Journal of Impact Engineering, 2000,* 24 (3), 259–275.

[11] Shatynski, S.R. The Thermochemesty of Transition Metal Carbides. – *Oxidation of Metals, 1978,* 13(2), 105–118.

[12] Ткаченко Ю.Г., Орданьян С.С., Юлюгин В.К. Характеристики трения, особенности деформаций в зоне контакта TiC области гомогенности. – *Порошковая металлургия* 1979, 6, 45–51.

[13] Weast, R. CRC Handbook of Chemisrty and Physics. Cleaveland : CRC Publications, 1980.

[14] Cho, K., Katz, R.N., Bar-On, I. Mechanical Properties of Hot Pressed Titnium Diboride. Aberdeen : U.S. Army Research Laboratory, 1996.

[15] Anthony, J.W. Handbook of Mineralogy, Volume III. Chantilly : Mineral Data Publishing, 1997.

[16] Petersen, K.E. Silicon as a Mechanical Material. – *Proceedings of the IEEE,* USA. San Diego : IEEE Group, 1982, 70(5).

[17] Bauer, E. Epitaxy of metals on metals. – *Applications of Surface Science,* 1982, 11–12, 479–494.

[18] Pierson, H.O. Handbook of refractory carbides and nitrides: properties, characteristics, processing, and applications. Westwood : Noyes Publications, 1996.

[19] Zhang, S. Titanium carbonitride-based cermets: processes and properties. – *Materials Science and Engineering: A,* 1993, 163, 141–148.

[20] Murno, R.G. Material Properties of Titanium Diboride. – *Journal of Research of the National Institute of Standards and Technology,* 2000, 105, 709–720.

[21] Pettersson, A., Magnusson, P., Lundberg, P., Nygren, M. Titanium–titanium diboride composites as part of a gradient armour material. – *International Journal of Impact Engineering,* 2005, 32(1–4), 387–399.

[22] Rajenderan, A., Grove, D. Modeling the shock response of silicon carbide, boron carbide and titanium diboride. – *International Journal of Impact Engineering,* 1996, 18(6), 611–631.

[23] Clayton, J. Penetration resistance of armor ceramics: Dimensional analysis and property correlations. – *International Journal of Impact Engineering,* 2015, 85, 124–131.

[24] Vance, M.W. Low cost Sintering of Titnium Diboride for Armor. Watertown : U.S. Army Materials Technology Laboratory, 1988.

[25] Azo Materials. [WWW] http://www.azom.com/article.aspx?ArticleID=492 (29.01.2016)

[26] CeraShield. [WWW] http://www.coorstek.com/resource-library/library/8510-1091_ceramic_armor.pdf (29.01.2016)

[27] Nurol Technologies. [WWW] http://nurolteknoloji.com/en/materials/titanium-diboride-tib2.html (29.01.2016)

[28] Ettmayer, P. Hardmetals and Cermets. – *Annual Review of Material Science,* 1989, 19, 145–164.

[29] Compton, B., Zok, F. Impact resistance of TiC-based cermets. – *International Journal of Impact Engineering,* 2013, 62, 75–87.

[30] Davis, J. ASM Specialty Handbook: Tool Materials. Russell Township: ASM International, 1995.

[31] Humenik, M., Kingery, W. Metal-Ceramic Interactions: III, Surface Tension and Wettability of Metal-Ceramic Systems. – *Journal of American Ceramic Society,* 1954, 37, 18–23.

[32] Humenik, M., Parikh, N. Cermets: I, Fundamental Concepts Related to Micro-structure and Physical Properties of Cermet Systems. – *Journal of the American Ceramic Society,* 1956, 39(2), 60–63.

[33] Wu, Q., Yang, C., Xue, F., Sun, Y. Effect of Mo addition on the microstructure and wear resistance of in situ TiC/Al composite. – *Materials and Design,* 2011, 32, 4999–5003.

[34] Kudaka, K., Onishi, T. – *Journal of Japan Society of Powder and Powder Metallurgy,* 1971, 17 (6), 267–269.

[35] Kübarsepp, J., Klaasen, H., Pirso, J. Behaviour of TiC-base cermets in different wear conditions. – *Wear,* 2001, 249, 229–234.

[36] Tanaka, T., Matsuura, K., Kojima, K., Ohno, M. Combustion Synthesis of Titanium-based Cemented Carbides. – *Materials Science Forum,* 2010, 638–642, 1860–1865.

[37] Farid, A., Guo, S., Shah, J., Feng, P. Effect of Adding a Type of Binder Phase on The Microstructure, Properties and Heat Treatment of Steel Bonded TiC Cermets. – *Materials Science Forum,* 2007, 534–536, 1161–1164.

[38] Dai, H., Li, J., Zhai, F., Cheng, X., Wang, Y. Effect of molybdenum on the microstructure and mechanical properties of TiC-Fe cermets. – *Advanced Materials Research,* 2012, 557–559, 205–208.

[39] Li, B., Liu, Z., Chen, Y., Zhao, L. Erosion Resistance of TiC/Fe Composite at High Temperatures. – *Advanced Materials Research,* 2009, 79-82, 1087–1090.

[40] Xiao, Z., Wu, Y., Shen, Y., Zou, Z., Long, F., Liu, K. First-principles Study of the Properties of Clean and Ni-doped TiC/Fe Interfaces. – *Advanced Materials Research,* 2012, 415-417, 166–169.

[41] Liu, H., Hong, ;., Huang, C., Zou, B. Experimental Study on the Cutting Performance of TiC-based Nanocomposite Ceramic Tools in turning 40Cr Steel. – *Advanced Materials Research,* 2011, 325, 309–314.

[42] Subramanian, R., Schneible, J., Alexander, K. Iron aluminide-titanium carbide composites - microstructure and mechanical properties, Oak Ridge: Oak Ridge National Laboratory, 1996.

[43] Pirso, J., Viljus, M., Juhani, K., Kuningas, M. Three-body abrasive wear of TiC-NiMo cermets. – *Tribology International,* 2010, 43 (1-2), 340–346.

[44] Kwon, H., Jung, S., Kim, W. (Ti,Cr)C Synthesized In Situ by Spark Plasma Sintering of TiC/Cr3C2 Powder Mixtures. – *Materials Transactions,* 2015, 56 (2), 264–268.

[45] Han, C., Kong, M. Fabrication and properties of TiC-based cermet with intra/intergranular microstructure. – *Materials and Design,* 2009, 30, 1205–1208.

[46] Choi, Y., Baik, N., Lee, J., Hong, S., Hahn, Y. Corrosion and wear properties of TiC/Ni-Mo composites produced by direct consolidation during a self-propagating high-temperature reaction. – *Composites Science and Technology,* 2001, 61, 981–986.

[47] Choi, C. Densification process of TiCx–Ni composites formed by self-propagating high-temperature synthesis reaction. – *Journal of Materials Science,* 1997, 32, 1717–1724.

[48] Kobayashi, K., Ozaki, K. Fabrication of TiC-20 mass%Ni Cermet Using MA-PCS Process. – *Materials Transactions,* 2006, 47 (10), 2561–2565.

[49] Schatt, W., Wieters, K. Powder Metallurgy, Processing and Materials. Shrewbury: European Powder Metallurgy Association, 1997.

[50] Razavi, M., Rahimipour, M., Kaboli, R. Synthesis of TiC nanocomposite powder from impure TiO2 and carbon black by mechanically activated sintering. – *Journal of Alloys and Compounds,* 2008, 460, 694–698.

[51] Jiang, Z., Rhine, R. Preparation of titanium nitride (TiN) and titanium carbide (TiC) from a polymeric precursor. – *Chemestry of Materials,* 1991, 3 (6), 1132–1137.

[52] Stanley, D., Birchall, J., Hyland, J., Thomas, L., Hodgetts, K. Carbothermal synthesis of binary (MX) and ternary (M1, M2X) carbides, nitrides and borides from polymeric precursors. – *Journal of Materials Chemistry,* 1992, 2, 149–156.

[53] Alexandereshu, R., Borsella, E., Botti, S., Cesile, M., Martelli, S., Georgi, R., Turtu, S., Zappa, G. Synthesis of TiC and SiC/TiC nanocrystalline powders by gas-phase laser-induced reaction. – *Journal of Materials Science,* 1997, 32 (21), 5629–5635.

[54] Ma, J., Wu, M., Du, Y., Chen, S., Li, G., Hu, J. Synthesis of nanocrystalline titanium carbide with a new convenient route at low temperature and its thermal stability. – *Materials Science and Engineering: B,* 2008, 153 (1-3), 96–99.

[55] Lohse, B., Calka, A., Wexler, D. Effect of Moisture on the Synthesis of TiC by Mechanically-Induced Self-Propagating Reaction. – *Journal of Metastable and Nanocrystalline Materials,* 2005, 26, 8–15.

[56] Jia, H., Zhang, Z., Qi, Z., Liu, G., Bian, X. Formation of nanocrystalline TiC from titanium and different carbon sources by mechanical alloying. – *Journal of Alloys and Compounds,* 2009, 472, 97–103.

[57] Suryanarayana, C. Mechanical alloying and milling. – *Progress in Materials Science,* 2001, 46 (1-2), 1–184.

[58] Jin, H., Li, J., Cao, M., Agathopoulos, S. Influence of mechanical activation on combustion synthesis of fine silicon carbide (SiC) powder. – *Powder Technology,* 2009, 196 (2), 229–232.

[59] Tsuchida, T., Morita, N. Formation of ternary carbide Co6W6C by mechanical activation assisted solid-state reaction. – *Journal of the European Ceramic Society,* 2002, 22 (13), 2401–2407.

[60] Zhu, X., Zhao, K., Cheng, B., Lin, Q., Zhang, X., Chen, T., Su, Y. Synthesis of nanocrystalline TiC powder by mechanical alloying. – *Materials Science and Engineering: C,* 2001, 16 (1-2), 103–105.

[61] Chaira, D., Mishra, B., Sangal, S. Synthesis and characterization of nanocrystalline carbides By reaction milling. – *Proceedings of INCOME 2008 NML Jamshedpur. India : VI International Conference on Mechanochemistry and Mechanical Alloying*, 2008.

[62] Choi, C. Preparation of ultrafine TiC–Ni cermet powders by mechanical alloying. – *Journal of Materials Processing Technology,* 2000, 104 (1-2), 127–132.

[63] Pirso, J., Viljus, M., Letunovitš, S., Juhani, K. Reactive carburizing sintering—A novel production method for high quality chromium carbide–nickel cermets. – *International Journal of Refractory Metals and Hard Materials,* 2006, 24 (3), 263–270.

[64] Pirso, J., Juhani, K., Viljus, M., Joost, R., Letunovits, S. Microstructure evolution in WC-Co composites during reactive sintering from nanocrystalline powders. – *Proceedings of the PM08 World Congress on Powder Metallurgy and Particulate Materials, USA. Washington, NY : PM08 Wordl Congress,* 2008.

[65] Hosokawa, H., Katou, K., Shimojima, K., Furushima, R., Matsumoto, A. Effect of Ni Contents on Microstructures and Mechanical Properties for (Ti0.8Mo0.2)C-Ni Cermets. – *Materials Transactions,* 2014, 55 (9), 1451–1454.

[66] Storms, E. The Refractory Metals Carbides. New York : Academic Press, 1967.

[67] Jõeleht, M., Pirso, J., Juhani, K., Viljus, M. The influence of TiC powder to reactive sintered TiC-NiMo cermets. – *Proceedings of the. Austria. Reutte : 18th Plansee Seminar, 2013*.

[68] Jõeleht, M., Pirso, J., Juhani, K., Viljus, M., Traksmaa, R. The formation of reactive sintered (Ti, Mo)C-Ni cermet from nanocrystalline powders. –

International Journal of Refractory Metals and Hard Materials, 2014, 43, 284–290.

[69] Lawn, H.R., Fuller, E.R. Equilibrium penny-like cracks in indentation fracture. – *Journal of Materials Science*, 1975, 10, 2016–2024.

[70] Jõeleht, M., Pirso, J., Juhani, K., Viljus, M. The Influence of Sintering Temperature of Reactive Sintered (Ti, Mo)C-Ni Cermets. – *Materials Science,* 2015, 21 (3), 435–438.

[71] Kübarsepp, J., Pirso, J., Juhani, K. Developments in cermet design, technology and performance. – *International Journal of Materials and Product Technologies,* 2014, 49, 160–179.

[72] Sánchez, J., Ordóñeza, A., González, R. HIP after sintering of ultrafine WC–Co hardmetals. – *International Journal of Refractory Metals and Hard Materials,* 2005, 23 (3), 193–198.

[73] Wei, C., Song, X., Zhao, S., Zhang, L., Liu, W. In-situ synthesis of WC–Co composite powder and densification by sinter-HIP. – *International Journal of Refractory Metals and Hard Materials,* 2010, 28 (5), 567–571.

[74] Klaasen, H., Kollo, L., Kübarsepp, J. Mechanical properties and wear performance of compression sintered TiC based cermets. – *Powder Metallurgy,* 2007, 28 (5), 132–136.

[75] Kübarsepp, J., Klaasen, H., Tsinjan, A., Juhani, K., Kollo, L., Viljus, M. Influence of pressurized sintering on the performance of TiC-based cermets. – *Key Engineering Materials,* 2013, 527, 56–61.

[76] Jõeleht, M., Pirso, J., Juhani, K., Viljus, M., Traksmaa, R. The influence of high energy milling and sintering parameters on reactive sintered (Ti, Mo)C-Ni cermets. – *Journal of Alloys and Compounds,* 2015, 636, 381–386.

[77] Lohse, B., Calka, A., Wexler, D. Effect of starting composition on the synthesis of nanocrystalline TiC during milling of titanium and carbon. – *Journal of Alloys and Compounds,* 2005, 394, 148–151.

[78] Zhang, W., Wang, H., Yin, S., Jiang, Q. Effect of Ti/C ratio on the SHS reaction on the SHS reaction of Cr-Ti-C system. – *Materials Letters,* 2007, 61, 3075–3078.

[79] Calphad. [WWW] http://www.calphad.com/pdf/Ni_Cr_Phase_Diagram.pdf (25.02.2016)

[80] Jõeleht, M., Pirso, J., Juhani, K., Viljus, M. The influence of carbon and molybden in reactive sintered Ti(Mo)C-NiCr cermets. – *PM2015 Proceedings, France. Reims : PM2015, 2015*.

[81] Hazell, P.J., Appleby-Thomas, G., Philbey, D., Tolman, W. The effect of gilding jacket material on the penetration mechanics of a 7.62 mm armour-piercing projectile. – *International Journal of Impact Engineering,* 2013, 54, 11–18.

[82] Savio, S., Senthil, P., Singh, V., Ghoshal, P., Madhu, V., Gogia, A. An experimental study on the projectile defeat mechanism of hard steel projectile against boron carbide tiles. – *International Journal of Impact Engineering,* 2015, 86, 157–166.

[83] Chi, R., Serjouei, A., Sridhar, I., Geoffrey, T. Pre-stress effect on confined ceramic armor ballistic performance. – *International Journal of Impact Engineering,* 2015, 84, 159–170.

[84] Liu, J., Yuan, J. Effects of Specimen Size and Boundary Conditions on the Penetration Depth of Metal Ceramic Structure. – *Procedia Engineering,* 2014, 75, 71–77.

[85] Hazell, P.J., Appleby-Thomas, G., Toone, S. Ballistic compaction of a confined ceramic powder by a non-deforming projectile: Experiments and simulations. *Materials & Design,* 2014, 56, 943–952.

[86] Savio, S., Ramanjaneyulu, K., Madhu. V., Bhat, B. An experimental study on ballistic performance of boron carbide tiles. – *International Journal of Impact Engineering,* 2011, 38, 535–541.

[87] Lundberg, P., Lundberg, B. Transition between interface defeat and penetration for tungsten projectiles and four silicon carbide materials. – *International Journal of Impact Engineering,* 2005, 31 (7), 781–792.

[88] Westerling, L., Lundberg, P., Lundberg, B. Tungsten long-rod penetration into confined cylinders of boron carbide at and above ordnance velocities. – *International Journal of Impact Engineering,* 2001, 25 (7), 703–714.

[89] Climax Molybdenum Company. The use of molybdenum in TiC-base cermets. New York: Communication Corporation, 1967.

[90] Accuratus. [WWW]. http://accuratus.com/alumox.html (15.02.2016)

[91] Saint-Gobain. [WWW] http://www.refractories.saint-gobain.com/uploadedFiles/SGCeramicsHPR/Documents/Hexoloy/Hexoloy-SA-SiC-TDS.pdf (15.02.2016)

[92] Davis, J. ASM Specialty Handbook: Aluminum and Aluminum Alloys. ASM International, 1993.

[93] Krell, A., Strassburger, E. Order of influences on the ballistic resistance of armor ceramics and single crystals. – *Materials Science and Engineering A,* 2014, 597, 422–430.

[94] TenCate. [WWW] http://www.tencate.com/emea/advanced-armour/brands/tencate-liba/tencate-liba-al.aspx (15.02.2016)

[95] Cohen, M. Composite armor plates and panel : US6289781 B1, 2001. [Online] http://www.google.com/patents/US6289781 (18. 02. 2016).

LIST OF PUBLICATIONS

1. Jõeleht, M., Pirso, J., Juhani, K., Viljus, M., Traksmaa, R. The formation of reactive sintered (Ti, Mo)C-Ni cermet from nanocrystalline powders. – *International Journal of Refractory Metals and Hard Materials*, 2014, 43, 284–290. doi:10.1016/j.ijrmhm.2013.12.016

2. Jõeleht, M., Pirso, J., Juhani, K., Viljus, M., Traksmaa, R. The influence of high energy milling and sintering parameters on reactive sintered (Ti, Mo)C-Ni cermets. – *Journal of Alloys and Compounds*, 2015, 636, 381–386. doi:10.1016/j.jallcom.2015.02.071

3. Jõeleht, M., Pirso, J., Juhani, K., Viljus, M. The influence of sintering temperature of reactive sintered (Ti, Mo)C-Ni cermets. – *Materials Science*, 2015, 21 (3), 435–438. http://dx.doi.org/10.5755/j01.ms.21.3.7179

Participation at international conferences

1. Jõeleht, M., Pirso, J., Juhani, K., Viljus, M. The influence of TiC powder to reactive sintered TiC-NiMo cermets. – *Proceedings of the 18th Plansee Seminar 2013, Austria, Reutte : 18th Plansee Seminar 2013, 3–7 June*.

2. Jõeleht, M., Pirso, J., Juhani, K., Viljus, M., Traksmaa, R. The influence of sintering temperature of reactive sintered (Ti, Mo)C-Ni cermets. – *Materials Engineering (Medžiagotyra)*, 2015, 21 (3), 435–438 *: 23rd International Baltic Conference on Materials Engineering Kaunas, Lithuania, 2014. (2. paper was presented at this conference.)*

3. Jõeleht, M., Pirso, J., Juhani, K., Viljus, M. The influence of carbon and molybden in reactive sintered Ti(Mo)C-NiCr cermets. – *PM2015 Proceedings, France. Reims : EURO PM 2015*.

ACKNOWLEDGEMENTS

First and foremost, I would like to thank sincerely my supervisor D. Eng. Jüri Pirso for accepting to mentor my research activities and to take full control on the research direction for myself and for steering to the correct direction when needed. In addition, I would like to thank my second supervisor Kristjan Juhani, PhD, for helping with research related activities as well as other important aspects for a successful doctorate period.

My learning from experiments and analysis would have been significantly impaired if I had not had the chance of exchanging ideas and discussing my work with colleagues in the laboratory and in other departments. I would therefore like to thank my fellow doctorate students Marek Tarraste, Kaspar Kallip, Aare Aruniit (now already PhD), Märt Kolnes, Marina Aghayan and Der-Liang Yung as well as more experienced colleagues Lauri Kollo, PhD, Jaan Kers, PhD, Mart Viljus, PhD and Rainer Traksmaa, MSc.

Additional appreciation goes to the Ministry of Defence for supporting my research on a personal level and especially, Mr Dmitri Teperik and Ms Kristiina Kütt for giving me the possibility to expand my understanding from the governmental side of defence management on a national scale. Also, help from the Estonian Defence forces for organizing and conducting ballistic testing came from mjr Risto Pärtel and msg Margus Simson.

Finally, I would like to thank my mum and grandparents for supporting me in the pursuit of higher education with motivation, encouragement and the occasional warm meal and place to sleep.

ABSTRACT

Titanium Carbide based Cermets as Ballistic Protection Material

In this study, titanium carbide based cermets were investigated as alternative material for ballistic protection. Firstly, reactive sintering technology was implemented to improve the mechanical properties and to reduce the manufacturing costs of TiC based cermets. Secondly, the material was assessed by ballistic performance and compared to other materials that are currently on the market.

Different aspects of material preparation showed that as compared to conventional methods, reactive sintering technology enables similar or in some cases, superior mechanical properties to be achieved. Powder milling, chemical composition and sintering regimes were developed to acquire a set of properties suitable for ballistic performance against hardmetal projectiles.

Ballistic testing methods were also developed to compare TiC based cermets to Al_2O_3 and SiC ceramic materials. Single tile testing experiments were designed to closely resemble the conditions of a tile in a full armour panel solution. In addition, armour tiles were tested in an armour panel configuration where the final thickness of the tiles was optimised. It was concluded that TiC based cermets are able to destroy the hardmetal core of the 7.62x51 AP round at a mass efficiency between that of SiC and Al_2O_3. These results indicate that TiC based cermets could offer an alternative material in designing armour solutions at a competitive weight and cost.

KOKKUVÕTE

Titaankarbiidi baasil kermis ballistilise kaitse materjalina

Käesoleval tööl oli kaks põhilist eesmärki. Esimeseks oli välja töötada tehnoloogia reaktsioonpaagutatavatele titaankarbiidi baasil kermised, mille mehaanilised omadused oleksid samaväärsed või paremad tavatehnoloogiaga valmistatud ekvivalentidest. Teisalt uuriti titaankarbiidi baasil kermiste kasutamist võimaliku alternatiivse materjalina kõvasulamsüdamikuga 7.62x51 soomustläbistavate kuulide vastu. Püstitati järgnevad hüpoteesid:

Hüpotees I. *Reaktsioonpaagutuse tehnoloogiaga on võimalik saavutada titaankarbiidi baasil kermiseid, mis on paremate mehaaniliste omadustega kui tavatehnoloogiaga valmistatud materjal.*

Hüpotees II. *Titaankarbiidkermised on võimelised töötama kõvasulamsüdamikuga 7.62x51 soomustläbistavate kuulide vastu.*

Hüpotees III. *Titaankarbiidkermistel on konkureeriv kaal võrreldes laialtlevinud keraamiliste soomusmaterjalidega, milledeks on alumiiniumoksiid (Al_2O_3) ning ränikarbiid (SiC).*

Uurimustöö tulemused on jagatud kahte gruppi. Esimene grupp hõlmab reaktsioonpaagutatud titaankarbiidkermiste materjali arendust. Teine grupp annab ülevaate titaankarbiidkermiste sobimisest kõvasulamist südamikuga 7.62x51 soomustläbistavate kuulide vastu toimimisest. Peale järeldusi on vastatud eelnevalt püstitatud hüpoteesidele.

Järeldused reaktsioonpaagutatud titaankarbiidi baasil kermiste arendusest:

1. Karbiidi süntees toimub kolmes faasis ning enne nikli sideaine vedelfaaspaagutust. Esmane karbiidi süntees algab kõrgenergeetilisel jahvatamisel. Titaan- ja molübdeenkarbiidi süntees toimub paagutamisel alla 800 ˚C, millele järgneb Ti(Mo)C kaksikkarbiidi moodustumine. Lõplik mikrostruktuur on kahefaasiline komposiitmaterjal koosnedes Ti(Mo)C kaksikkarbiidist, mis on ümbritsetud nikli maatriksiga. Tavatehnoloogial baseeruvad materjalid on aga seevastu kolmefaasilised. Kõvafaasi moodustavad terad koosnedes titaankarbiid südamikest ja kaksikkarbiidist ümbrisega, mis on paigutatud nikli maatriksisse.
2. Ühtlase molübdeeni jaotumisega karbiidi terade sees on minimaalne vajalik molübdeeni kogus karbiidi metalli aatomitest 6%. Vastasel juhul on oht, et sideaine ei suuda karbiidi terasid piisaval määral märjata ning materjali tekib mikropoorsus.
3. Kroomi metalli aatomid lahustuvad niklis suurendades nihete arvu nikli terade kristalli võres ja tasapindades. Antud nihked suurendavad sideaine võre vastupanu kristallitasapindade liikumisele tõstes sideaine kõvadust, mis

omakorda suurendab terve materjali kõvadust. Kroomi jagunemine sideaines toimub aga ebaühtlaselt, mis tähendab, et tekkivad nihked sideaine kristallvõres koonduvad ning sellega kaasnevad pingekontsentraatorid. Sellega kaasneb ka materjali tugevuse kahanemine, sest tugevuse mõõtes on pinge all kogu materjal ning purunemine algab pragudest.

4. Optimaalne paagutusrežiim sisaldab endas lisahoidmist 1270˚C juures tagamaks ühtlast mikrostruktuuri ja vähendatud poorsust. Parima tulemuse andsid katsekehad, mida hoiti 1270˚C ja 1500˚C juures 60 minutit.
5. Vaakumi suurus paagutuse käigus mõjutab materjali omadusi, kuna kõrge vaakumiga võib vedelfaasi ajal sideaine aurustuda. Rakendades isostaatilist kuumpressimiste vedelfaasi ajal argooni gaasiga on võimalik tõsta materjali tihedust kuni 3%. Materjali tiheduse suurenimine sõltub materjali eelnevast suhtelisest tihedusest enne isostaatilist kuumpressimist.
6. Optimaalseim jahvatusaeg reaktsioonpaagutatavale pulbrile on 6 tundi kõrgenergeetilises jahvatuses. Jahvatuse käigus toimub volframkarbiidiga saastumine jahvatusseadme ja -kuulide kulumisest tingituna 0,27 kaalu% tunnis. Suure tihedusega volframkarbiidiga saastumine suurendab kermise tihedust, mis antud rakenduses soomusmaterjalina ei ole soovitud.

Järeldused titaankarbiidist kermisest soomusplaatide arendusest on järgnevad:

1. Titaankarbiidkermistel on piisavad ballistilised omadused, et purustada volframkarbiid-nikkel kõvasulamsüdamikuga kuule. Tähtsaim materjali mehaaniline omadus tagamaks soomusplaadi võimet kuuli südamikus pragude tekkimist on materjali kõvadus. Vastava madala sideainekogusega on titaankarbiidkermistel suurem kõvadus kui kõvasulam, mida kasutatakse kuuli südamikes.
2. Kermise materjalis toimub pragude tekkimise protsess suuremate pragude vahelise kaugusega võrreldes keraamikaga. Selle tulemusel on purunemise tagajärjel tekkivad soomusplaadi killud suuremad, mis töötavad kuuli südamiku kulutamisel efektiivsemalt kui väiksed killud sama kõvaduse juures. Ränikarbiidist plaadi pragunemise tulemusel tekib küll peenem kildude fraktsioon, kuid omades oluliselt suuremat kõvadust (HV10 2420) võrreldes titaankarbiidkermisega (HV10 1510) on ränikarbiidist killud suurema kulutamisvõimega. Arvestades erinevaid kildude suurusi ja kõvadusi on titaankarbiidkermiste ja ränikarbiidist kildude kuuli südamiku kulutamise efektiivsus samaväärne sama mahu juures. Alumiiniumoksiid on sarnase kõvadusega (HV10 1580) võrreldes titaankarbiidkermisega, kuid peenema kildude fraktsiooniga on titaankarbiidkermised võimelised kuuli kulutama paremini omades seega ka paremat kaaluefektiivsust alumiiniumoksiidi ees.
3. Sissetungimissügavuse katsetused pakkusid soovitatavaks titaankarbiid-kermiste ja ränikarbiidi soomusplaatide paksuseks 12 mm. Heksagonaalse

kujuga soomusplaatide kõrgus on 30 mm. Üksikute soomusplaatide katsetused viidi läbi alumiiniumi sulamist tausta peal. Tingituna keerukast soomus- ja alusplaadi koostoimest dünaamilistel koormustel suudeti soomusplaadi paksusi vähendada kasutades taustaplaadina sihtotstarbelisi komposiitmaterjale. Titaankarbiidkermisest soomusplaatide paksust vähendati 9 mm peale ning ränikarbiidist soomusplaatide paksust 10 mm-ni. Antud paksuste juures on titaankarbiidist plaatide ruutmeetri kaal 48,6 kg/m^2 ning ränikarbiidist plaatide ruutmeetri kaal 32,1 kg/m^2. Katsetused näitasid, et edasise soomuspaneeli arendusega oleks võimalik mõlemast materjalist plaadi paksust vähendada 1 mm võrra.

4. Titaankarbiidkermised töötavad võrreldes keraamiliste materjalidega paremini mitme lähestikku paikneva tabamuse korral, kuna nende tugevusnäitajad on suuremad. Tabamuse korral kutsutakse soomusplaadis esile pingelained, mis kantakse üle kõrval paiknevatele plaatidele. Kõrval-asetsevad plaadid võivad puruneda ka ilma otsetabamust saamata plaadis peegelduvate pingelainete mõjul kutsutes esile pinged, mis ületavad materjali tugevust, kui soomusplaat ei ole piisavalt suurte mõõtmetega.
5. Võrreldes titaankarbiidkermiseid turul pakutavate soomusmaterjalina kasutavate keraamiliste plaatidega on titaankarbiidkermised kaalu efektiivsuse osas ränikarbiidi ja alumiiniumoksiidi vahel. Ränikarbiid on kõige kergem materjal pakkumaks kaitset sama ohutaseme korral ning alumiiniumoksiid kõige raskem.

Põhijäreldused püstitatud hüpoteesidele on järgnevad:

I. *Reaktsioonpaagutuse tehnoloogiaga on võimalik valmistada titaankarbiidi baasil kermiseid, millede mehaanilised omadused on samaväärsed või osaliselt paremad võrreldes ekvivalentse koostisega kermistega, mis on valmistatud tavatehnoloogilisel viisil.*

II. *Titaankarbiidkermised piisava sideainega on võimelised purustama volframkarbiidist kõvasulamiga 7.62x51 soomustläbistavaid kuuli südamikku.*

III. *Titaankarbiidkermisest valmistatud soomusplaadid on kaalu efektiivsuse osas ränikarbiidi ja alumiiniumoksiidi vahel.*

CURRICULUM VITAE

1. Personal data

Name and surname	Marek Jõeleht
Date and place of birth	July 24, 1988, Tallinn, Estonia
Nationality	Estonian
E-mail address	marek.joeleht@gmail.com

2. Education

Educational institution (name during graduation)	Graduation	Education (degree)
Tallinn University of Technology	2012	Master of Science
Tallinn University of Technology	2011	Bachelor of Science
Tallinn Arte Gymnasium	2007	Secondary education

3. Language skills (basic, good, fluent)

Language	Skill
Estonian	Fluent
English	Fluent
German	Basic

4. Additional training

Training period	Additional training facility
2010–2011	Aalto University Product Development Project
2015–2015	Fraunhofer IWS Additive manufacturing training

5. Professional employment

Period	Employer	Position
2011– *to date*	Tallinn University of Technology	Engineer
2013– *to date*	Ministry of Defence of Estonia	Expert

6. Research activities and awards

Projects	LKM12179 "Light-weight hard armour panels for armoured vehicles" (December 1, 2012 – November 30, 2016) Tallinn University of Technology, Faculty of Mechanical Engineering, Department of Materials Engineering AR12131 "Permanent magnets for sustainable energy application (MagMat)" (March 17, 2012 – June 30, 2015) Renno Veinthal, Tallinn University of Technology, Faculty of Mechanical Engineering, Department of Materials Engineering, Tallinn University of Technology, Faculty of Power Engineering, Department of Electrical Engineering
Patents	Method and device for manufacturing sintered material products; Owner: Tallinn University of Technology; Authors: Lauri Kollo, Kaspar Kallip, Zorjana Mural, Hans Vallner, Renno Veinthal, Märt Kolnes, Marek Tarraste, Marek Jõeleht; Priority number: P201500021; Priority date: May 13, 2015
Supervised theses	Master thesis "Technology of Titaniumcarbonotride Cermets" Kened Aavamägi
Awards	Graduates of 2012 Reception by the President of the Republic of Estonia

ELULOOKIRJELDUS

1. Isikuandmed

Ees- ja perekonnanimi	Marek Jõeleht
Sünniaeg ja -koht	24 juuli 1988, Eesti
Kodakondsus	Eesti
E-posti aadress	marek.joeleht@gmail.com

2. Hariduskäik

Õppeasutus (nimetus lõpetamise ajal)	Lõpetamise aasta	Haridus (eriala/kraad)
Tallinna Tehnikaülikool	2012	Tehnikateaduse magister
Tallinna Tehnikaülikool	2011	Tehnikateaduse bakalaureus
Tallinna Arte Gümnaasium	2007	Üldharidus

3. Keelteoskus (alg-, kesk- või kõrgtase)

Keel	Tase
Eesti	Kõrgtase (emakeel)
Inglise	Kõrgtase
Saksa	Algtase

4. Täiendusõpe

Õppimise aeg	Täiendusõppe korraldaja nimetus
2010–2011	Aalto Ülikool Tootearendusprojekt
2015–2015	Fraunhofer IWS Metalliprintimise uurimine

5. Teenistuskäik

Töötamise aeg	Tööandja nimetus	Ametikoht
2011– *praeguseni*	Tallinna Tehnikaülikool	Insener
2013– *praeguseni*	Kaitseministeerium	Ekspert

6. Teadustegevus, sh tunnustused ja juhendatud lõputööd

Projektid	LKM12179 „Kergsoomuspaneelid transpordivahendite soomustamiseks (1.12.2012−30.11.2016) Tallinna Tehnikaülikool, Mehaanikateaduskond, Materjalitehnika instituut AR12131 Püsimagnetid jätkusuutliku energeetika rakendustes (MagMat).“ (17.03.2012−30.06.2015)", Renno Veinthal, Tallinna Tehnikaülikool, Tallinna Tehnikaülikool, Mehaanikateaduskond, Materjalitehnika instituut, Tallinna Tehnikaülikool, Energeetikateaduskond, Elektrotehnika instituut
Patendid	Meetod ja seade pulbermaterjalist toodete valmistamiseks; Omanik: Tallinna Tehnikaülikool; Autorid: Lauri Kollo, Kaspar Kallip, Zorjana Mural, Hans Vallner, Renno Veinthal, Märt Kolnes, Marek Tarraste, Marek Jõeleht; Prioriteedi number: P201500021; Prioriteedi kuupäev: 13.05.2015
Juhendatud lõputööd	Magistritöö „Titaankarbonitriid kermiste tehnoloogia“ Kened Aavamägi
Tunnustused	EV presidendi 2012. aasta lõpetajate vastuvõtt Kadriorus

DISSERTATIONS DEFENDED AT TALLINN UNIVERSITY OF TECHNOLOGY ON *MECHANICAL ENGINEERING*

1. **Jakob Kübarsepp**. Steel-Bonded Hardmetals. 1992.

2. **Jakub Kõo**. Determination of Residual Stresses in Coatings &Coated Parts. 1994.

3. **Mart Tamre**. Tribocharacteristics of Journal Bearings Unlocated Axis. 1995.

4. **Paul Kallas**. Abrasive Erosion of Powder Materials. 1996.

5. **Jüri Pirso**. Titanium and Chromium Carbide Based Cermets. 1996.

6. **Heinrich Reshetnyak**. Hard Metals Serviceability in Sheet Metal Forming Operations. 1996.

7. **Arvi Kruusing**. Magnetic Microdevices and Their Fabrication methods. 1997.

8. **Roberto Carmona Davila**. Some Contributions to the Quality Control in Motor Car Industry. 1999.

9. **Harri Annuka**. Characterization and Application of TiC-Based Iron Alloys Bonded Cermets. 1999.

10. **Irina Hussainova**. Investigation of Particle-Wall Collision and Erosion Prediction. 1999.

11. **Edi Kulderknup**. Reliability and Uncertainty of Quality Measurement. 2000.

12. **Vitali Podgurski**. Laser Ablation and Thermal Evaporation of Thin Films and Structures. 2001.

13. **Igor Penkov**. Strength Investigation of Threaded Joints Under Static and Dynamic Loading. 2001.

14. **Martin Eerme**. Structural Modelling of Engineering Products and Realisation of Computer-Based Environment for Product Development. 2001.

15. **Toivo Tähemaa**. Assurance of Synergy and Competitive Dependability at Non-Safety-Critical Mechatronics Systems design. 2002.

16. **Jüri Resev**. Virtual Differential as Torque Distribution Control Unit in Automotive Propulsion Systems. 2002.

17. **Toomas Pihl**. Powder Coatings for Abrasive Wear. 2002.

18. **Sergei Letunovitš**. Tribology of Fine-Grained Cermets. 2003.

19. **Tatyana Karaulova**. Development of the Modelling Tool for the Analysis of the Production Process and its Entities for the SME. 2004.

20. **Grigori Nekrassov**. Development of an Intelligent Integrated Environment for Computer. 2004.

21. **Sergei Zimakov**. Novel Wear Resistant WC-Based Thermal Sprayed Coatings. 2004.

22. **Irina Preis**. Fatigue Performance and Mechanical Reliability of Cemented Carbides. 2004.

23. **Medhat Hussainov**. Effect of Solid Particles on Turbulence of Gas in Two-Phase Flows. 2005.

24. **Frid Kaljas**. Synergy-Based Approach to Design of the Interdisciplinary Systems. 2005.

25. **Dmitri Neshumayev**. Experimental and Numerical Investigation of Combined Heat Transfer Enhancement Technique in Gas-Heated Channels. 2005.

26. **Renno Veinthal**. Characterization and Modelling of Erosion Wear of Powder Composite Materials and Coatings. 2005.

27. **Sergei Tisler**. Deposition of Solid Particles from Aerosol Flow in Laminar Flat-Plate Boundary Layer. 2006.

28. **Tauno Otto**. Models for Monitoring of Technological Processes and Production Systems. 2006.

29. **Maksim Antonov**. Assessment of Cermets Performance in Aggressive Media. 2006.

30. **Tatjana Barashkova**. Research of the Effect of Correlation at the Measurement of Alternating Voltage. 2006.

31. **Jaan Kers**. Recycling of Composite Plastics. 2006.

32. **Raivo Sell**. Model Based Mechatronic Systems Modeling Methodology in Conceptual Design Stage. 2007.

33. **Hans Rämmal**. Experimental Methods for Sound Propagation Studies in Automotive Duct Systems. 2007.

34. **Meelis Pohlak**. Rapid Prototyping of Sheet Metal Components with Incremental Sheet Forming Technology. 2007.

35. **Priidu Peetsalu**. Microstructural Aspects of Thermal Sprayed WC-Co Coatings and Ni-Cr Coated Steels. 2007.

36. **Lauri Kollo**. Sinter/HIP Technology of TiC-Based Cermets. 2007.

37. **Andrei Dedov**. Assessment of Metal Condition and Remaining Life of In-service Power Plant Components Operating at High Temperature. 2007.

38. **Fjodor Sergejev**. Investigation of the Fatigue Mechanics Aspects of PM Hardmetals and Cermets. 2007.

39. **Eduard Ševtšenko**. Intelligent Decision Support System for the Network of Collaborative SME-s. 2007.

40. **Rünno Lumiste**. Networks and Innovation in Machinery and Electronics Industry and Enterprises (Estonian Case Studies). 2008.

41. **Kristo Karjust**. Integrated Product Development and Production Technology of Large Composite Plastic Products. 2008.

42. **Mart Saarna**. Fatigue Characteristics of PM Steels. 2008.

43. **Eduard Kimmari**. Exothermically Synthesized B_4C-Al Composites for Dry Sliding. 2008.

44. **Indrek Abiline**. Calibration Methods of Coating Thickness Gauges. 2008.

45. **Tiit Hindreus**. Synergy-Based Approach to Quality Assurance. 2009.

46. **Karl Raba**. Uncertainty Focused Product Improvement Models. 2009.

47. **Riho Tarbe**. Abrasive Impact Wear: Tester, Wear and Grindability Studies. 2009.

48. **Kristjan Juhani**. Reactive Sintered Chromium and Titanium Carbide-Based Cermets. 2009.

49. **Nadežda Dementjeva**. Energy Planning Model Analysis and Their Adaptability for Estonian Energy Sector. 2009.

50. **Igor Krupenski**. Numerical Simulation of Two-Phase Turbulent Flows in Ash Circulating Fluidized Bed. 2010.

51. **Aleksandr Hlebnikov**. The Analysis of Efficiency and Optimization of District Heating Networks in Estonia. 2010.

52. **Andres Petritšenko**. Vibration of Ladder Frames. 2010.

53. **Renee Joost**. Novel Methods for Hardmetal Production and Recycling. 2010.

54. **Andre Gregor**. Hard PVD Coatings for Tooling. 2010.

55. **Tõnu Roosaar**. Wear Performance of WC- and TiC-Based Ceramic-Metallic Composites. 2010.

56. **Alina Sivitski**. Sliding Wear of PVD Hard Coatings: Fatigue and Measurement Aspects. 2010.

57. **Sergei Kramanenko**. Fractal Approach for Multiple Project Management in Manufacturing Enterprises. 2010.

58. **Eduard Latõsov**. Model for the Analysis of Combined Heat and Power Production. 2011.

59. **Jürgen Riim**. Calibration Methods of Coating Thickness Standards. 2011.

60. **Andrei Surzhenkov**. Duplex Treatment of Steel Surface. 2011.

61. **Steffen Dahms**. Diffusion Welding of Different Materials. 2011.

62. **Birthe Matsi**. Research of Innovation Capasity Monitoring Methodology for Engineering Industry. 2011.

63. **Peeter Ross**. Data Sharing and Shared Workflow in Medical Imaging. 2011.

64. **Siim Link**. Reactivity of Woody and Herbaceous Biomass Chars. 2011.

65. **Kristjan Plamus**. The Impact of Oil Shale Calorific Value on CFB Boiler Thermal Efficiency and Environment. 2012.

66. **Aleksei Tšinjan**. Performance of Tool Materials in Blanking. 2012.

67. **Martinš Sarkans**. Synergy Deployment at Early Evaluation of Modularity of the Multi-Agent Production Systems. 2012.

68. **Sven Seiler**. Laboratory as a Service – A Holistic Framework for Remote and Virtual Labs. 2012.

69. **Tarmo Velsker**. Design Optimization of Steel and Glass Structures. 2012.

70. **Madis Tiik**. Access Rights and Organizational Management in Implementation of Estonian Electronic Health Record System. 2012.

71. **Marina Kostina**. Reliability Management of Manufacturing Processes in Machinery Enterprises. 2012.

72. **Robert Hudjakov**. Long-Range Navigation for Unmanned Off-Road Ground Vehicle. 2012.

73. **Arkadi Zikin**. Advanced Multiphase Tribo-Functional PTA Hardfacings. 2013.

74. **Alar Konist**. Environmental Aspects of Oil Shale Power Production. 2013.

75. **Inge Roos**. Methodology for Calculating CO_2 Emissions from Estonian Shale Oil Industry. 2013.

76. **Dmitri Shvarts**. Global 3D Map Merging Methods for Robot Navigation. 2013.

77. **Kaia Lõun**. Company's Strategy Based Formation of e-Workplace Performance in the Engineering Industry. 2013.

78. **Maido Hiiemaa**. Motion Planner for Skid-Steer Unmanned Ground Vehicle. 2013.

79. **Dmitri Goljandin**. Disintegrator Milling System Development and Milling Technologies of Different Materials. 2013.

80. **Dmitri Aleksandrov**. Light-Weight Multicopter Structural Design for Energy Saving. 2013.

81. **Henrik Herranen**. Design Optimization of Smart Composite Structures with Embedded Devices. 2014.

82. **Heiki Tiikoja**. Experimental Acoustic Characterization of Automotive Inlet and Exhaust System. 2014.

83. **Jelena Priss**. High Temperature Corrosion and Abrasive Wear of Boiler Steels. 2014.

84. **Aare Aruniit**. Thermoreactive Polymer Composite with High Particulate Filler Content. 2014.

85. **Dmitri Gornostajev**. Development of the Calculation Method for Barge Hull. 2014.

86. **Liina Lind**. Wear of PVD Coatings on Fineblanking Punches. 2014.

87. **Nikolai Voltšihhin**. Design and Technology of Oxides-Containing Ceramic-Based Composites. 2014.

88. **Aleksander Šablinski**. RANS Numerical Modelling of Turbulent Polydispersed Flows in CFB Freeboard. 2015.

89. **Tanel Aruväli**. Wireless Real-time Monitoring of Machining Processes. 2015.

90. **Andrei Bogatov**. Morphological Changes on Diamond and DLC Films During Sliding Wear. 2015.

91. **Raimo Kabral**. Aero-Acoustic Studies and Innovative Noise Control with Application to Modern Automotive Gas Exchange System. 2015.

92. **Jevgeni Sahno**. Dynamic Management Framework for Continuous Improvement of Production Processes. 2015.

93. **Ott Pabut**. Optimal Design of Slotless Permanent Magnet Generators. 2015.

94. **Merili Kukuškin**. Value Centric Business Development for Estonian Manufacturing Small and Medium Sized Enterprises. 2015.

95. **Kaimo Sonk**. Development of Additive Manufacturing Based on Functional Requirements. 2015.